

For Reference

NOT TO BE TAKEN FROM THIS ROOM

Ex LIBRIS
UNIVERSITATIS
ALBERTAENSIS



THE UNIVERSITY OF ALBERTA

SOME EFFECTS OF NON-SYSTEMATIC REFLECTIONS IN
ELECTRON DIFFRACTION

by



CARMAN DENNIS CANN

A THESIS

SUBMITTED TO THE FACULTY OF GRADUATE STUDIES AND RESEARCH
IN PARTIAL FULFILLMENT OF THE REQUIREMENTS FOR THE DEGREE

OF DOCTOR OF PHILOSOPHY

IN

SOLID STATE PHYSICS

DEPARTMENT OF PHYSICS

EDMONTON, ALBERTA

SPRING 1973

ABSTRACT

The effects of the presence of non-systematic reflections on extinction distance, anomalous absorption, and image intensity have been studied for different electron diffraction situations. In the course of these studies a criterion for inclusion of reflections in a many-beam calculation has been developed and the question of Bloch wave labelling in the presence of a non-systematic reflection examined.

In the extinction distance study it was found that, in the presence of a single non-systematic reflection, the largest changes in extinction distance occurred at small positive and negative deviations of the non-systematic reflection from its Bragg condition. Associated with these regions of maximum change were small ranges of deviation over which the variation of the diffracted beam intensity with depth became non-sinusoidal. An analysis in terms of Bloch wave parameters showed that the changes in extinction distance could be explained by relative displacements of the important branches of the dispersion surface. In addition, the regions of non-sinusoidal intensity variations occurred when more than two Bloch waves made significant contributions to the diffracted beam intensity. A further analysis using three-beam analytical

solutions of the dynamical theory showed that the deviations at which the non-sinusoidal intensity variations occurred could be predicted by examining the wave vectors corresponding to the important Bloch waves in the systematic case. It was also found that, for one particular deviation of the systematic reflection from its Bragg condition, one of the non-sinusoidal regions disappeared due to the degeneracy of two of the Bloch waves.

Marked changes in anomalous absorption effects and image intensity were also observed in the presence of non-systematic reflections. Variations in Bloch wave absorption coefficients arising from alterations in the channelling characteristics of the wave under such circumstances resulted in corresponding changes in anomalous absorption effects. These effects were found to be enhanced for negative deviations of the non-systematic reflection from its Bragg condition but diminished for positive deviations. In the case of image intensity, it was found that, in the bright field rocking curve, marked changes in the position of the intensity maximum from that obtained in the systematic case could occur in the presence of non-systematic reflections. No such changes were observed, however, in the dark field case.

As an aid in carrying out many-beam calculations involving non-systematic reflections, a criterion was developed for choosing the reflections to be included in such calculations. This criterion, based on the predicted effect of a reflection on the systematic extinction distance, allowed a calculation to be carried out with the minimum number of reflections included to obtain the desired convergence.

Finally, the labelling of Bloch waves in the presence of a non-systematic reflection was examined. It was found that, under such circumstances, it is no longer possible to associate certain characteristics with particular Bloch wave numbers as is done in the systematic case.

ACKNOWLEDGEMENTS

I wish to express my sincere gratitude to Dr. S.S. Sheinin, my research supervisor, for his guidance and encouragement during the course of this work. In addition, I would like to thank Dr. P.S. Turner, Mr. K.Z. Botros, Mr. J.W. Andrew and Mr. A.E.B. Monk for many helpful discussions and suggestions.

For assistance in many of the technical aspects of the work I wish to thank Mr. J.C. Brunel.

For typing of the manuscript and figure captions I wish to express my sincere appreciation to Mrs. M. Yiu.

For her patience and encouragement during the latter part of this work I wish to express my sincere thanks to Miss Shirley Adelung.

Finally, I wish to thank the National Research Council of Canada and the University of Alberta for financial support throughout the course of this project.

TABLE OF CONTENTS

	Page
ABSTRACT	iv
ACKNOWLEDGEMENTS	vii
TABLE OF CONTENTS	viii
LIST OF TABLES	xiv
LIST OF FIGURES	xv

Chapter

1	A REVIEW OF ELECTRON DIFFRACTION EFFECTS AND PURPOSES OF THE PRESENT WORK	
1:1	Introduction	1
1:2	Historical Background	1
1:3	Bloch Wave Concepts in the Dynamical Theory	5
1:4	Systematic and Non-Systematic Reflections	6
1:5	Studies of the Effects of Systematic Reflections	11
1:6	Studies of the Effects of Non-Systematic Reflections	14
1:7	Purposes of the Present Investigation	18
1:7.1	To Investigate the Effects of a Non-Systematic Reflection on Extinction Distance	18
1:7.2	To Examine the Effects of a Non-Systematic Reflection on Anomalous Absorption	19
1:7.3	To Examine the Effects of Non-Systematic Reflections on Image Intensity	20

Chapter		Page
	1:7.4 To Develop a Criterion for the Inclusion of Non-Systematic Reflections in Many-Beam Calculations	21
	1:7.5 To Examine the Problem of Bloch Wave Labelling in the Presence of Non-Systematic Reflections	22
2	ASPECTS OF THE DYNAMICAL THEORY OF ELECTRON DIFFRACTION	
	2:1 Introduction	24
	2:2 Basic Outline of the Dynamical Theory	25
	2:2.1 Two-Beam Approximation	28
	2:2.2 Second Bethe Approximation	33
	2:2.3 Many-Beam Approximation	35
	2:3 Effects of Inelastic Scattering	40
	2:3.1 Inelastic Scattering Processes	40
	2:3.2 Phenomenological Treatment of Inelastic Scattering	43
	2:3.3 Anomalous Absorption Effects	45
	2:4 Additional Corrections to the Dynamical Theory	48
3	THEORETICAL CALCULATIONS	
	3:1 Introduction	50
	3:2 Setting up the <u>A</u> Matrix	50
	3:2.1 Indexing of Non-Systematic Reflections	51
	3:2.2 Non-Systematic Reflections Included in a Many-Beam Calculation	58

Chapter		Page
	3:2.3 Determination of the Diagonal Elements of \underline{A}	62
	3:2.4 Determination of the Off-Diagonal Elements of \underline{A}	67
	3:3 Calculations of the Effects of Non-Systematic Reflections	68
	3:4 Programs, Computers and Displays	69
4	EXPERIMENTAL PROCEDURES	
	4:1 Introduction	71
	4:2 Specimen Preparation	72
	4:3 Electron Microscope Examination	74
	4:4 Analysis of Observations	78
	4:5 Experimental Errors	83
	4:6 Experimental Procedures in Observing the Effects on Anomalous Absorption of the Presence of a Non-Systematic Reflection	88
5	RESULTS AND DISCUSSION	
	5:1 Introduction	90
	5:2 The Effects of a Non-Systematic Reflection on Extinction Distance	90
	5:2.1 The Variation of the (220) Extinction Distance with $\Delta\theta_{\bar{1}33}$ for $\Delta\theta_{220} = 0.0$	91
	5:2.2 Explanation of the Observed Variation of ξ/ξ_0 with $\Delta\theta_{\bar{1}33}$ for $\Delta\theta_{220} = 0.0$	95
	5:2.3 The Variation of the (220) Extinction Distance with $\Delta\theta_{\bar{1}33}$ for $\Delta\theta_{220} = 0.25$	103
	5:2.4 Explanation of the Observed Variation of ξ/ξ_0 with $\Delta\theta_{\bar{1}33}$ for $\Delta\theta_{220} = 0.25$	105

Chapter	Page
5:2.5 A Discussion of the Results Obtained at $\Delta\theta_{220} = 0.0$ and $\Delta\theta_{220} = 0.25$	110
5:2.6 Analysis of Extinction Dis- tance Behaviour in Terms of the Three-Beam Analytical Solution of the Dynamical Theory	114
5:2.7 The Variation of Extinction Distance in the Presence of Higher Order Non-Systematic Reflections	122
5:2.8 Explanation for the Observed Behaviour in the Presence of Higher Order Reflections	126
5:3 The Effects of a Non-Systematic Reflection on Anomalous Absorption	131
5:3.1 Variation of Bloch Wave Absorp- tion Coefficients in the Presence of a Non-Systematic Reflection	133
5:3.2 Effects of the Variation of the Absorption Coefficients with $\Delta\theta_{133}$ on the Contributions of the Different Bloch Waves to the Diffracted Beam Intensity	139
5:3.3 Effects of Beam Divergence on Thickness Fringe Contrast	146
5:4 Variation of Bright and Dark Field Rocking Curves in the Presence of Non-Systematic Reflections	151
5:4.1 Procedures Used in Calculating Theoretical Rocking Curves	154
5:4.2 The Variation of Bright and Dark Field Intensity at an Accelerat- ing Voltage of 150 kV	156
5:4.3 The Variation of Bright Field Intensity at an Accelerating Voltage of 1000 kV	161

Chapter		Page
5:5	The Development of a Criterion for the Inclusion of Non-Systematic Reflections in Many-Beam Calculations	163
5:5.1	Ranking at Non-Systematic Reflections in Order of Their Importance for Inclusion in a Many-Beam Calculation	165
5:5.2	Development of a Criterion for Including Non-Systematic Reflections in a Many-Beam Calculation	170
5:5.3	Additional Considerations in Using the Criterion	175
5:5.4	Application of the Criterion to Calculations Carried Out in this Thesis	179
5:6	Bloch Wave Labelling in the Presence of Non-Systematic Reflections	180
5:6.1	Bloch Wave Labelling at a Degeneracy Resulting from the Presence of a Non-Systematic Reflection	181
5:6.2	The Effect of the Presence of a Non-Systematic Reflection on Bloch Wave Labelling	187
6	SUMMARY AND SUGGESTIONS FOR FURTHER WORK	
6:1	Variation of Extinction Distance in the Presence of a Non-Systematic Reflection	189
6:1.1	Experimental Observations	189
6:1.2	Bloch Wave Analysis	191
6:1.3	Three-Beam Analytical Theory	191
6:1.4	Effects of Higher Order Non-Systematic Reflections	193

Chapter	Page
6:2 The Effect of the Presence of a Non-Systematic Reflection on Anomalous Absorption	193
6:3 Effects of the Presence of Non- Systematic Reflections on Image Intensity	194
6:4 Development of a Criterion for Inclusion of Reflections in a Many-Beam Calculation	195
6:5 The Effect of the Presence of a Non-Systematic Reflection on Bloch Wave Labelling	196
6:5 Suggestions for Further Work	196
REFERENCES	199
APPENDIX A	206
APPENDIX B	210

LIST OF TABLES

Table		Page
1	The calculated extinction distance ξ found from many-beam calculations in which the reflections included were determined by the parameter ϵ . Only systematic reflections are considered.	172
2	The calculated extinction distance ξ found from many-beam calculations in which the reflections included were determined by the parameter ϵ . The orientation is an exact $[1\bar{1}1]$.	172
3	The calculated extinction distance ξ found from many-beam calculations in which the reflections included were determined by the parameter ϵ . The orientation is such that $\Delta\theta_{220} = 0.0$ while $\Delta\theta_{\bar{1}33} = -.50$.	173
4	The calculated extinction distance ξ found from many-beam calculations in which the reflections included were determined by the parameter ϵ . At the orientation considered $\Delta\theta_{220} = 0.0$ and $\Delta\theta_{\bar{1}33} = .10$.	173

LIST OF FIGURES

Figure		Page
1	A computed diffraction pattern for an f.c.c. crystal at an exact $[\bar{1}\bar{1}2]$ orientation with respect to the incident beam.	8
2	A computed diffraction pattern for an f.c.c. crystal at an orientation obtained by tilting 10° from an exact $[\bar{1}\bar{1}2]$ orientation about an axis parallel to the $[111]$ direction.	9
3	The dispersion surface in the two-beam approximation.	30
4	Waves propagating through a thin slab of crystal.	37
5	The variation of diffracted beam intensity with depth in the presence of (a) no absorption, (b) normal absorption and (c) anomalous absorption.	47
6	A computed diffraction pattern for a $[\bar{1}11]$ orientation in Si.	53
7	Experimental electron diffraction patterns showing $\{137\}$ and $\{220\}$ type reflections simultaneously at their Bragg conditions but with different other non-systematic reflections excited.	55
8	A computed electron diffraction pattern for an orientation near the $[\bar{7}7\bar{4}]$ direction in Si.	57

Figure		Page
9	A cross section of a reciprocal lattice showing the position of the Ewald sphere for the incident beam in a direction of (a), high symmetry and (b), low symmetry in the lattice.	59
10	A diagram drawn of reciprocal lattice space showing the vectors and their relationships used for the calculation of s_g .	65
11	An experimental dark field electron micrograph of a wedge-shaped Si specimen showing thickness extinction contours.	76
12	(a) Microdensitometer system for measuring the distance between extinction contours. (b) A microdensitometer trace across an electron micrograph of a wedge-shaped crystal showing the regular periodic variation of the (220) diffracted beam intensity with depth.	80 81
13	The variation with $\Delta\theta_{220}$ of ξ/ξ_0 , the normalized extinction distance of the (220) reflection, at an accelerating voltage of 150 kV.	87
14	The experimental and theoretical variation of ξ/ξ_0 for the (220) reflection in Si as a function of $\Delta\theta_{133}$ for the case $\Delta\theta_{220} = 0.0$.	92

Figure		Page
15	A microdensitometer trace showing complex structure in the variation of the (220) intensity with depth.	94
16	The excited branches of the dispersion surface as given by a 25 beam calculation.	96
17	The variation with $\Delta\theta_{\bar{1}33}$ of the branches of the dispersion surface as given by a three-beam calculation including the (000), (220) and ($\bar{1}33$) reflections.	98
18	The variation with $\Delta\theta_{\bar{1}33}$ of the contributions, $ \phi_{220}^{(j)} $, of the different Bloch waves to the (220) amplitude as given by a three-beam calculation. $\Delta\theta_{220} = 0.0$.	99
19	The experimental and theoretical variation of the ratio ξ/ξ_0 for the (220) reflection in Si as a function of $\Delta\theta_{\bar{1}33}$ for the case $\Delta\theta_{220} = 0.25$.	104
20	The variation with $\Delta\theta_{\bar{1}33}$ of the branches of the dispersion surface as given by a three-beam calculation. $\Delta\theta_{220} = 0.25$.	107
21	The variation with $\Delta\theta_{\bar{1}33}$ of the three-beam $ \phi_{220}^{(j)} $ values. $\Delta\theta_{220} = 0.25$.	108
22	The experimental and theoretical variation of the ratio ξ/ξ_0 for the (220) reflection in Si as a function of $\Delta\theta_{\bar{1}35}$. $\Delta\theta_{220} = 0.0$.	123

Figure		Page
23	The experimental and theoretical variation of the ratio ξ/ξ_0 for the (220) reflection in Si as a function of $\Delta\theta_{\bar{1}37}$. $\Delta\theta_{220} = 0.0$.	124
24	(a) The variation with $\Delta\theta_{\bar{1}35}$ of the dispersion surface branches as given by a three-beam calculation including the (000), (220) and ($\bar{1}35$) reflections. (b) The variation with $\Delta\theta_{\bar{1}35}$ of the contributions to the (220) amplitude of the Bloch waves corresponding to the branches in (a).	127
25	(a) The variation with $\Delta\theta_{\bar{1}37}$ of the dispersion surface branches as given by a three-beam calculation including the (000), (220) and ($\bar{1}37$) reflections. (b) The variation with $\Delta\theta_{\bar{1}37}$ of the contributions to the (220) amplitude of the Bloch waves corresponding to the branches in (a).	128
26	The variation of the Bloch wave absorption coefficients, $q^{(j)}$, with $\Delta\theta_{\bar{1}33}$.	134
27	The intensity distributions of the 3 Bloch waves across a section of crystal perpendicular to the direction of current flow at values of $\Delta\theta_{\bar{1}33}$ of (a) $-.30$, (b) $.02$ and (c) $.30$.	137

Figure		Page
28	The variation of the $ \phi_g^{(j)}(z) $'s, the contributions of the different Bloch waves to the (220) diffracted beam amplitude, with $\Delta\theta_{\bar{1}33}$ at (a), the top surface of the crystal and (b), a depth of 10000Å.	142
29	A computed, (a), and experimental, (b), (220) dark field image of a bent wedge-shaped silicon crystal.	145
30	The computed variation of the (220) intensity with depth, z , for $\Delta\theta_{\bar{1}33} = .09$ for the cases of (a) a parallel incident electron beam and (b) an incident electron beam with an angular divergence of $.015^\circ$.	149
31	The computed variation of the (220) intensity with depth, z , taking into account a beam divergence of $.015^\circ$ for (a) $\Delta\theta_{\bar{1}33} = -.09$ and (b) $\Delta\theta_{\bar{1}33} = .70$.	150
32	Bright and dark field rocking curves for molybdenum at an accelerating voltage of 150 kV and a crystal thickness of 5000 Å.	157
33	Bright field rocking curves for molybdenum at an accelerating voltage of 1000 kV and for crystal thicknesses of 2 and 4 μ .	162
34	The three branches of the dispersion surface as a function of $\Delta\theta_{\bar{1}33}$ for a three-beam situation. $\Delta\theta_{220} = 0.0$.	183

- 35 The variation with $\Delta\theta_{\bar{1}33}$ of the contributions, $|\phi_{220}^{(j)}|$, of the different Bloch waves to the (220) amplitude assuming that branches 2 and 3 of the dispersion surface cross over at the degeneracy point. 184
- A1 A diagram in reciprocal space showing the allowed orientations $\overrightarrow{OR1}$ and $\overrightarrow{OR2}$ of the crystal when the reflections corresponding to \vec{g} and \vec{h} are in their exact Bragg conditions. 207

CHAPTER 1

A REVIEW OF ELECTRON DIFFRACTION EFFECTS AND PURPOSES OF THE PRESENT WORK

1:1 Introduction

Electron diffraction is an important tool in the study of the structure of materials. Both the surface characteristics and internal features of a crystalline specimen can be examined by using this phenomenon. In the case of internal structure, such examination is most often carried out in an electron microscope. The interpretation of contrast effects in electron microscope images of crystals in terms of electron diffraction interactions has played an important role in the development of electron microscopy as applied to problems in material science. It was with a view to examining one particular aspect of these interactions, namely, electron diffraction effects in the presence of strongly excited non-systematic reflections, that the work described in this thesis was undertaken.

1:2 Historical Background

Electron diffraction was first observed experimentally in 1927 by Davisson and Germer (1927) and almost simultaneously by Thomson and Reid (1927). Their work

confirmed the de Broglie postulate for electrons (de Broglie, 1924) and provided the basis for the development of the electron microscope. In the year following the first experimental observation of electron diffraction, Bethe (1928) published a quantum mechanical theory for the motion of a high energy electron in a crystal potential. This theory, known as the dynamical theory of electron diffraction, has come to play a very important role in the analysis of electron diffraction effects.

Initially, however, after the development of the electron microscope by Knoll and Ruska (1932), interpretation of the image contrast observed in these instruments was carried out in terms of the simpler kinematical theory of electron diffraction. This theory was developed from the corresponding kinematical theory of X-ray diffraction, which had been found adequate in explaining most effects observed when using X-radiation. However, in the case of electrons, the assumptions of the kinematical theory of single scattering and of negligible diffracted beam intensity in comparison to that of the directly transmitted beam, are not usually fulfilled. Thus, when a number of authors (von Borries and Ruska, 1940; Hillier and Baker, 1942; Heidenreich, 1942; Boersch, 1943; Kinder, 1943; Heidenreich and Sturkey, 1945) reported experimental results which could be only partially explained in terms of the kinematical theory, interest

returned to the dynamical theory.

In Bethe's theory neither of the assumptions of the kinematical approach were required. Both multiple scattering of the electrons and comparable diffracted and directly transmitted beam intensities were allowed. Also, any number of strong diffracted beams could, in principle, be taken into consideration. It was found in practice, however, that analytical solutions for the intensities of the different beams could be easily obtained only for the case where two reflections, the directly transmitted and one diffracted beam, were considered. These analytical solutions gave good agreement with experiment in the usual strong beam imaging situations where only one low-order reflection was close to its Bragg condition. As a result the use of this two-beam approximation of the dynamical theory became widespread.

In order to take the effects of additional weak diffracted beams into account and yet retain the simplicity of the two-beam analytical solutions, it is possible to use Bethe's Second Approximation. In this, the effects of the additional reflections are included by adding correction terms to the lattice potentials corresponding to the directly transmitted and strongly diffracted beams. However, these corrections result in lattice potentials which are functions of crystal

orientation. Moreover, Bethe's Second Approximation is found to break down whenever any of the additional reflections are close to their Bragg conditions. For these reasons this Approximation was not widely used to study situations where a number of strong beams were present. Instead, interest turned to the numerical solution of the dynamical equations when it was desired to take into account more than two reflections.

In this regard, a number of theoretical formulations were put forward during the late 1950's for calculating intensities in a many-beam situation. Cowley and Moodie (1957) developed such a theory using scattering principles carried over from light optics. In the same year Sturkey (1957) reported results of many-beam calculations employing an exponential expansion of the scattering matrix in the dynamical theory. Additional matrix approaches were also reported by Niehrs (1959) and Fujimoto (1959) in which they formulated the dynamical theory in terms of an eigenvalue equation. Howie and Whelan (1960) were the first to carry out many-beam calculations using this formulation. Their method has gradually gained wide acceptance for calculating many-beam effects. It is their approach that has been used in the work presented in this thesis.

1:3 Bloch Wave Concepts in the Dynamical Theory

Although the dynamical theory of electron diffraction will be treated in detail in Chap. 2, it is useful to introduce some of its concepts at this point. In the formulation of this theory in terms of an eigenvalue equation, as given by Howie and Whelan (1960), the motion of the high energy electrons in a crystal are described in terms of a set of Bloch waves. The wave vector corresponding to each of these Bloch waves is associated with an eigenvalue of the initial equation and, in fact, these eigenvalues give the differences between the wave vectors of the different waves. The eigenvector associated with each of these eigenvalues gives the components of the corresponding Bloch wave in the directions of the directly transmitted and diffracted beams considered. The effects of inelastic scattering of the incident electrons, referred to as absorption in the dynamical theory, is taken into account by allowing the Bloch waves to attenuate as they propagate through the crystal.

Contrast observed in electron microscope images of perfect crystals can be explained quite easily in terms of Bloch waves. Thickness extinction contours, which arise from a periodic variation of transmitted or diffracted beam intensity with depth in a crystal, can be interpreted in terms of beating between Bloch waves due to differences

in their wave vectors. The period of this beating, known as the extinction distance, is then directly related to the eigenvalues of the Bloch waves involved. The contribution of a Bloch wave to a particular diffracted beam is determined by both the extent to which it is excited and the magnitude of its component in the direction of the beam as given by the eigenvector. Usually, only a few waves make a significant contribution to the intensity of a given reflection. Differences in the absorption of these waves can, however, give rise to anomalous absorption effects such as the disappearance of extinction contours in thick crystals although appreciable intensity is still transmitted.

It was partly with a view of investigating the changes in the Bloch wave eigenvalues, eigenvectors and absorption coefficients in the presence of two strongly diffracted beams that the work reported here was undertaken.

1:4 Systematic and Non-Systematic Reflections

When a high energy electron beam is incident on a crystal it is generally found that a number of different sets of planes are close to satisfying their Bragg conditions. In forming conventional strong beam images the crystal is usually oriented so that only one low-order diffracted beam is strongly excited. If this reflection

has a reciprocal lattice vector, \vec{g} , then all reflections corresponding to the vectors $n\vec{g}$ where n is an integer are called systematic reflections (Hoerni, 1956). Similarly, those reflections which have a reciprocal lattice vector, \vec{h} , not collinear with \vec{g} are called accidental or non-systematic reflections. Whether a particular reflection is termed systematic or non-systematic depends entirely upon the low-order diffracted beam being used for imaging purposes. Thus, a reflection which is termed systematic in one situation may, upon choosing a different low-order reflection for study, be termed non-systematic. This is illustrated in Fig. 1, which shows a computed electron diffraction pattern for a $[\bar{1}\bar{1}2]$ orientation in a crystal with f.c.c. structure. If the (111) reflection is the primary reflection being used in image formation, then the reflections (222), (333), ($\bar{1}\bar{1}\bar{1}$), ($\bar{2}\bar{2}\bar{2}$) and ($\bar{3}\bar{3}\bar{3}$) are designated as systematic and all other reflections such as ($2\bar{2}0$), ($5\bar{3}1$) etc. as non-systematic. Similarly, if the ($2\bar{2}0$) reflection is the primary diffracted beam, ($4\bar{4}0$), ($\bar{2}20$) and ($\bar{4}40$) are termed systematic and all other reflections such as (111), (222) etc. are then called non-systematic.

The importance of this differentiation between systematic and non-systematic reflections can be seen by examining Fig. 2. This Figure shows the calculated diffraction pattern for the above crystal after it has

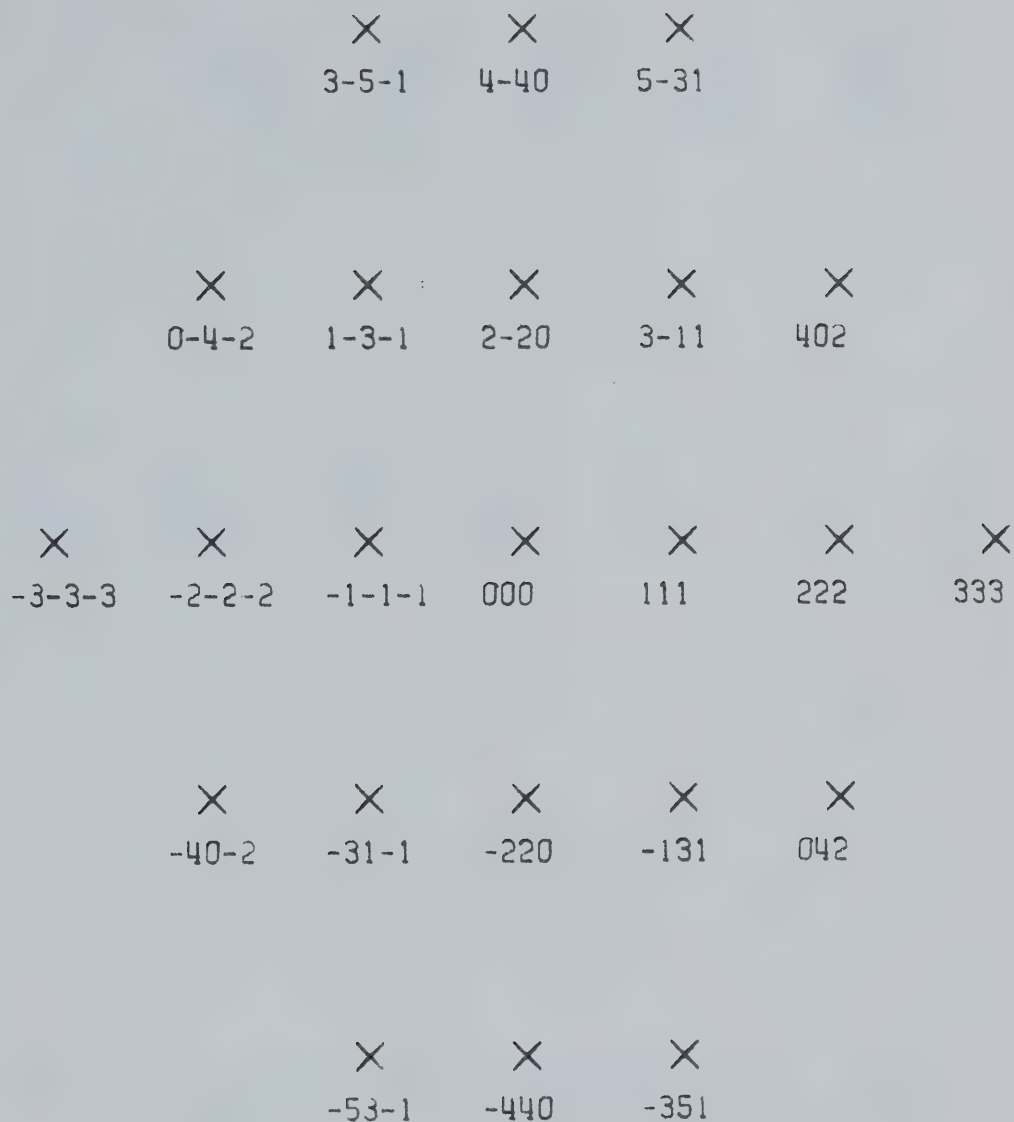


Fig. 1. A computed diffraction pattern for an f.c.c. crystal at an exact $[\bar{1}\bar{1}2]$ orientation with respect to the incident beam.

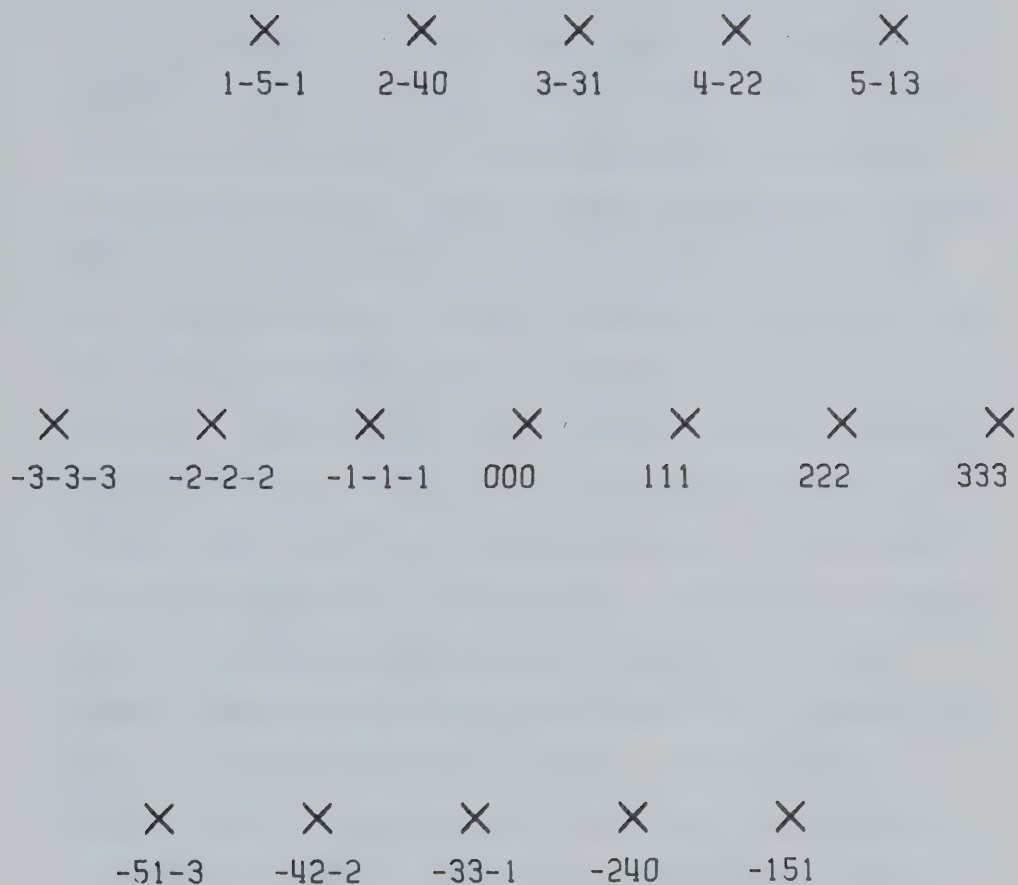


Fig. 2. A computed diffraction pattern for an f.c.c. crystal at an orientation obtained by tilting 10° from an exact $[\bar{1}\bar{1}2]$ orientation about an axis parallel to the $[111]$ direction.

been rotated 10 degrees about an axis parallel to the $[111]$ direction. As can be seen, the (111) row of systematic reflections are still present after carrying out the 10° tilt but the corresponding non-systematic reflections visible in Fig. 1 have disappeared. Instead other non-systematic reflections such as $(3\bar{3}1)$, $(\bar{2}40)$ etc. are now excited. These two Figures illustrate the importance of differentiating between systematic and non-systematic reflections. For example, if it is desired to use the (111) reflection in forming a conventional strong beam image, this reflection must be set close to its Bragg condition. The effects of systematic reflections are thereby determined and cannot be changed without changing the deviation of the (111) reflection from its Bragg condition. However, by rotating the crystal about an axis parallel to $[111]$ direction, the excitations of the non-systematic reflections can be drastically altered without affecting the deviation from the Bragg condition of the (111) reflection. This fact is commonly used by electron microscopists in order to orient their specimens so that the only low-order reflections strongly excited lie along the systematic row. In doing this they hope to minimize the effects of non-systematic reflections on their images.

In the next section a brief review of the effects of systematic reflections will be given for purposes of comparison with the effects of non-systematic reflections to be discussed later.

1:5 Studies of the Effects of Systematic Reflections

It was shown in the previous section that systematic reflections must always be present whenever a low-order reflection is excited. Because of this, most of the many-beam calculations which have been carried out in the past have been to investigate the effects of these reflections.

In their original paper on the numerical solution of the dynamical equations of electron diffraction, Howie and Whelan (1960) carried out seven-beam calculations to take into account the lower order systematic reflections associated with the (111) reflection in Al. They found that the presence of these additional reflections can result in significant effects. In the case of the (111) extinction distance, marked changes in its magnitude from the two-beam value were predicted to occur both at the exact (111) Bragg condition and at deviations from this condition. In addition, they found that the rate of absorption of the different Bloch waves was also sensitive to the presence of the systematic

reflections. The first experimental measurements showing the effect of systematic reflections were those of Dupouy, Perrier, Uyeda, Ayroles, and Mazel (1965) who reported measurements of extinction distance in MgO as a function of accelerating voltage for a range of voltages from 100 to 1200 kV. At the higher voltages the results obtained were found to deviate from those predicted by the two-beam theory. Goringe, Howie and Whelan (1966) showed that these results were in good accord with many-beam calculations in which systematic reflections were included.

Sheinin (1967) reported measurements of the variation of extinction distance with deviation from the exact Bragg condition of the (110) reflection in Mo. He found that the effects of systematic reflections became important at deviations of approximately 1.5 Bragg angles. Here the extinction contours became quite complex in nature. When, for larger deviations, they again became sinusoidal in form the extinction distance was found to have increased markedly in magnitude. Cann and Sheinin (1968) reported similar measurements for the (111) reflection in Si in which they found systematic reflections to have a strong effect, even quite close to the exact Bragg condition. The greater effect of the systematic reflections in this case was primarily

attributed to the presence of the (222) reflection which is kinematically forbidden in the diamond cubic structure. Similar measurements for the (220) reflection in Si (Cann, 1967; Sheinin, 1970A) showed that the effects of systematic reflections were negligible for deviations within one Bragg angle of the (220) reflection from its Bragg condition. Mazel (1971) also carried out similar measurements in MgO but for a range of accelerating voltages. She found good agreement between her experimental results and many-beam calculations taking 10 systematic reflections into account. Finally, Spring and Steeds (1970) and Steeds (1970), using a different approach, examined images of extinction contours in bent wedge-shaped crystals for the primary purpose of obtaining absorption coefficients. They found that many-beam calculations taking into account systematic reflections were necessary in order to obtain good agreement between theory and experiment.

The effects of systematic reflections have also been studied in the case of images obtained from defect containing crystals. Humphreys, Howie and Booker (1967) considered the effect of these reflections on stacking fault intensity profiles in Si and Au. For the (220) reflection in Si they found the effects to be quite weak. However, for the (111) reflection in Au the many-beam

intensity profiles were markedly different from the computed two-beam profiles. Sheinin and Botros (1970) examined stacking fault contrast in Co as a function of the deviation of the ($\bar{1}11$) reflection from its Bragg condition for the case of both bright and dark field images. They found that the good contrast obtained in dark field images at large deviations could be explained by the presence of the additional Bloch waves excited when systematic reflections were considered. In the case of dislocations, Cann, Foxon and Sheinin (1968) reported calculations of many-beam dislocation profiles that showed marked effects due to the presence of systematic reflections. Finally, Cockayne (1972) stated that, in general, his weak-beam technique for obtaining high resolution images of defects should not be applied when a systematic reflection is close to its Bragg condition. This is because the intensity profiles may be perturbed in such a situation, thus leading to possible errors in measurements of features such as the splitting of partial dislocations.

1:6 Studies of the Effects of Non-Systematic Reflections

In comparison with the extensive research done in the case of systematic reflections only recently has attention turned to the problem of interpretation of

electron images in the presence of non-systematic reflections. A number of authors (Hibi, Kambe and Honjo, 1955; Uyeda and Nonoyama, 1965; Uyeda, 1968; Takahashi, 1969) have observed complex periodicity in thickness extinction contours when the non-systematic reflections present were close to their Bragg conditions. Lehmpfuhl (1970) showed that the presence of three strongly excited Bloch waves at the crystal orientations involved could result in the complexities observed. Uyeda and Nonoyama (1965) also observed that outside the region of complex periodicity the extinction distance varied with the deviation of the non-systematic reflection from its Bragg condition. For positive deviations the extinction distance was larger than that measured when the non-systematic reflection was absent while for negative deviations it was smaller. They showed that this was in qualitative agreement with the predictions of Bethe's Second Approximation.

Although the dynamical theory in the formulation presented by Howie and Whelan (1960) handles the case of non-systematic reflections quite readily, a number of analytical approximations of the theory have also been developed. Kambe (1967) derived approximate analytical expressions for the beam intensities of three non-collinear reflections which could be used to deter-

mine the differences between the phase angles of the structure amplitudes for the reflections involved. Fukuhara (1966) developed analytical expressions for the Bloch wave vectors and amplitudes for a number of configurations involving both systematic and non-systematic reflections. The arrangement of the reflections in these configurations were, however, required to obey certain symmetry conditions. Hirsch, Howie, Nicholson, Pashley and Whelan (1965) and Reynaud (1971) have examined orientations of high symmetry in order to determine the channelling characteristics of the Bloch waves present. Using a different approach, Gjønnes (1966) and Gjønnes and Høier (1969, 1971) investigated the essentially strong non-systematic situations arising at Kikuchi line intersections. They interpreted their results in terms of three and four-beam analytical solutions of the dynamical theory. From these solutions they derived rules, depending upon the Fourier coefficients of the lattice potential involved, for the behaviour of the Kikuchi lines at the intersections.

Recently, since the commencement of the work reported in this thesis, a number of papers have been published in which aspects of the effects of non-systematic reflections have been interpreted in terms of the dynamical theory by using many-beam calculations.

Lehmpfuhl and Reissland (1968) and Lehmpfuhl (1970, 1972) have examined the intensities of the Bloch waves excited in the presence of non-systematic reflections. These intensities were studied experimentally by observing the fine structure of diffraction spots obtained from wedge-shaped crystals. The results were compared with many-beam calculations including up to 108 reflections and good agreement obtained when absorption was taken into account. Fisher (1968) also carried out many-beam calculations including a large number of reflections. He found that, at an accelerating voltage of 100 kV, it was necessary to include approximately 50 systematic and non-systematic reflections in order to obtain convergence for the extinction distance obtained at a [100] orientation in CuAu_3 .

In the case of electron microscope images, Ayroles and Mazel (1970) reported measurements in MgO of the (200) extinction distance with deviation of the (024) and (224) reflections from their Bragg conditions. They obtained good agreement between their observed results and many-beam calculations. Ayroles (1971) went on to show that the changes in extinction distance and the appearance of complex periodicity, reported by him and Mazel, could be explained by the dynamical theory in terms of variations in the Bloch wave vectors and

the contributions of the different Bloch waves to the (200) diffracted beam intensity. Finally, Lynch (1971) investigated fine-focus convergent-beam images in Au [111] oriented foils. He found it necessary to take into account 139 reflections in his calculations including second zone spots in order to obtain agreement with experiment.

1:7 Purposes of the Present Investigation

In carrying out the work presented in this thesis the effects of non-systematic reflections in five general areas have been considered. The first three of these involved electron microscope imaging and were concerned with the effect of non-systematic reflections on extinction distance, anomalous absorption and image intensity. The fourth area considered was the question of the number of non-systematic reflections which should be included in a many-beam calculation. The fifth study was concerned with an investigation of Bloch wave labeling in the presence of a non-systematic reflection. The purposes of these studies are discussed in detail below.

1:7.1 To Investigate the Effects of a Non-Systematic Reflection on Extinction Distance

A detailed examination was undertaken of the

variation of the (220) extinction distance in Si as a function of the deviation of the ($\bar{1}33$) reflection from its Bragg condition. This study was carried out for the (220) reflection both in its Bragg condition and at a deviation from this condition of a quarter of a Bragg angle. The first aim of this study was to examine the behaviour of the Bloch waves in a situation where only one non-systematic reflection was close to its Bragg condition in hope that the interpretation would be simpler than in the case considered by Ayroles (1971). In his study two strong non-systematic reflections were present resulting in the simultaneous excitation of up to four strong Bloch waves in the crystal. With a single non-systematic reflection three Bloch waves, at most, should be important.

The second aim was to compare the results obtained for the (220) reflection in its Bragg condition with those found at a deviation from this condition of a quarter of a Bragg angle. This was done to determine whether or not there were any significant differences in the effects of the non-systematic reflection in these two cases.

1:7.2 To Examine the Effects of a Non-systematic Reflection on Anomalous Absorption

Anomalous absorption effects in electron microscope

images, as stated in Section 1:3, arise from differences in the absorption coefficients of the Bloch waves. The variation of the absorption coefficients corresponding to the important Bloch waves in the case of the (220) reflection in Si have been studied as a function of the deviation of the ($\bar{1}33$) reflection from its Bragg condition. This was done to determine the changes in anomalous absorption effects which might result from the presence of a non-systematic reflection.

1:7.3 To Examine the Effect of Non-Systematic Reflections on Image Intensity

In electron microscopy, especially of thick materials, it is usually desirable to use a crystal orientation for which the imaging beam has a maximum intensity. The orientation at which this maximum occurs is usually found theoretically by calculating the variation of the beam intensity as a function of orientation. The resulting plots are referred to as rocking curves. In the case where only systematic reflections are considered and for an accelerating voltage of the order of 100 kV these rocking curves predict maximum image intensity in the dark field to occur at the exact Bragg condition of the diffracted beam. For the bright field image, however, the maximum intensity occurs at a small positive deviation of the diffracted beam from its Bragg condition.

In order to test whether the presence of non-systematic reflections would significantly alter these effects, many-beam calculations of rocking curves were carried out in the presence of different non-systematic reflections. The orientations at which the average intensity was a maximum, as obtained from these curves, were then compared with the predictions in the systematic case.

1:7.4 To Develop a Criterion for the Inclusion of Non-Systematic Reflections in Many-Beam Calculations

In Bethe's original dynamical theory an infinite number of reflections are considered. However, in a many-beam calculation only a finite number can be included. Moreover, in order to minimize computing time it is desirable that this number should be no larger than necessary. In the case where only systematic reflections are considered, the number of reflections to be included is usually found by a convergence criterion. This consists of including higher and higher order reflections until there is no significant change in the results obtained. A similar convergence technique can also be used when a crystal is near a low-order orientation such that all the systematic and non-systematic reflections excited lie in the same plane or zone. The justification for this method of determining the reflections to be

included in a calculation lies in the fact that the effect of a reflection decreases with both increasing order and increasing deviation from its Bragg condition.

When spots from different zones are present, however, the problem of deciding which reflections to include is more difficult. This is because, in this case, the question arises as to the relative importance of a low-order reflection far from its Bragg condition as compared to a higher order reflection close to its Bragg condition. It was for this latter situation, in particular, that a criterion for the inclusion of reflections in a many-beam calculation was developed.

1:7.5 To Examine the Problem of Bloch Wave Labelling in the Presence of Non-Systematic Reflections

It has been stated in Section 1:3 that the motion of the high energy electrons in a crystal can be described in terms of a set of Bloch waves. In the case where only systematic reflections are considered it is found that the properties associated with each of these Bloch waves depend upon the relative magnitudes of their wave vectors. On the basis of this dependence of the Bloch wave characteristics on the wave vector,

Humphreys and Fisher (1971) proposed a Bloch wave numbering system which consisted of numbering the Bloch waves in increasing order with decreasing magnitude of the corresponding Bloch wave vector. In this numbering system Bloch wave 1 is always found to be symmetric and to have a high absorption coefficient. Bloch wave 2, on the other hand, is found to be anti-symmetric below the critical voltage and to have a low absorption coefficient.

It was desired in the work undertaken here to examine the effects of a non-systematic reflection on Bloch wave characteristics. This was done with a view to finding the significance of these effects in relation to the characteristics usually associated with the different Bloch wave numbers in the systematic case.

CHAPTER 2

ASPECTS OF THE DYNAMICAL THEORY OF ELECTRON DIFFRACTION

2:1 Introduction

The dynamical theory of diffraction of high energy electrons in a crystal can be developed in a number of ways. One approach is based on a formulation of the dynamical theory of X-ray diffraction due to Darwin (1914). In this treatment the behaviour of the electrons is determined by considering single Bragg reflection events in successive slices of a crystal. A second formulation of the theory was developed from a physical optics basis by Cowley and Moodie (1957). Here, Huygens' Principle was applied to electron waves in a three-dimensional periodic system in order to determine electron beam intensities. In this thesis, however, the effects of non-systematic reflections in electron diffraction have been studied by employing the Bloch wave formulation of the dynamical theory as developed by Bethe (1928). The basic reason for doing so is the insight into the physical mechanisms responsible for electron diffraction effects which can be obtained from a study of Bloch wave interactions. A second reason is that the scattering matrix representation of this formulation is amenable to standard computing techniques (Howie and Whelan, 1960).

2:2 Basic Outline of the Dynamical Theory

The dynamical theory of electron diffraction, as first proposed by Bethe (1928), starts with the Schrödinger equation for an electron in a crystal potential $V(\vec{r})$. This equation can be written as

$$\nabla^2 \psi(\vec{r}) + \left(\frac{8\pi^2 m e}{h^2} \right) (E + V(\vec{r})) \psi(\vec{r}) = 0, \quad (2.1)$$

where $\psi(\vec{r})$ is the wave function of the electron, and E is the potential through which the electron was accelerated before entering the crystal. Also, m and e are the rest mass and charge of the electron respectively, and h is Planck's constant. Due to the periodic nature of the crystal potential, $V(\vec{r})$ can be expressed by a Fourier series of the form

$$V(\vec{r}) = \sum_{\vec{g}} V_{\vec{g}} \exp(2\pi i \vec{g} \cdot \vec{r}) \quad (2.2)$$

where the summation is over all reflections, \vec{g} , and $V_{\vec{g}}$ is the Fourier coefficient of the potential corresponding to the reflection \vec{g} . In the notation to be used here \vec{g} denotes the reciprocal lattice vector associated with the reflection \vec{g} . It is useful, when considering the Schrödinger equation, to rewrite equation (2.2) in the form

$$V(\vec{r}) = \frac{h^2}{2me} \sum_{\vec{g}} U_{\vec{g}} \exp(2\pi i \vec{g} \cdot \vec{r}) \quad (2.3)$$

where $U_g = \frac{2me}{h^2} V_g$. Since the potential energy of the crystal must be real, $V(\vec{r}) = V^*(\vec{r})$ and, therefore,

$$U_g = U_{-g}^* \quad (2.4)$$

Also, if the crystal is centro-symmetric as they are in the cases to be considered in this thesis, an origin can be chosen such that $V(\vec{r}) = V(-\vec{r})$. Then

$$U_g = U_{-g} = U_g^* \quad (2.5)$$

and the U_g 's are all real.

In the case of electrons with energies of the order of those found in the electron microscope, (10-3000 keV), E is much greater than $V(\vec{r})$ and the Schrödinger equation can be solved using a nearly-free electron approximation. Outside the crystal where $V(\vec{r}) = 0$ the solutions of the equation are plane waves of the form

$$\psi(\vec{r}) = \exp(2\pi i \vec{\chi} \cdot \vec{r}) \quad , \quad (2.6)$$

where the wave vector $\vec{\chi}$ has magnitude

$$\chi = \left(\frac{2mE}{h^2} \right)^{\frac{1}{2}} \quad (2.7)$$

In the crystal, the effect of the lattice potential $V(\vec{r})$ would be expected to result in solutions to the Schrödinger equation which are Bloch waves, i.e. plane

waves modulated by a function with the period of the lattice. Thus, solutions to equation 2.1 are looked for in the form

$$\psi(\vec{r}) = \sum_{\vec{g}} C_{\vec{g}}(\vec{k}) \exp\{2\pi i (\vec{k} + \vec{g}) \cdot \vec{r}\} \quad . \quad (2.8)$$

Here, \vec{k} is a wave vector and $C_{\vec{g}}(\vec{k})$ is the amplitude of the Bloch wave, corresponding to \vec{k} , in the direction $\vec{k} + \vec{g}$. If equations 2.3 and 2.8 are substituted back into equation 2.1 the following expression is obtained

$$\sum_{\vec{g}} [\{ -(\vec{k} + \vec{g})^2 + \chi^2 + U_0 \} C_{\vec{g}}(\vec{k}) + \sum_{\vec{h}}' C_{\vec{g}-\vec{h}}(\vec{k}) U_{\vec{h}}] \exp\{2\pi i (\vec{k} + \vec{g}) \cdot \vec{r}\} = 0 \quad , \quad (2.9)$$

where the prime on the second summation means that the term $\vec{h} = 0$ is omitted. Since the terms $\exp\{2\pi i (\vec{k} + \vec{g}) \cdot \vec{r}\}$ are linearly independent, the coefficients of these exponentials must all equal zero. This condition results in a set of equations of the form

$$(K^2 - k_{\vec{g}}^2) C_{\vec{g}}(\vec{k}) + \sum_{\vec{h}}' U_{\vec{h}} C_{\vec{g}-\vec{h}}(\vec{k}) = 0 \quad , \quad (2.10)$$

where $K^2 = \chi^2 + U_0$ and $\vec{k}_{\vec{g}} = \vec{k} + \vec{g}$.

This set of equations, called the "dispersion equation" by Bethe, gives the general relations among the amplitudes, $C_{\vec{g}}(\vec{k})$, the Fourier coefficients, $U_{\vec{g}}$, and the Bloch wave vectors, \vec{k} . It is from these relations that the two and many-beam approximations of the dynamical theory have been derived.

2:2.1 Two-Beam Approximation

Although it is not used directly in the work described in this thesis, it is useful to develop the two-beam approximation in order to illustrate the origin of some of the basic concepts in the dynamical theory. In this approximation only the directly transmitted and one diffracted beam, g , are considered. In this case the set of equations 2.10 reduces to two equations of the form

$$(K^2 - k^2)C_o(\vec{k}) + U_{-g}C_g(\vec{k}) = 0$$

and

(2.11)

$$U_gC_o(\vec{k}) + (K^2 - k_g^2)C_g(\vec{k}) = 0 \quad .$$

Non-zero solutions exist for $C_o(\vec{k})$ and $C_g(\vec{k})$ in equations 2.11 only if the determinant formed by their coefficients vanishes. Therefore, using equation 2.11 and the fact that $U_g = U_{-g}$

$$(K^2 - k^2)(K^2 - k_g^2) - U_g^2 = 0 \quad . \quad (2.12)$$

Since K is much larger than U_g or $|\vec{g}|$, K and k must be nearly equal and, to a good approximation, equation 2.12 can be rewritten

$$(k - K)(k_g - K) = \frac{U_g^2}{4K^2} \quad . \quad (2.13)$$

This is a quadratic equation in k and the values $k^{(1)}$ and $k^{(2)}$ satisfying it lie on a surface in k -space called the dispersion surface (see Fig. 3). Note, for conduction electrons, dispersion surfaces are more commonly known as Fermi surfaces. The particular points on the dispersion surface satisfying the quadratic equation are determined by the direction of the incident electron beam in the crystal as given by \vec{k} . In Fig. 3, for the situation shown, \vec{k} is a vector from the point E to the point O. As the point E moves along the sphere centred at O different points F and H on the two branches $D^{(1)}$ and $D^{(2)}$ of the dispersion surface will satisfy the quadratic equation.

Physically, the two-beam approximation predicts that the motion of a high energy electron in a crystal can be described in terms of two Bloch waves. These waves have the same total energy as that of the incident electron, $\hbar^2 \chi^2 / 2m$, but different kinetic energies as determined by the vectors $\vec{k}^{(1)}$ and $\vec{k}^{(2)}$.

In order to determine the relative magnitudes of these Bloch waves the boundary conditions at the top surface of the crystal must be considered. The condition that electron density is conserved requires that the wave function at the surface be continuous. The fact that this condition must hold at any point on the boundary surface also requires that the wave vectors

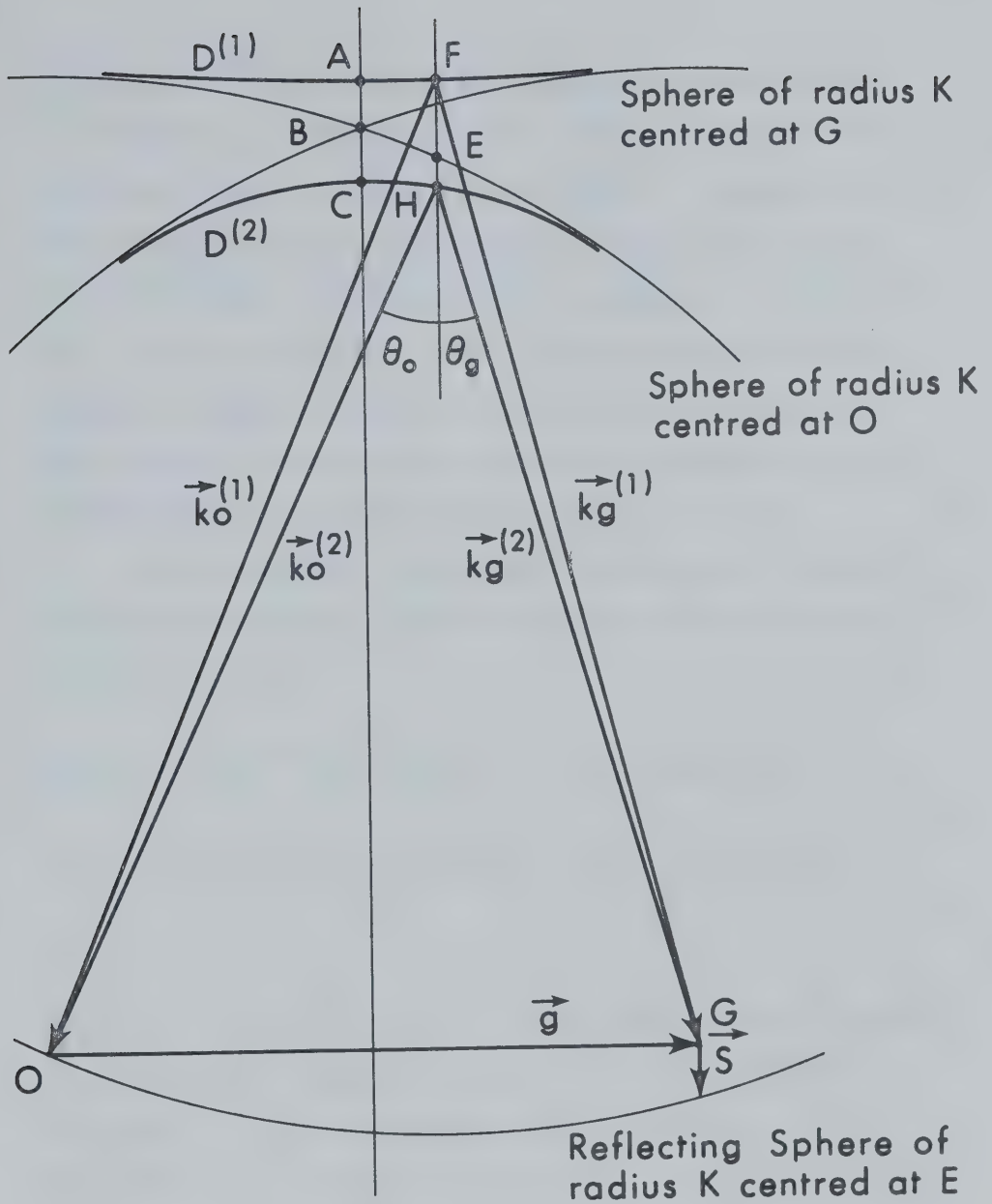


Fig. 3. The dispersion surface in the two-beam approximation. $D^{(1)}$ and $D^{(2)}$ are the upper and lower branches of the surface respectively. In this drawing $\gamma^{(1)} = EF$, the distance from the tie point E to branch 1 and $\gamma^{(2)} = EH$, the distance from the tie point E to branch 2.

$\vec{k}^{(1)}$ and $\vec{k}^{(2)}$ have the same tangential components as $\vec{\lambda}$. Generally, reflected waves from the surface can be ignored up to angles of incidence of greater than 80° (Hirsch et al; 1965) because of the large difference between the energy of the incident electron and the lattice potentials. The boundary conditions then reduce to simple continuity of the incident wave at the top surface and continuity of the transmitted and diffracted waves at the bottom or exit surface.

In the crystal the total electron wave function can be written as a linear combination of the Bloch waves of the form

$$\begin{aligned} \psi(\vec{r}) = & \psi^{(1)} \{ C_O^{(1)} \exp(2\pi i \vec{k}^{(1)} \cdot \vec{r}) + C_g^{(1)} \exp(2\pi i \vec{k}_g^{(1)} \cdot \vec{r}) \} + \\ & \psi^{(2)} \{ C_O^{(2)} \exp(2\pi i \vec{k}^{(2)} \cdot \vec{r}) + C_g^{(2)} \exp(2\pi i \vec{k}_g^{(2)} \cdot \vec{r}) \} \end{aligned} \quad (2.14)$$

where $\psi^{(1)}$ and $\psi^{(2)}$ are the excitations of Bloch waves 1 and 2 respectively as determined by the boundary conditions at the top surface of the crystal. Also, for brevity in the notation $C_O(k^{(i)})$ and $C_g(k^{(i)})$ have been replaced by $C_O^{(i)}$ and $C_g^{(i)}$ respectively. The amplitude, $u_g(z)$, of the diffracted beam g at a depth z in the crystal is equal to the sum of the Bloch wave components in the direction $\vec{k} + \vec{g}$. Using equation 2.14 and the

requirement that the tangential components of the wave vectors are equal, $u_g(z)$ is then given by the expression

$$u_g(z) = \psi^{(1)} C_g^{(1)} \exp(2\pi i \gamma^{(1)} z) + \psi^{(2)} C_g^{(2)} \exp(2\pi i \gamma^{(2)} z) \quad (2.15)$$

where $\gamma^{(1)}$ and $\gamma^{(2)}$ are defined as shown in Fig. 3.

The intensity of the diffracted beam g at a depth z , $u_g^*(z)u_g(z)$, is then given by the expression

$$u_g^*(z)u_g(z) = \phi_g^{(1)2} + \phi_g^{(2)2} + 2\phi_g^{(1)}\phi_g^{(2)} \cos\{2\pi(\gamma^{(1)} - \gamma^{(2)})z\} \quad (2.16)$$

where $\phi_g^{(1)} = \psi^{(1)} C_g^{(1)}$ and $\phi_g^{(2)} = \psi^{(2)} C_g^{(2)}$.

By examining equation 2.16 it can be seen that the diffracted beam intensity will vary sinusoidally with depth with a period equal to $1/(\gamma^{(1)} - \gamma^{(2)})$. This distance is called the extinction distance. By examining Fig. 3 it can be seen that $\gamma^{(1)} - \gamma^{(2)}$ and, therefore, the extinction distance varies with s_g , the deviation of the g 'th reflection from its Bragg condition. For $s_g = 0$, $\gamma^{(1)} - \gamma^{(2)}$ is equal to the distance AC which is less than the distance FH, the value of $\gamma^{(1)} - \gamma^{(2)}$ at the deviation shown. This is due to the hyperbolic curvature of the dispersion surfaces.

The situation, as shown here, is very similar to the many-beam situation to be discussed in Section 2:2.3 when only two Bloch waves are important. It was shown by Howie and Whelan (1960), however, that the actual curvature of the dispersion surfaces is somewhat altered from the two-beam case.

2:2.2 Second Bethe Approximation

Bethe, in his original paper, proposed a method for taking into account the effects of additional weak reflections in the two-beam approximation. This is done by introducing "dynamic" potentials. When an attempt is made to solve the "dispersion equation" 2.10 by progressively eliminating all terms in C_h , where h is one of the weak reflections, it is found that equation 2.10 reduces to two equations of the form

$$(K_{oo}^2 - k_o^2)C_o + U_{og}C_g = 0$$

and

(2.17)

$$U_{o-g}C_o + (K_{gg}^2 - k_g^2)C_g = 0$$

where

$$K_{oo}^2 = K^2 - \sum_h \frac{U_h U_{-h}}{K^2 - k_h^2}$$

$$K_{gg}^2 = K^2 - \sum_h \frac{U_{h-g} U_{g-h}}{K^2 - k_h^2}$$

and the dynamic potential U_{og} has the form

$$U_{og} = U_g - \sum_h \frac{U_{g-h} U_{-h}}{K^2 - k_h^2} .$$

By comparing equations 2.17 to equation 2.11 it is seen that they are of the same form as the equations in the two-beam approximation. However, the actual values of the coefficients of the C_o 's and C_g 's are different due to the presence of the additional summation terms.

Herzberg (1971) has carried out a thorough investigation of the accuracy of the Second Bethe Approximation. He found that, as long as no terms whose denominators were close to zero occurred in the sums, the results of the approximation were in very good agreement with experiment and many-beam calculations using the eigenvalue approach. Also, Watanabe, Uyeda and Fukuhara (1968) used the Second Bethe Approximation to explain the disappearance of the second order Kikuchi line at a particular accelerating voltage or, as it is now known, the critical voltage effect. They found that the dynamic potential of the reflection concerned went to zero at the critical voltage due to the summation term becoming equal to U_g . In general, however, the approximation has not been widely used to take into account additional reflections because of the orientation dependence of the

dynamic potentials and the breakdown of the approximation when a reflection h is close to its Bragg condition.

2:2.3 Many-Beam Approximation

Although the dynamical theory takes into account an infinite number of diffracted beams, in practice, only a finite number can be included in a many-beam calculation. Usually from 3 to 100 reflections are considered depending upon the accuracy desired and the orientations involved. The many-beam formulation of Howie and Whelan (1960) used in the calculations carried out here starts from the dispersion equation 2.10. As in the two-beam approximation, non-trivial solutions exist for the amplitudes $C_g^{(i)}$ only if the determinant of the coefficients is equal to zero. By analogy with the two-beam case and by reference to Fig. 3 the diagonal elements of the determinant can be written

$$K^2 - k^{(i)2} \approx 2K(K - k^{(i)}) \approx -2K\gamma^{(i)}$$

and

(2.18)

$$K^2 - k_g^{(i)2} \approx 2K(K - k_g^{(i)}) \approx 2K(s_g - \gamma^{(i)}) .$$

When these expressions are substituted back into the determinant and a division by $2K$ carried out, the dispersion equation 2.10 can be written in the form of the

eigenvalue equation

$$\underline{A} \underline{C}^{(i)} = \gamma^{(i)} \underline{C}^{(i)} \quad . \quad (2.19)$$

Here $\underline{C}^{(i)}$ is a column vector whose elements, $C_g^{(i)}$ are the components of the Bloch eigenvector and \underline{A} is a matrix with elements $A_{oo} = 0$, $A_{gg} = s_g$ and $A_{gh} = U_{g-h}/2K$ where $g \neq h$. The eigenvalues, $\gamma^{(i)}$, define the positions of the branches of the dispersion surface in K-space corresponding to the Bloch waves excited.

Consider now the situation shown in Fig. 4. Waves in the directions of the n beams being considered, are incident upon a slab of crystal of thickness δz . In the case shown n is equal to three. These waves can be represented by a column vector \underline{u} whose components are the amplitudes of the various waves. The boundary conditions at the upper surface of the slab, $z = 0$, result in a set of equations of the form

$$\sum_i \psi^{(i)} C_g^{(i)} = u_g \quad (2.20)$$

or, in matrix notation

$$\underline{C} \underline{\psi} = \underline{u} \quad , \quad (2.21)$$

where \underline{C} is a matrix whose columns are the eigenvectors of equation 2.19 and $\underline{\psi}$ is a column vector whose elements give the excitation of the Bloch waves corresponding to

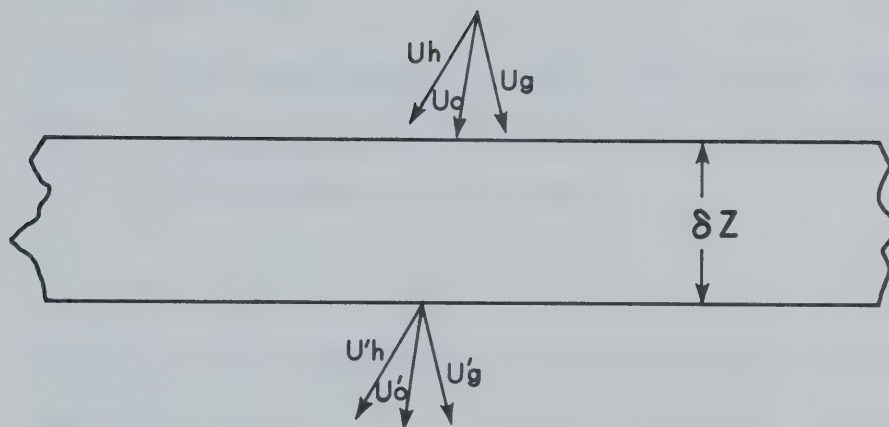


Fig. 4. Waves propagating through a thin slab of crystal (From Howie and Whelan, 1961).

the different branches of the dispersion surface. $\underline{\psi}$ can be found by multiplying both sides of equation 2.21 by \underline{C}^{-1} to give

$$\underline{\psi} = \underline{C}^{-1} \underline{u} \quad . \quad (2.22)$$

Since \underline{A} is a real Hermitian matrix, the eigenvectors $\underline{C}^{(i)}$ are orthogonal and if they are also normalized, $\underline{C}^{-1} = \tilde{\underline{C}}$ and equation 2.22 becomes

$$\underline{\psi} = \tilde{\underline{C}} \underline{u} \quad , \quad (2.23)$$

where $\tilde{\underline{C}}$ is the transpose of \underline{C} . The amplitude of the diffracted beam g at the bottom of the slab is equal to the sum of the components of the Bloch waves in the direction $\vec{k}^{(i)} + g$ and is given by the expression

$$u'_g = \sum_i \psi^{(i)} C_g^{(i)} \exp(2\pi i \gamma^{(i)} \delta z) \quad . \quad (2.24)$$

Here, the exponential terms take into account the phase differences among the waves corresponding to different branches of the dispersion surface. In matrix form this expression can be written

$$\underline{u}' = \underline{C} \underline{\gamma} \underline{\psi} \quad , \quad (2.25)$$

where $\underline{\gamma}$ is a diagonal matrix whose i 'th component is $\exp(2\pi i \gamma^{(i)} \delta z)$. Upon substitution for $\underline{\psi}$ from equation 2.23 the following expression is obtained for \underline{u}' .

$$\underline{u}' = \underline{C} \underline{\gamma} \tilde{\underline{C}} \underline{u} = \underline{P} \underline{u} , \quad (2.26)$$

where $\underline{P} = \underline{C} \underline{\gamma} \tilde{\underline{C}}$. \underline{P} is, thus, a scattering matrix relating the amplitude vector \underline{u}' at the bottom of the slab to the incident wave \underline{u} at the top surface. For any finite number of beams, the components of the scattering matrix \underline{P} can be computed and, thus, the amplitude of any reflection found.

For the case where the top surface of the slab corresponds to the top surface of the crystal, the incident wave has a component only in the direction of the directly transmitted beam. If this beam has unit amplitude then the components of \underline{u} are $u_0 = 1$ and $u_g = 0$ for $g \neq 0$. When this value of \underline{u} is substituted into equation 2.21 it is found that $\underline{\psi}$ is a column vector whose i 'th element is $C_0^{(i)}$. Substituting this into equation 2.24 the following expression is obtained for the amplitude of the diffracted beam g at a depth z

$$u_g'(z) = \sum_i C_0^{(i)} C_g^{(i)} \exp(2\pi i \gamma^{(i)} z) \quad (2.27)$$

or

$$u_g'(z) = \sum_i \phi_g^{(i)} \exp(2\pi i \gamma^{(i)} z) \quad (2.28)$$

where $\phi_g^{(i)} = C_0^{(i)} C_g^{(i)}$. Thus, it is seen that the contribution of a particular Bloch wave to the g 'th diffracted beam amplitude is determined by the magnitude

of $\phi_g^{(i)}$. When only two of the waves make significant contributions to this amplitude, equation 2.28 has the same form as equation 2.15 obtained in the two-beam approximation. However, the actual values of the $\gamma^{(i)}$'s, $\psi^{(i)}$'s and $C_g^{(i)}$'s will be different due to the inclusion of the additional beams in the many-beam calculation.

2:3 Effects of Inelastic Scattering

High energy electrons incident on a crystal can undergo both elastic and inelastic scattering. The dynamical theory as presented by Bethe took into consideration only elastic scattering. We will now consider the modifications to the theory which allow the effects of inelastic scattering of electrons on electron microscope images to be taken into account.

2:3.1 Inelastic Scattering Processes

In a crystal a high energy electron may be involved in three different types of inelastic scattering processes. These are plasmon scattering, electron-electron interactions and phonon or thermal diffuse scattering.

Plasmon scattering results from the long range Coulomb interaction between the high energy electron and the valence electron gas as a whole. The incident

electron excites oscillations called plasmons in the electron gas losing energy in the process. The interaction here can be considered to occur between the electron and the crystal as a whole rather than any individual element of the crystal and is referred to as a collective excitation.

Electron-electron scattering, on the other hand, consists of a short range Coulomb interaction between the high energy electron and the valence and core electrons of the individual atoms. In the case of the valence electrons, these particles are only weakly localized at the ion positions and the scattering cross section is nearly uniformly distributed in the crystal. Core electrons, on the other hand, are localized near the ions. However, the range of the interaction (Williams, 1933) and exchange effects (Shimamoto, Fukamachi and Ohtsuki, 1972) effectively enlarge the scattering cross section so that it also is nearly uniform in the crystal.

Thermal diffuse scattering involves interactions between the incident electrons and the ions. This scattering results in the ion being displaced from its equilibrium position thereby creating lattice waves or phonons in the crystal. Calculations (Whelan, 1965; Hall and Hirsch, 1965; Humphreys and Hirsch, 1968) have shown that the scattering here is localized at the

atomic positions and is, therefore, of great importance in explaining anomalous absorption effects.

It should be noted that, for crystals of the thicknesses commonly examined in the electron microscope, nearly all the electrons are predicted to have undergone inelastic scattering. This point is of interest when it is considered that a diffraction theory ignoring the effects of inelastic scattering usually gives good agreement with experiment. This apparent contradiction is resolved when it is noted that small angle inelastic scattering processes, especially plasmon scattering retains the same coherence between the Bloch waves after scattering as was present before scattering. Thus, the inelastically scattered electrons give the same image contrast as those undergoing only elastic scattering. This was shown to be so experimentally by Kamiya and Uyeda (1961) who obtained images from both elastically and inelastically scattered electrons. These images showed very good agreement with regard to contrast features.

Finally, the term absorption is often used in describing inelastic scattering processes. Although the electrons cannot be physically absorbed, those that are scattered outside the objective aperture do not contribute to the image and can be considered to be

effectively absorbed. It is in this context that the term absorption will be used here.

2:3.2 Phenomenological Treatment of Inelastic Scattering

Inelastic scattering or absorption of the incident electrons is taken into account in electron diffraction by using the phenomenological concept of a complex lattice potential as introduced by Molière (1939). This concept was substantiated theoretically by Yoshioka (1957). It consists of adding a small complex component $iV'(\vec{r})$ to the real part of the lattice potential $V(\vec{r})$. Equation 2.3 then becomes

$$V(\vec{r}) + iV'(\vec{r}) = \frac{\hbar^2}{2me} \sum_{\vec{g}} (U_{\vec{g}} + iU'_{\vec{g}}) \exp(2\pi i \vec{g} \cdot \vec{r}). \quad (2.29)$$

In general, $U'_{\vec{g}} \approx U_{\vec{g}}/10$ and a perturbation approach is used to take into account this additional complex term. The Schrödinger equation is first solved for the case of the real part of the lattice potential and solutions obtained as shown in Sect. 2:2.3. First order perturbation theory is then applied with the perturbing potential being this additional complex term $iU'(\vec{r})$. When this is done it is found that each Bloch wave vector has associated with it an additional imaginary part $i\vec{q}^{(j)}$ where

$$q^{(j)} = \frac{1}{2K} \int_{\text{B}} B^{(j)}(\vec{r})^* U'(\vec{r}) B^{(j)}(\vec{r}) d\tau \quad (2.30)$$

and the Bloch wave $B^{(j)}(\vec{r})$ is given by

$$B^{(j)}(\vec{r}) = \sum_{\vec{g}} C_g^{(j)} \exp\{2\pi i(\vec{k}^{(j)} + \vec{g}) \cdot \vec{r}\} . \quad (2.31)$$

In matrix notation the expression for $q^{(j)}$ reduces to

$$q^{(j)} = \frac{1}{2K} \tilde{\underline{C}}^{(j)} \underline{U}' \underline{C}^{(j)} \quad (2.32)$$

where $\tilde{\underline{C}}^{(j)}$ is the transpose or row vector corresponding to the column vector $\underline{C}^{(j)}$. \underline{U}' is a matrix whose diagonal elements are all equal to U'_0 and whose gh 'th off-diagonal element is equal to U'_{g-h} . When this new wave vector $\vec{k}^{(j)} + i\vec{q}^{(j)}$, resulting from the inclusion of absorption, is substituted back into equation 2.31 the expression for the Bloch wave becomes

$$B^{(j)}(\vec{r}) = \sum_{\vec{g}} C_g^{(j)} \exp\{2\pi i(\vec{k}^{(j)} + \vec{g}) \cdot \vec{r}\} \exp(-2\pi \vec{q}^{(j)} \cdot \vec{r}) . \quad (2.33)$$

By examining this relation it can be seen that the Bloch wave is effectively attenuated or absorbed with depth in the crystal due to the presence of the $\exp(-2\pi \vec{q}^{(j)} \cdot \vec{r})$ term. Thus, the $q^{(j)}$'s have become known as Bloch wave absorption coefficients.

The differences that are commonly found between these coefficients, $q^{(j)}$, have been explained by a number of authors (Hashimoto, Howie and Whelan, 1962;

Howie, 1966; Reynaud, 1971) in terms of the channelling of Bloch waves. In general, the intensity, $B^{(j)}(\vec{r})B^{(j)*}(\vec{r})$ of a Bloch wave as it propagates through a crystal is not evenly distributed but instead is localized or channelled into certain regions either at or between the atomic positions. On the other hand, the imaginary component, $V''(\vec{r})$, of the potential which represents the inelastic scattering is positive and also, due to thermal diffuse scattering, localized at the atomic positions. Thus, it can be seen by examining equation 2.30 that a Bloch wave whose intensity is also concentrated at these positions will have a larger positive value of $q^{(j)}$ than a wave whose intensity is a maximum between the atoms.

2:3.3 Anomalous Absorption Effects

The differences between the $q^{(j)}$'s have been used to explain contrast effects commonly classified under the term of anomalous absorption. The anomalous absorption effect in the case of thickness extinction contours in wedge-shaped crystals consists of the disappearance of thickness contours in thicker regions of the crystal together with the retention of significant diffracted beam intensity. As discussed in Sections 2:2.1 and 2:2.3 these contours occur because of interference effects between the different Bloch waves excited. The magnitude

of the image contrast associated with this interference is determined by the contributions of the different Bloch waves to the diffracted beam amplitude. When absorption is taken into account the expression for this amplitude is of the form

$$u'_g(z) = \sum_j C_o^{(j)} C_g^{(j)} \exp(2\pi i \gamma^{(j)} z) \exp(-2\pi q^{(j)} z) \quad (2.34)$$

or

$$u'_g(z) = \sum_j \phi_g^{(j)}(z) \exp(2\pi i \gamma^{(j)} z) \quad (2.35)$$

where

$$\phi_g^{(j)}(z) = C_o^{(j)} C_g^{(j)} \exp(-2\pi q^{(j)} z) \quad (2.36)$$

In the case where only two Bloch waves make significant contributions to the diffracted beam amplitude, the contours vary in a regular sinusoidal manner with depth as shown in Fig. 5a. Here can be seen the calculated variation of a diffracted beam intensity with depth in a crystal when only two Bloch waves make significant but equal contributions to the corresponding amplitude. Absorption has been neglected in this case. Fig. 5b shows the same situation except that both Bloch waves are attenuated at the same rate, i.e. they have equal absorption coefficients. As can be seen the mean intensity decreases with increasing thickness but the

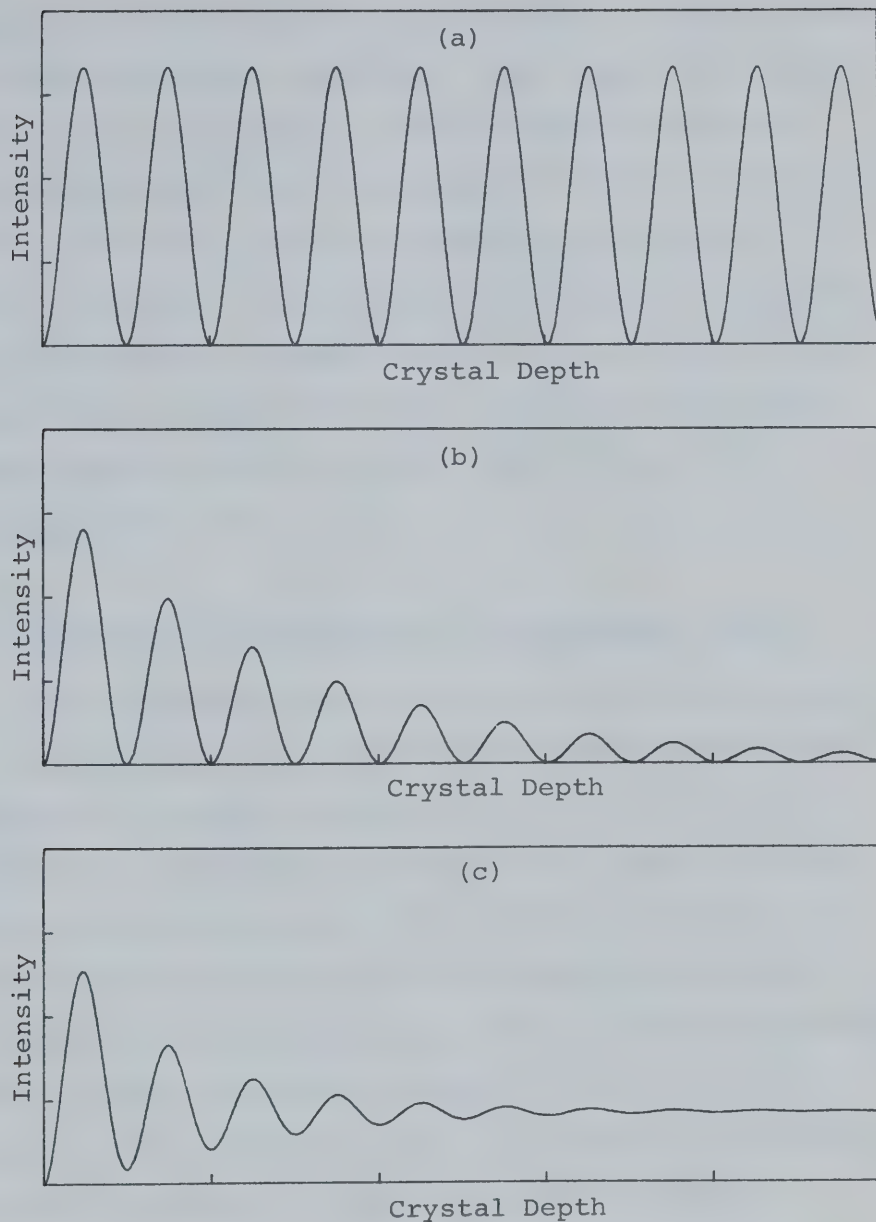


Fig. 5. The variation of diffracted beam intensity with depth in the presence of (a) no absorption (b) normal absorption and (c) anomalous absorption.

sinusoidal variations are still present. This is termed a normal absorption situation. Fig. 5c, on the other hand, shows the intensity profile obtained when one Bloch wave is absorbed much more strongly than the other. Here is seen the effects of anomalous absorption. In thicker regions of the crystal the intensity variations have essentially disappeared due to the strong attenuation of one of the Bloch waves. However, diffracted beam intensity is still present due to the weakly absorbed Bloch wave.

2:4 Additional Corrections to the Dynamical Theory

The dynamical theory as it was originally formulated did not take into consideration either relativistic effects or thermal vibrations of the atoms about their equilibrium positions in the lattice. Since the velocities of the electrons in the electron microscope are approaching that of the speed of light, relativistic effects will be of importance. Fujiwara (1962) developed a relativistic dynamical electron diffraction theory using the Dirac wave equation. His results showed that the non-relativistic theory developed using the Schrödinger wave equation can be corrected for relativistic effects by two simple substitutions. These consist of replacing of the non-relativistic

wavelength by a relativistically corrected one and multiplying the Fourier coefficient term U_g by β where

$$\beta = \left(1 - \frac{v^2}{c^2}\right)^{-\frac{1}{2}}.$$

Here v and c are the velocities of the electrons and light respectively. This second substitution corrects for the relativistic mass of the electron. The imaginary part of U_g , U'_g is relativistically corrected by multiplying the uncorrected U'_g by $v^{-1}\beta$ (Howie, 1962). The accuracy of these corrections have been confirmed experimentally by Hashimoto (1964) and also in the results of Dupouy et al. (1965) as interpreted by Goringe et al. (1966).

Thermal vibrations of the atoms result in a decrease in the Fourier potential coefficients U_g by a factor $\exp(-B|\vec{g}|^2/4)$ where B is the Debye-Waller B factor and $|\vec{g}|$ is the magnitude of the reciprocal lattice vector \vec{g} . This correction at room temperature is usually of the order of a few per cent for low order reflections but due to the $|\vec{g}|^2$ dependence can be quite significant for higher order reflections. The accuracy of this correction has also been confirmed experimentally by Horstmann and Meyer (1963).

CHAPTER 3

THEORETICAL CALCULATIONS

3:1 Introduction

The use of many-beam calculations has become necessary in interpreting many effects in electron diffraction. The basic procedure used in these calculations has been described in detail by Goringe (1971). The procedure used in the calculations in this thesis, although developed independently, is, in general, similar to his procedure. However, it was found that particular problems arise when it is desired to include non-systematic as well as systematic reflections in such calculations. In the discussion which follows these problems are considered in detail, as well as their relationship to the general procedure used in carrying out many-beam calculations.

3:2 Setting Up the A Matrix

The first step in a many-beam calculation using the eigenvalue approach of Hirsch et al. (1965) is to set up the matrix A as defined in equation 2.19. Before evaluating the elements of this matrix, however, it is first necessary to decide what reflections are to be

included in the many-beam calculation. In the case where only systematic reflections are taken into account, the reflections included are usually determined by a convergence criterion. Higher and higher order systematic reflections are added to the calculation until no significant change in the results is obtained. This approach is based on the generally accepted fact that a low-order reflection has a larger effect on the results obtained than a high-order reflection provided that both reflections have the same deviation from their respective Bragg conditions.

When non-systematic reflections are considered, the question of what reflections to include in a calculation can become much more complicated. There are two basic problems in this case. The first is the identification of the non-systematic reflections present in the experimental situation. The second is deciding which of these reflections it is necessary to include in a many-beam calculation. These problems will be discussed in the following two sections.

3:2.1 Indexing of Non-Systematic Reflections

In indexing spots in an electron diffraction pattern, the following procedure is usually employed. First, the distance from the diffraction spot corresponding to the directly transmitted beam to a spot

arising from a low-order reflection is measured. Using the camera length at the diffraction condition and the lattice constant of the crystal, the order, $h^2 + k^2 + \ell^2$, of the reflection can then be determined. From the order and a knowledge of the crystal structure, the type, $\{h\ k\ \ell\}$, of the reflection can be found. From the different possible permutations of h , k and ℓ one set (h_1, k_1, ℓ_1) is usually arbitrarily chosen and the rest of the spots in the diffraction pattern indexed in accordance with it. This is done by measuring the distance from each of these spots to the (000) and (h_1, k_1, ℓ_1) spots and choosing the appropriate h , k , and ℓ values.

When the orientation of the crystal is close to a low-order zone axis the diffraction pattern is of a high symmetry such as shown in Fig. 6. This Figure shows a computed diffraction pattern for a $[\bar{1}11]$ orientation in Si. For such a pattern, it is only necessary to index two spots on different systematic rows in the manner described above. The rest of the spots can then be quickly indexed from symmetry arguments. For the more general case when the crystal orientation does not lie close to a low-order zone axis, the indexing process can be more involved. This is due to the presence of spots corresponding to points of the reciprocal lattice lying on different planes (see Section 3:2.2).

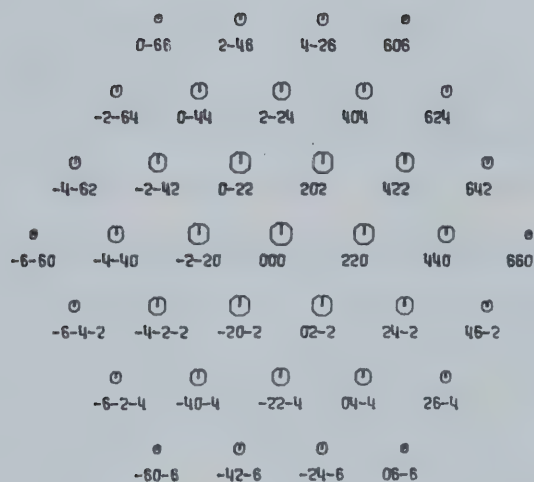


Fig. 6. A computed diffraction pattern for a $[\bar{1}11]$ orientation in Si showing the high symmetry present when the crystal orientation lies close to a low-order zone axis.

In this case, indexing of two non-collinear spots in the pattern does not immediately lead to the indices of all other spots, as in the high symmetry case. This can be seen by examining Figs. 7a and 7b. These Figures show experimental electron diffraction patterns in which a $\{220\}$ systematic row is present. Also visible in each pattern is a second row parallel to the $\{220\}$ row in which a $\{137\}$ type reflection is close to its Bragg condition. However, with the exception of the reflections lying on these two rows, these diffraction patterns have no other common reflections. Thus, indexing of the $\{220\}$ and $\{137\}$ type spots does not immediately lead to the Miller indices of the other diffraction spots present. In order to index these other spots, different allowed combinations for the indices of the $\{220\}$ and $\{137\}$ spots must be considered until a self-consistent set of indices is obtained for all spots in the pattern.

If the spot in the $\{220\}$ systematic row directly to the left of the (000) spot is indexed as a $(\bar{2}\bar{2}0)$ spot, then there are eight possible ways of indexing the 137 spot. These are $(\bar{1}37)$, $(1\bar{3}7)$, $(3\bar{1}7)$, $(\bar{3}17)$, $(\bar{1}3\bar{7})$, $(1\bar{3}\bar{7})$, $(3\bar{1}\bar{7})$ and $(\bar{3}1\bar{7})$. In order to aid in choosing which of these reflections lead to the correct diffraction pattern, and to quickly index the other reflections present, a method involving the computer generation of

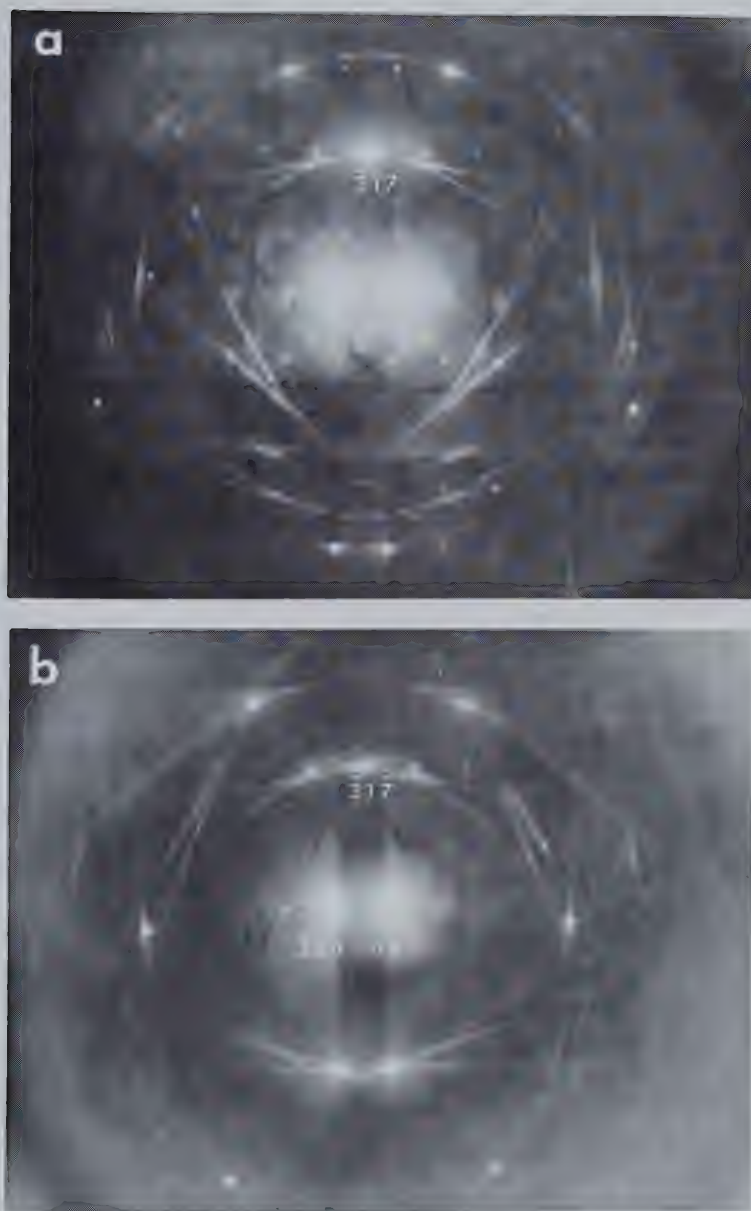


Fig. 7. Experimental electron diffraction patterns showing $\{137\}$ and $\{220\}$ type reflections simultaneously at their Bragg conditions but with different other non-systematic reflections excited.

diffraction patterns was developed. In this method, a computer program was written which displayed the indexed diffraction pattern expected when two non-collinear reflections were in their Bragg conditions. Thus, to index the diffraction pattern shown in Fig. 7a, the computer program was run with different combinations of the $(\bar{2}\bar{2}0)$ and allowed $\{137\}$ reflections in their Bragg conditions. The resulting computed diffraction patterns were then compared with the experimental pattern until one was obtained in which there was a one to one correspondence between the spots in the two patterns. When this was obtained, a correct indexing of all the spots in the experimental pattern was immediately available from the computed pattern. Such a computed pattern for the experimental situation shown in Fig. 7a can be seen by examining Fig. 8. A comparison of these patterns shows a one to one correspondence of the diffraction spots. Thus, the spots in the experimental pattern are correctly indexed using the indices shown in Fig. 8. A similar calculation for Fig. 7b shows that the $\{137\}$ reflection can be correctly indexed as a $(\bar{3}1\bar{7})$ reflection and the rest of the spots indexed accordingly.

It should be noted that, although there are eight allowed combinations for the $(\bar{2}\bar{2}0)$ and $\{137\}$ type



Fig. 8. A computed electron diffraction pattern for an orientation near the $[\bar{7}7\bar{4}]$ direction in Si.

reflections the diffraction patterns corresponding to these combinations are not all necessarily unique. The number of different diffraction patterns obtained will depend on the symmetry of the crystal.

3:2.2 Non-Systematic Reflections Included in a Many-Beam Calculation

Once the non-systematic reflections present have been identified, it is then necessary to determine which of these reflections should be included in a many-beam calculation to obtain the desired convergence. When the crystal orientation lies close to a low-order zone axis, the electron diffraction pattern demonstrates a high symmetry as was seen in Fig. 6. In this case, the reciprocal lattice points corresponding to the reflections excited, all lie in the same plane in reciprocal space as shown schematically in Fig. 9a. This Figure shows a cross section of reciprocal space with the incident beam direction denoted by the arrow and the corresponding position of the Ewald sphere by the solid curved line segment. In this Figure the electron beam is shown incident in a direction of high symmetry in the lattice and the lower order points lying closest to the Ewald sphere all lie in the same plane or zone denoted by the dashed line. Due to the curvature of the

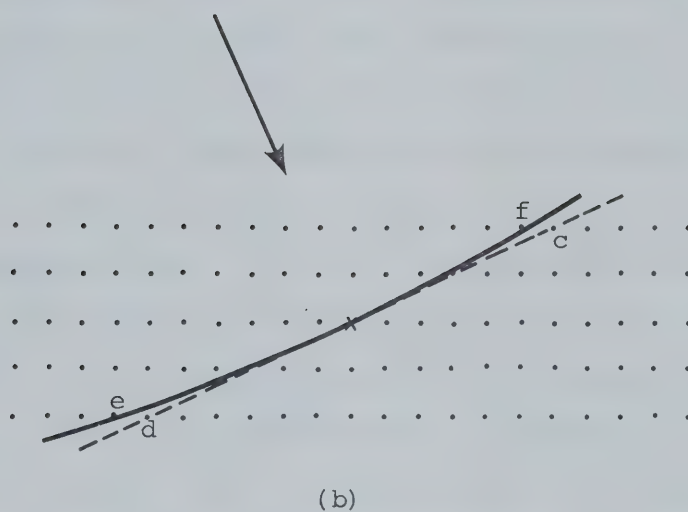
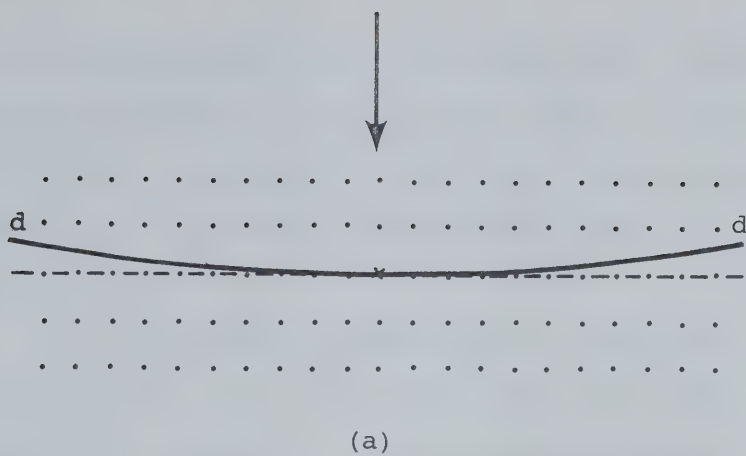


Fig. 9. A cross section of a reciprocal lattice showing the position of the Ewald sphere for the incident beam in a direction of (a), high symmetry and (b), low symmetry in the lattice.

Ewald sphere, points, d , on the plane above the one denoted may also lie close to the sphere. However, these points correspond to high order reflections and generally, do not have a significant effect on calculated results.

For the situation where all the reciprocal lattice points lie on the same plane, the number of reflections included in a many-beam calculation can be determined by the same convergence technique as used in the systematic case. This technique consists of including higher and higher order reflections until the desired accuracy is obtained. In the non-systematic case, however, these reflections lie on annular rings in the plane in reciprocal space rather than along only a systematic row. It is high symmetry situations of this type that have been studied by Howie and Basinski (1968) in Cu, and Lehmpfuhl(1972) and Ayroles(1971) in MgO. Lynch (1971) also examined such a situation in Au. He found, however, that it was necessary to include reflections corresponding to reciprocal lattice points lying in planes above and below the principal plane in reciprocal space in his many-beam calculations in order to obtain agreement with experiment. This was due to the strong dynamic coupling in the presence of the heavy gold atoms.

In the more general case, where the incident electron beam direction does not lie close to a low-order zone axis, the electron diffraction pattern demonstrates a low symmetry as was seen in Fig. 8. In this case, the reciprocal lattice points, corresponding to the reflections excited, do not all lie in the same plane in reciprocal space. The explanation for this can be seen by examining Fig. 9b. In the cross section of reciprocal space shown here, the incident beam is in a direction of low-symmetry in the lattice. The Ewald sphere then passes closer to reciprocal lattice points, *e* and *f*, lying off the principal plane than to points, *d* and *c*, lying on this plane.

This result poses a problem in carrying out many-beam calculations. To obtain convergence when only systematic reflections or high symmetry non-systematic situations are considered, it is only necessary to include higher and higher order reflections until the desired accuracy is obtained. This is because, in general, in these situations the deviation from the Bragg condition increases with increasing order of the reflection considered. However, for a general low symmetry non-systematic situation, this relation of the deviation from the Bragg condition to the order of the

reflection does not necessarily hold. Here, a high-order reflection may be strongly excited and, thus, have an important effect on the results of a calculation while a low order reflection may have a large deviation from the Bragg condition and, therefore, have a relatively small effect. Thus, the order in which non-systematic reflections should be added in carrying out convergence calculations may differ depending upon the orientation of the crystal. The method used for determining this order, for the many-beam calculations carried out at the low-symmetry situations considered in this thesis, will be discussed in detail in Section 5:5. Once the reflections to be included in a many-beam calculation have been chosen in some manner, however, one can then proceed to evaluate the elements of the A matrix.

3:2.3 Determination of the Diagonal Elements of A

The g 'th diagonal element of the matrix A is equal to $s_g = \pm |\vec{s}_g|$ where \vec{s}_g is a deviation parameter equal to the distance from the g 'th reciprocal lattice point to the Ewald sphere. The sign chosen for s_g is given by a convention which will be described later.

A good approximation, used by many workers when considering the two-beam or a systematics only case, is to

assume the Ewald sphere can be approximated by a plane and then set $s_g = |\vec{g}| \Delta\theta$ where $\Delta\theta$ is the angle that the reflection has been tilted away from its exact Bragg condition. More recent work, however, has taken into account the curvature of the Ewald sphere in order to more accurately determine the values of the deviation parameters when higher order reflections are considered. Ayroles (1971), in his work on non-systematic reflections, developed an algebraic relationship for \vec{s}_g for the case where all the corresponding reciprocal lattice points lie in the same plane. However, because in the situations investigated in this thesis non-coplanar reciprocal lattice points were involved, a more general approach, described below, for calculating the \vec{s}_g 's was used.

When the boundary conditions at the top surface of the crystal are taken into consideration, it is found that the distance s_g is measured in a direction normal to the crystal surface. For the calculations carried out in this thesis it was assumed that the incident electron beam was also perpendicular to the crystal surface. Therefore, if the directly transmitted beam has a wave vector \vec{k} in the crystal, \vec{s}_g is measured in a direction parallel to \vec{k} . It should be noted that

modifications to the matrix approach may be required when the angle of the incident beam makes with the crystal surface is not 90° . However, Spencer and Humphreys (1971) have found that these modifications are only significant for large variations from normal incidence.

When the incident beam direction is perpendicular to the crystal surface, the deviation parameter \vec{s}_g is as shown in Fig. 10. By convention, s_g is positive if the reciprocal lattice point g lies inside the Ewald sphere and is negative if it lies outside the sphere. From Fig. 10 it can be seen that

$$\vec{K}' = \vec{K} + \vec{g} + \vec{s}_g \quad . \quad (3.1)$$

Squaring this equation and using the relations $|\vec{K}'| = |\vec{K}| = \frac{1}{\lambda}$ and $\vec{s}_g \parallel \vec{K}$ one then obtains, after a rearrangement of terms, the following quadratic equation in s_g ,

$$s_g^2 + s_g \left[\frac{2}{\lambda} (\vec{K} \cdot \vec{g} + 1) \right] + g^2 + 2\vec{K} \cdot \vec{g} = 0 \quad . \quad (3.2)$$

Since \vec{K} and \vec{g} are known, this equation can be evaluated for the two roots using the standard techniques. These two values correspond to the distance from g to the points of intersection with the Ewald sphere of a line passing through g parallel to \vec{K} . One of these points of intersection is at B and the other where the line cuts

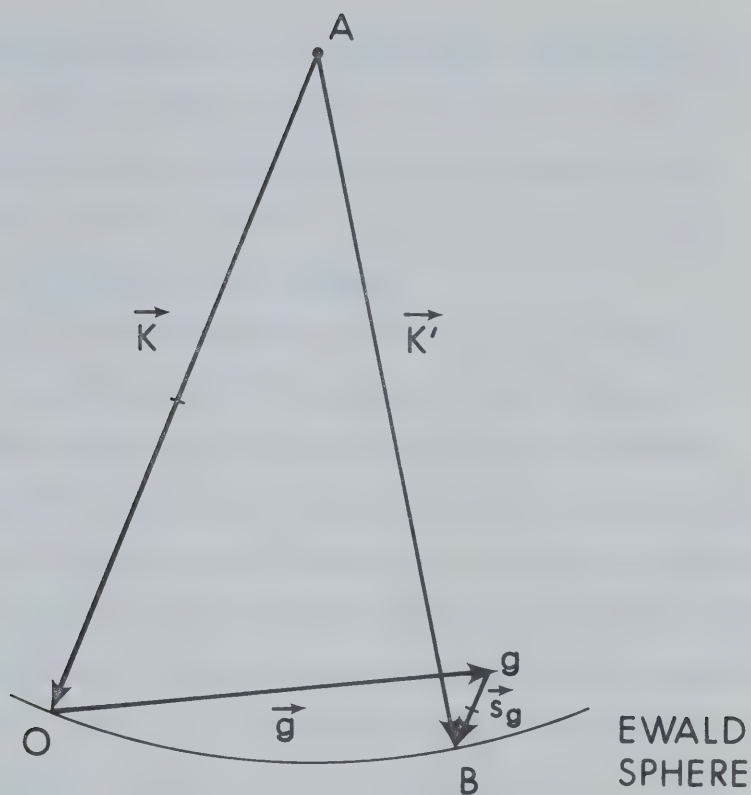


Fig. 10. A diagram drawn of reciprocal lattice space showing the vectors and their relationships used for the calculation of \vec{s}_g . Here, $|\vec{K}| = |\vec{K}'| = \frac{1}{\lambda}$ and $\vec{g} = \frac{1}{a_0} (h, k, l)$. The Ewald sphere is a sphere of radius $\frac{1}{\lambda}$ with centre A located at the point $-\vec{K}$ from the origin of reciprocal space.

the sphere again beyond the upper right hand corner of Fig. 10. Since s_g must equal 0.0 when g is in the Bragg condition, it is seen that the distance gB is the correct value to use for s_g in the many-beam calculations of the dynamical theory.

Thus, if the direction of \vec{K} or its equivalent, the exact orientation of the crystal with respect to the incident beam, is known, the deviation parameter \vec{s}_g of any reflection g can be determined from equation 3.2. It was found useful, therefore, in the calculations carried out in this thesis, to consider tilting of the crystal in terms of the resulting changes in its exact orientation. This is in contrast to the situation when only systematic reflections are considered. In this case, a simple relationship exists between the deviations of all the systematic reflections from their Bragg conditions and tilts of the crystal are, therefore, usually expressed in terms of these deviations. In the non-systematic case, however, a simple relationship does not necessarily exist between the deviations of different reflections. It is therefore necessary, in this case, to consider tilting of the crystal from the point of view of orientation change rather than the resulting change in the deviation of a particular reflection from its Bragg condition.

3:2.4 Determination of the Off-Diagonal Elements of \underline{A}

The gh off-diagonal element of \underline{A} is equal to $U_{g-h}/2K$ where for a crystal composed of only one type of atoms

$$U_{g-h} = \frac{\beta}{\pi V_c} F_{g-h} f\left(\frac{\sin \theta_{g-h}}{\lambda}\right) \exp(-B|\vec{g}-\vec{h}|^2/4) .$$

Here, β is the relativistic mass correction for the incident electrons; V_c is the volume of the unit cell in the crystal; F_{g-h} is the kinematical structure factor for the $g-h$ reflection; $f(\sin \theta_{g-h}/\lambda)$ is the electron scattering factor of the atom for the reflection $(g-h)$ and B is the Debye-Waller factor for the material considered. In practice, K , which is equal to $1/\lambda^2 + U_0$, is usually set equal to $1/\lambda^2$ since the energy of the electrons is much greater than the mean potential of the crystal. For a cubic crystal $V_c = a_0^3$ where a_0 is the lattice parameter. F_{g-h} is equal to 2 for a b.c.c. crystal structure, 4 for a f.c.c. structure and $\pm 8, \pm 4\sqrt{2}$, or 0 for a diamond cubic structure depending upon the Miller indices of the reflection considered. Reflections, which in the diamond cubic structure have a $F_{g-h} = 0$, may still be present. These forbidden reflections occur through dynamic multiple scattering effects (Heidenreich, 1950; Hoerni, 1956; Fujimoto, 1960). The electron scattering factors for different atoms have

been tabulated by a number of authors (Ibers and Vainshtein, 1962; Smith and Burge, 1962; Doyle and Turner, 1968; Radi, 1970). Values for the Debye-Waller B factor are also given in the literature (Ibers and Vainshtein, 1962).

The values of the imaginary components of the lattice potential, U_g' , used in calculations of the absorption coefficients, $q^{(j)}$, can be found from the ratios given for U_g'/U_g by Humphreys and Hirsch (1968) or Radi (1970).

3:3 Calculations of the Effects of Non-Systematic Reflections

Three basic types of calculations of the effects of non-systematic reflections have been carried out. The first of these were calculations of the variation of the extinction distance of a low-order systematic reflection as a function of the deviation of a non-systematic reflection from its Bragg condition. The results obtained here were then compared with results of experimental measurements of the variation of extinction distance under the same circumstances. The second type of calculation involved finding the variation of Bloch wave parameters such as the $\gamma^{(j)}$'s, $\phi_g^{(j)}(z)$'s and

$q^{(j)}$'s, again as a function of the deviation of a non-systematic reflection from its Bragg condition. These parameters were studied in order to interpret the variations observed in the spacing and shape of the extinction contours in the presence of a non-systematic reflection. The third type of calculation undertaken was that of "rocking curves" i.e. the variation in intensity of a reflection measured at a constant depth in the crystal as the orientation of a crystal is changed. These calculations were carried out for both the directly transmitted and a low-order diffracted beam. The purpose was to determine the effects that the presence of non-systematic reflections might have on the positions of the maxima occurring in rocking curves.

The results of these three types of calculations will be discussed in detail in Chapter 5.

3:4 Programs, Computers and Displays

In general, many-beam calculations require the use of a computer for their execution. Thus, it was necessary to develop and write suitable computer programs in order to carry out such calculations. Versions of the programs, used in the calculations described in

the previous section, have not been included in this thesis but have been installed in the program library of the electron microscope group in the Physics Department of the University of Alberta. These programs, with the exception of the subprograms described below, were developed by the author with, however, many helpful suggestions from other members of the electron microscope group. Three subprograms used in the calculations were, however, developed elsewhere. These included the use of standard programs for finding the eigenvalues and eigenvectors of the real symmetric matrix \underline{A} . The version used in the calculations reported in this thesis was the Householder method program, available in the IMSL subroutine library (IMSL, 1972). The subprogram employed for obtaining the two-dimensional computer line printer plots was written by Monk (1972). Finally, the subroutine used for defining the exact orientation of a crystal was based on a method developed by Foxon (1968) (see Appendix A).

The programs were executed using the IBM 360/67 computer of the Department of Computing Services at the University of Alberta. The line printer two-dimensional displays were printed using an IBM 1403 line printer set at 8 lines per inch and using a TN print train. The calculated line graphs were plotted using an off-line model 770/663 Calcomp Plotter.

CHAPTER 4

EXPERIMENTAL PROCEDURES

4:1 Introduction

The effects of non-systematic reflections on extinction distance and anomalous absorption were examined experimentally. For these studies, wedge-shaped specimens of Si were used. The variation of the extinction distance of a low-order systematic reflection as a function of the deviation of a non-systematic reflection from its Bragg condition was determined by measurements of the average spacing of thickness extinction fringes. Also, the visibility of these fringes in thick crystals gave a means of determining anomalous absorption effects. Si was chosen as a specimen material primarily because its brittleness results in relatively strain-free specimens. This is very important in studies involving non-systematic reflections, since their effects can vary drastically over very small changes of the order of $.05^\circ$ in the crystal orientation. The (220) reflection was chosen as the low-order systematic reflection of interest. This reflection was employed rather than a $\{111\}$ type reflection as it had been found previously, by Cann (1967),

that the systematic reflections had only a small effect on the (220) extinction distance while having a very marked effect in the case of the (111) reflection. Thus, variations found in the (220) extinction distance in the presence of a non-systematic reflection should be relatively independent of systematic effects. The principal non-systematic reflections considered for study in the case of extinction distance were ($\bar{1}33$), ($\bar{1}35$) and ($\bar{1}37$). These reflections were chosen because, at the accelerating voltage of 150 kV at which all the experiments were carried out, orientations of the specimen could be obtained such that, when one of these reflections was close to its Bragg condition, no other low-order non-systematic reflection was strongly excited. Therefore, any variation in the (220) extinction distance would be due primarily to the presence of one of these principal reflections.

The actual procedure used in making measurements of the variation of extinction distance in the presence of a non-systematic reflection may be divided into three parts. These are specimen preparation, electron microscope examination and analysis of observations.

4:2 Specimen Preparation

Suitable wedge-shaped specimens of Si single crystals were obtained using a chemical polishing technique.

First, 3 mm discs were cut from commercially obtained (111) oriented silicon wafers, .25 mm in thickness. These discs were cut out by using a high speed drill in which was mounted a hollow brass cylindrical tool with inside diameter slightly greater than 3 mm. An abrasive paste was dabbed between the brass tool and the Si slice which had been previously glued to a brass block in order to hold it securely while the cutting operation was in progress. The 3 mm discs, obtained in this way, were then held at the edge by a set of teflon coated tweezers over an acid jet in an arrangement similar to that used by Booker and Stickler (1962). The composition of the acid was 9 parts HNO_3 (70%) and 1 part HF (48%). The disc was placed directly over and approximately 2 mm above the nozzle of the jet so that a constant column of acid was maintained between the nozzle and disc. The height was adjusted after commencement of polishing to eliminate any regions of etching. The flow rate of the acid was approximately 60 drops or 3 ml per minute. The polishing of one side was allowed to continue until a definite dished shape appeared. This occurred in approximately five minutes. The disc was then turned over and the other side placed over the jet until perforation was observed. It was then placed in a beaker containing the acid mixture for about 10 secs

to give a final polish to both sides before being alternately washed in distilled water and ethyl alcohol. After drying it was ready for examination in the electron microscope.

4:3 Electron Microscope Examination

The Si specimens were examined in a JEM 150 electron microscope at an accelerating voltage of 150 kV and with the second condenser lens partly defocused in order to minimize beam divergence and yet give reasonable image intensity. The orientation of the specimens with respect to the electron beam was varied by using a high precision double tilting and rotating stage (Brunel, 1968). This stage allowed tilting about mutually perpendicular main and secondary tilt axes of $\pm 13.0^\circ$ and $\pm 2.75^\circ$ respectively and rotation through a full 360° . Tilting about the main axis was accomplished by using a click-type control which allowed tilting in increments of $.0047^\circ$. On the secondary tilt a similar type of control allowed tilting in increments of $.0111^\circ$. The rotation was varied using a continuous drive control.

This type of stage, with its associated controls, allowed the effect of a non-systematic reflection on extinction distance to be examined in a systematic manner. From a known initial orientation, as determined from a diffraction pattern, a Si wedge specimen

was tilted in known increments through the Bragg condition of the non-systematic reflection using the main tilt control. For each increment, a dark field image, such as shown in Fig. 11, was recorded. Care was taken that these images were all recorded at the same magnification. The variation of the extinction distance with $\Delta\theta_{\text{NSR}}$, the deviation from the Bragg condition of the non-systematic reflection, could then be determined from measurements of the changes in thickness contour spacing between micrographs. Each micrograph could be related to a particular value of $\Delta\theta_{\text{NSR}}$ by an examination of the initial diffraction pattern and knowledge of the number of increments tilted to reach the position at which it was recorded.

Before carrying out this incremental tilting, however, it was necessary to orient the specimen carefully so that the {220} systematic row lay parallel to the main tilt axis of the stage. This is because the extinction distance of the (220) reflection is also dependent upon the deviation of that reflection from its exact Bragg condition. Thus, if in the incremental tilting procedure for observing the effect of a non-systematic reflection, $\Delta\theta_{220}$, the deviation of the (220) reflection from its Bragg condition, also changes, erroneous results could be obtained. In order to be

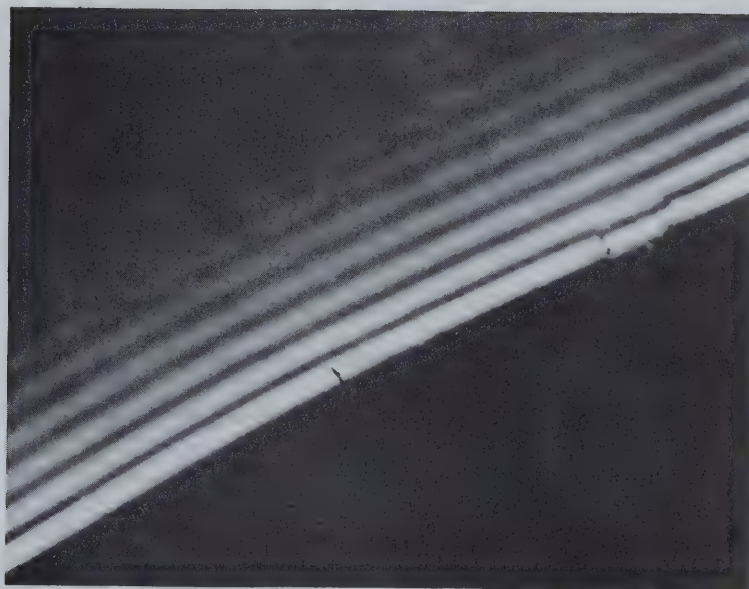


Fig.11. An experimental dark field electron micrograph of a wedge-shaped Si specimen showing thickness extinction contours.

assured that the (220) systematic row lay parallel to the main tilt axis, tilts of a few degrees about this axis were carried out. At the same time, the Kikuchi lines corresponding to the (220) systematic reflections were examined for movement with respect to the (220) diffraction spot. If any such movement was detected, the specimen was rotated slightly using the stage rotation control and the procedure repeated until no movement was found.

After the (220) systematic row had been oriented parallel to the main tilt axis, the desired value of $\Delta\theta_{220}$ was obtained by tilting about the secondary tilt axis. For measurements with the (220) reflection in the exact Bragg condition, such tilting was carried out until the (660) Kikuchi line was observed to pass directly through the (440) spot. Due to the nature of Kikuchi lines this situation corresponds to the (220) reflection in the exact Bragg condition. For measurements with $\Delta\theta_{220} = .25\theta_{220}$, where θ_{220} is equal to the (220) Bragg angle, the specimen was first tilted until the (440) reflection was in its exact Bragg condition as determined from Kikuchi line positions. It was then tilted through $.75\theta_{220}$ towards the Bragg condition of the (220) reflection by clicking through the appropriate number of increments on the secondary tilt control.

This procedure gave a deviation of approximately a quarter of a Bragg angle. The actual value for the deviation was found, however, by taking measurements from the diffraction patterns recorded with each series of micrographs.

In summary, when a specimen was examined in the electron microscope, the following procedure was carried out. First, the specimen was searched for a relatively uniform wedge-shaped region whose surfaces were free of polishing artifacts. It was then rotated until the (220) row of systematic reflections lay parallel to the main tilt axis. The non-systematic reflection of interest was then found by tilting about this axis. Following this, the (220) reflection was tilted to the required deviation from the Bragg condition using the secondary tilt. Then, using the main tilt again, the deviation of the non-systematic reflection from its Bragg condition was changed in a systematic manner using the incremental click control and electron micrographs of the specimen recorded for each increment.

4:4 Analysis of Observations

The electron micrographs of the wedge-shaped crystals were analysed in the following manner to determine the variation of ξ , the {220} extinction

distance, with $\Delta\theta_{\text{NSR}}$. First, a set of micrographs, obtained as described in Section 4:3, was examined and a reference point chosen along the edge of the image of the wedge. The location of this point marked a region where the thickness contours appeared to be uniformly spaced and the image free of other contrast perturbations such as those arising from surface irregularities. Microdensitometer traces, using the setup shown in Fig.12a, were then recorded along a line perpendicular to the image of the edge of the wedge and near the reference mark. These traces converted the density variations, corresponding to the extinction contours, to a periodic curve such as shown in Fig. 12b. An average spacing for the extinction contours could be found from measurements of the peak to peak spacing in these intensity profiles. Comparisons of this average spacing for different micrographs gave the variation of extinction distance as a function of the deviation of the non-systematic reflection from its Bragg condition.

It should be noted that this procedure did not give the actual extinction distance but only variations in it. To make measurements of the actual extinction distance requires a knowledge of either the wedge angle or the thickness of the specimen at a given point. Since neither of these can be easily ascertained for the case of a chemically polished specimen, no measure-

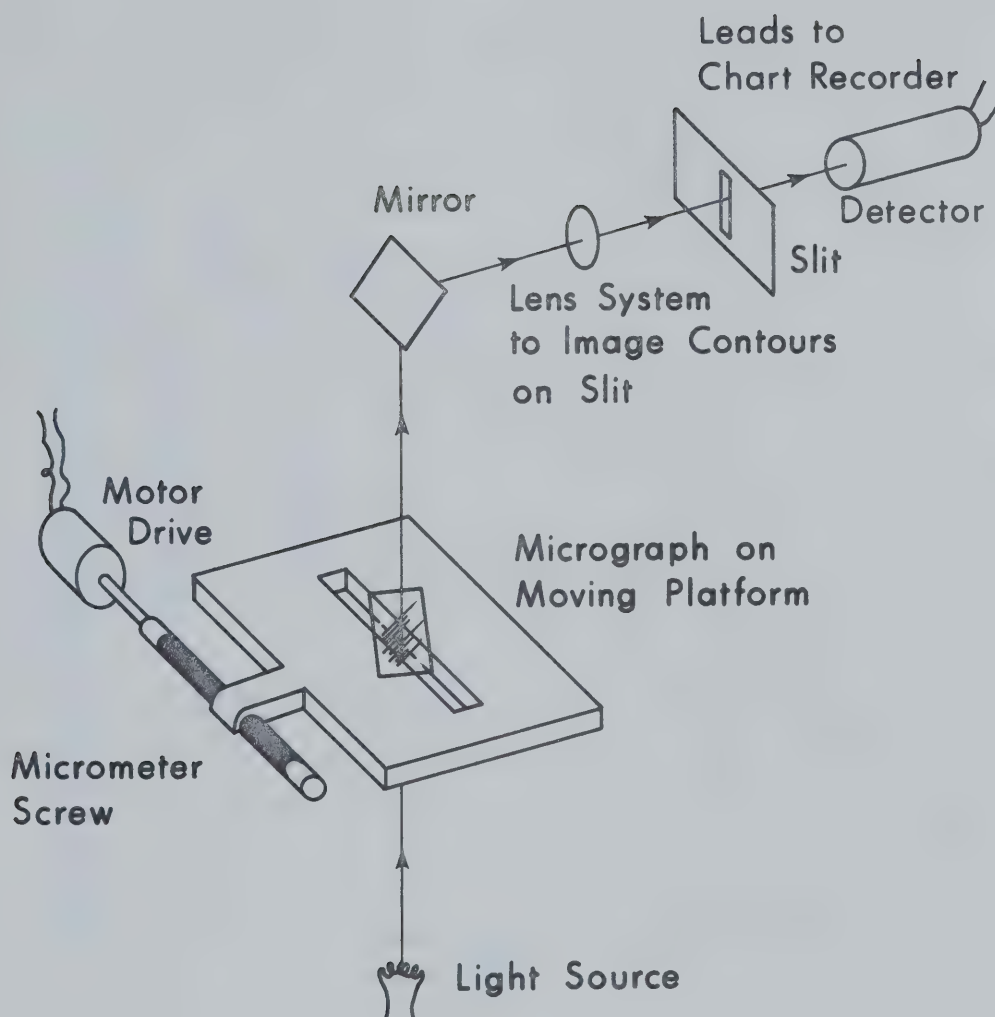


Fig. 12a. Microdensitometer system for measuring the distance between extinction contours.

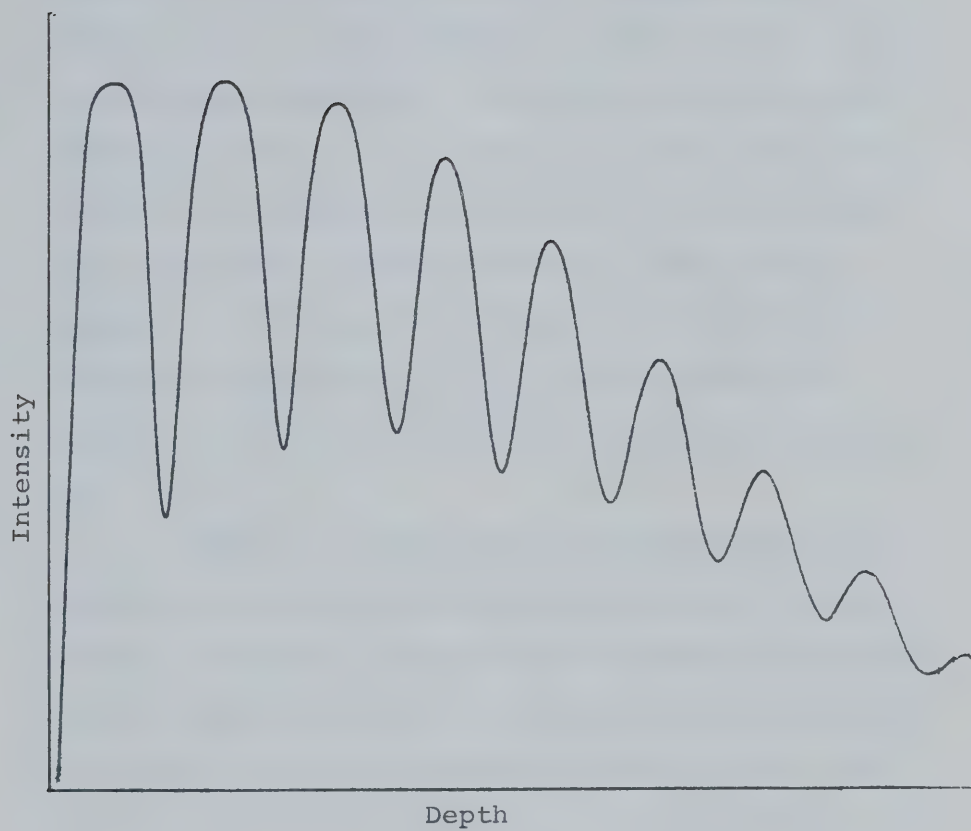


Fig. 12b. A microdensitometer trace across an electron micrograph of a wedge-shaped crystal showing the regular periodic variation of the (220) diffracted beam intensity with depth.

ments were made of actual values of extinction distance. The variation of the extinction distance, in the presence of a non-systematic reflection, could, however, be found by comparing the average spacing of the contours with the average spacing obtained when no non-systematic reflection was close to its Bragg condition. The ratio of these average spacings is equal to ξ/ξ_0 where ξ_0 is the extinction distance at the orientation where no non-systematic reflections were strongly excited. Thus, graphs, obtained by plotting these ratios of average peak spacing as a function of $\Delta\theta_{\text{NSR}}$, can be compared directly with the corresponding theoretical plots of ξ/ξ_0 .

In making the experimental measurements of the average spacing of the thickness extinction contours, care was taken that the measurements were carried out over the same region of the wedge. Since the polishing process results in slightly rounded rather than uniform wedges, it is important that measurements be made over the same region of the wedge each time in order to minimize the effect of unknown thickness variations.

4:5 Experimental Errors

There are two basic sources of error in the experimental results obtained by the methods outlined above. These are, first, in the determination of orientation and, second, in the measurement of the average peak to peak spacing of the thickness extinction contours. As stated in Section 4:3 the exact orientation at which a particular result was obtained was found by calculating how far it had been tilted from a reference orientation as determined from a diffraction pattern. Thus, knowledge of the exact orientation depends upon both the precision of the stage and the accuracy with which the reference orientation can be determined. Inaccuracies in the stage can arise in two areas. These are the size of the average tilt increment and the fluctuations of the increments about this mean value. The average tilt increment was checked by tilting through known angles as determined from Kikuchi patterns (Cann, 1967). These tests showed that the average increment on the primary tilt axis was equal to the designed value of $.0047^\circ$ within 1 per cent. The fluctuations of individual tilt increments from this value were checked both by observing the motion of Kikuchi lines and using the edge movement technique of Sheinin (1966). Variations

in the size of the increments were, in general, found to be small although fluctuations of the order of $.005^\circ$ or one tilt increment were observed on occasion. Such large variations, however, usually occurred in pairs such that the average increment remained close to $.0047^\circ$. Moreover, since 50 to 100 incremental tilts were carried out in obtaining each set of measurements, these short range variations would have little effect on the overall shape of the experimental curves.

Of equal importance to the accuracy of the stage, is the accuracy with which the initial deviation of the non-systematic reflection from its Bragg condition can be measured. This deviation, which is necessary for comparison of different sets of experimental and theoretical results, was found from measurements of the distance between corresponding Kikuchi lines and spots in the diffraction pattern. The accuracy of the deviations found in this manner depended upon a number of factors. These included errors in measuring the actual line and spot positions, as well as shifts in the Kikuchi line positions due to thickness effects (Tan, Bell and Thomas, 1971) and dynamic interactions (Shinohara, 1932; Pfister, 1953; Menzel-Kopp, 1962; Gjønnes and Watanabe, 1966; Gjønnes and Høier, 1969, 1971). Thickness effects, as determined from a comparison of the

spacing between the relevant excess and defect lines and the corresponding spot spacing in the diffraction pattern, were not found to be important. However, dynamical displacements of the lines were evident, especially in the case of the lines corresponding to the non-systematic reflection of interest. These effects, as well as errors in determining the exact positions of the Kikuchi lines and diffraction spots, resulted in uncertainties of the order of $\pm 0.02^\circ$ in determinations of the initial orientations. Thus, different sets of experimental results and the theoretical curve could only be compared with regard to deviation from the Bragg condition to within this range of accuracy.

The second basic source of error in the experimental results was in measuring the average peak to peak spacing of the thickness extinction contours. Errors may arise here from two sources. These are irregular peak spacings and inaccuracies in defining actual peak positions. The irregularities arise from two factors. The first of these is the unevenness of the wedges due to rounding of the specimen edges in the chemical polishing process. Efforts were made to minimize this effect by making measurements over the same region of the wedge. The second cause for the irregularities is due to the contribution of a third Bloch wave to the

diffracted beam amplitude. When three Bloch waves make nearly equal contributions to this amplitude, the extinction contours generally show a complex behaviour and no average spacing can be defined. For orientations slightly away from that at which the complex periodicity is obtained, the contribution of one of the Bloch waves diminishes. At these orientations the intensity profiles are generally sinusoidal in form, although variations in the peak to peak spacing due to the contribution of the third Bloch wave are evident. For the results obtained at $\Delta\theta_{220} = 0.0$, the errors due to these irregularities in the spacing as well as in defining the actual peak positions gave uncertainties of the order of ± 0.03 in the values of the ratio of the average peak to peak spacings (Section 4:4).

For the results obtained at $\Delta\theta_{220} = .25\theta_{220}$, an additional significant source of error must be considered with regard to the uncertainties in this spacing. This error arises from the sensitivity of the (220) thickness extinction contour spacing to small changes in $\Delta\theta_{220}$ at this deviation. As can be seen in Fig. 13, at $\Delta\theta_{220} = 0.0$ a change of $\pm 0.01^\circ$ or $\pm 0.023\theta_{220}$ results in a change of less than .01 in ξ/ξ_0 . However, at $\Delta\theta_{220} = .25\theta_{220}$ a similar error in $\Delta\theta_{220}$ results in an uncertainty of ± 0.025 in the values of ξ/ξ_0 . Thus, small variations in

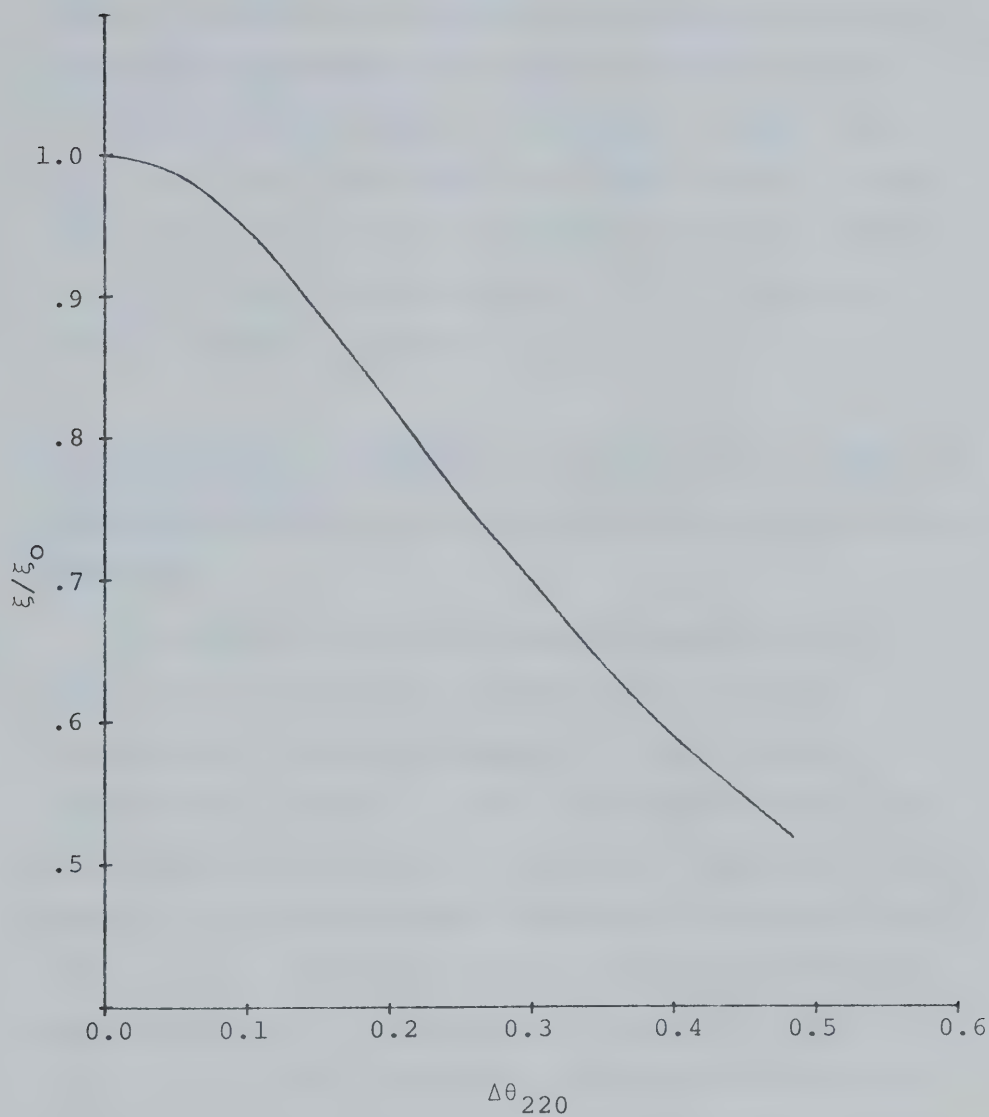


Fig. 13. The variation with $\Delta\theta_{220}$ of ξ/ξ_0 , the normalized extinction distance of the (220) reflection at an accelerating voltage of 150 kV. $\Delta\theta_{220}$ is given in units of θ_{220} .

$\Delta\theta_{220}$ due to slight movements about the secondary tilt axis on the stage, or beam drift in the electron microscope would be expected to result in larger scatter in the experimental results at $\Delta\theta_{220} = .25\theta_{220}$ than at $\Delta\theta_{220} = 0.0$. For this reason, the uncertainties in the value of the ratio of the average peak to peak spacings at $\Delta\theta_{220} = .25\theta_{220}$ are considered to be of the order of ± 0.04 as compared to ± 0.03 at $\Delta\theta_{220} = 0.0$.

4:6 Experimental Procedures in Observing the Effects on Anomalous Absorption of the Presence of a Non-Systematic Reflection

The effects of a non-systematic reflection on anomalous absorption were studied by examining the visibility of thickness contours in wedge-shaped Si specimens (see Section 2:3.3). The effect of the ($\bar{1}33$) non-systematic reflection on anomalous absorption in the case of the (220) dark field image was studied as a function of $\Delta\theta_{\bar{1}33}$. This was done by using regions of the wedge specimens which were bent so that the orientation changed in the $[\bar{1}33]$ direction but remained relatively constant in the [220] direction (see, for example, Fig. 29b in Section 5:3.2). Such regions were oriented, using the tilting stage, so that the (220) reflection was in its Bragg condition while $\Delta\theta_{\bar{1}33}$ varied from

negative to positive values. The variation in the effects of anomalous absorption with $\Delta\theta_{133}$ could then be found by observing the visibility of thickness contours in thick regions of the crystal.

CHAPTER 5

RESULTS AND DISCUSSION

5:1 Introduction

The effects of non-systematic reflections in electron diffraction have been studied in five different areas. These areas included the changes in extinction distance, anomalous absorption, and image intensity in the presence of such reflections, as well as the problems arising in many-beam calculations and Bloch wave labelling when non-systematic reflections are considered. The results of these five studies will be presented and discussed in the subsequent sections of this chapter. For brevity in these discussions, the following convention has been adopted. Whenever $\Delta\theta_{hkl}$, the deviation of the reflection (hkl) from its Bragg condition, is equated to a decimal fraction, it is to be interpreted as that fraction of θ_{hkl} , the Bragg angle of the (hkl) reflection.

5:2 The Effects of a Non-Systematic Reflection on Extinction Distance

The effects of the ($\bar{1}33$), ($\bar{1}35$) and ($\bar{1}37$) reflections on the (220) extinction distance in Si were examined as a function of the deviation of these reflections

from their Bragg conditions. In the case of the ($\bar{1}33$) reflection, these studies were carried out for both $\Delta\theta_{220} = 0.0$ and 0.25 . The range of deviations considered for the ($\bar{1}33$) reflection was $-.30 \leq \Delta\theta_{\bar{1}33} \leq +.30$. For the ($\bar{1}35$) and ($\bar{1}37$) reflections, the studies were only carried out for the case $\Delta\theta_{220} = 0.0$. The ranges of deviations involved for these reflections were $-.15 \leq \Delta\theta_{\bar{1}35} \leq +.15$ and $-.10 \leq \Delta\theta_{\bar{1}37} \leq +.10$ respectively.

5:2.1 The Variation of the (220) Extinction Distance with $\Delta\theta_{\bar{1}33}$ for $\Delta\theta_{220} = 0.0$

The results of three sets of measurements of the variation of the normalized (220) extinction distance, ξ/ξ_0 , with $\Delta\theta_{\bar{1}33}$ for $\Delta\theta_{220} = 0.0$ are shown in Fig. 14. For the experimental points in this Figure, the reference spacing of the thickness extinction contours for each set of results was taken to be the average value of this spacing as measured at $\Delta\theta_{\bar{1}33} \approx -.75$. Therefore, in calculating the corresponding theoretical variation of ξ/ξ_0 with $\Delta\theta_{\bar{1}33}$, the value of 844 \AA used for ξ_0 was the value found for the extinction distance from a many-beam calculation also carried out at approximately $\Delta\theta_{\bar{1}33} = .75$.

As can be seen in Fig. 14, there is good agreement between the experimental results and the theoretically

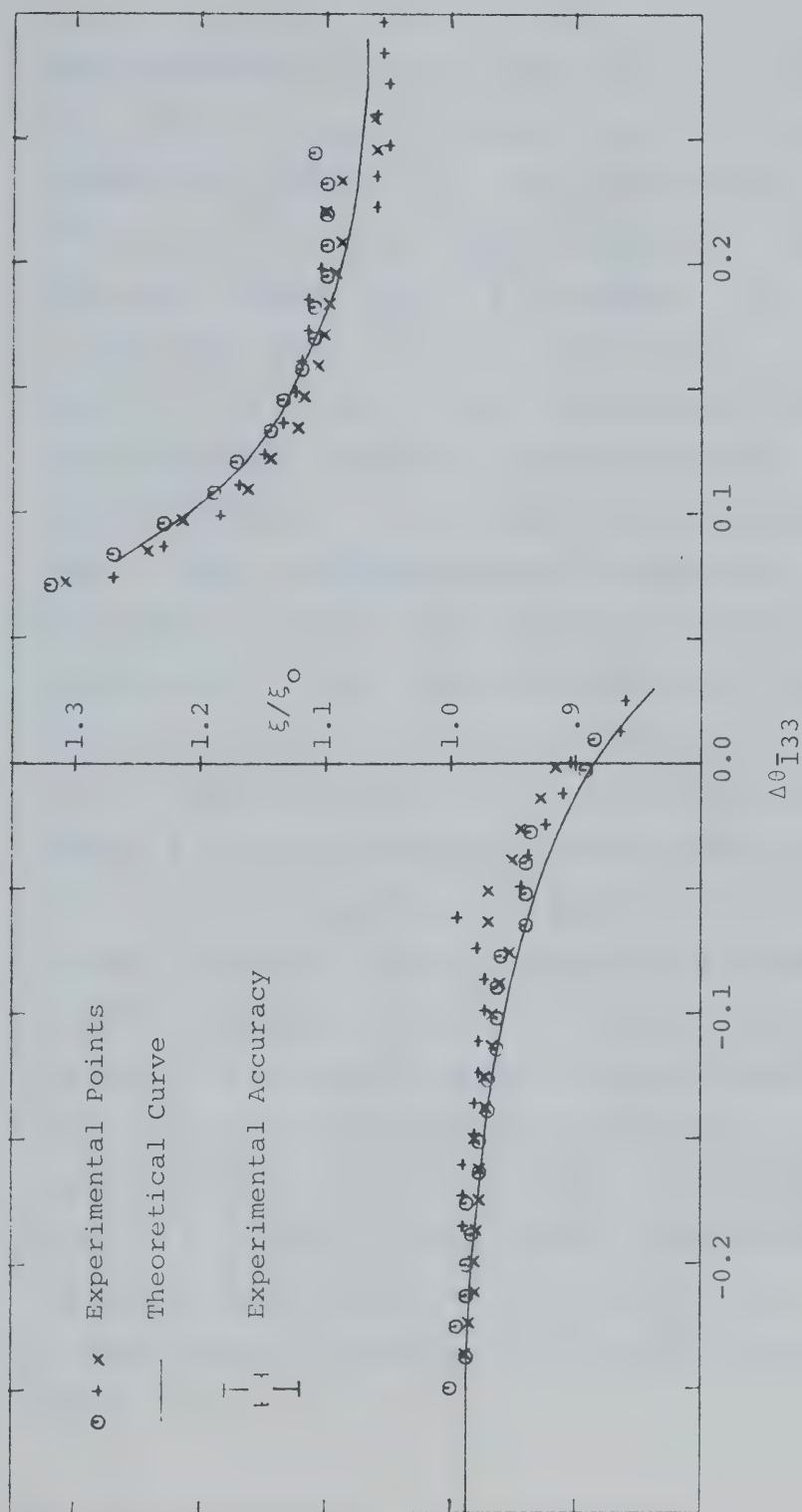


Fig. 14 The experimental and theoretical variation of ξ/ξ_0 for the (220) reflection in Si as a function of $\Delta\theta_{\bar{1}33}$ for the case $\Delta\theta_{220} = 0.0$.

predicted variation of ξ/ξ_0 with $\Delta\theta_{\bar{1}33}$. For large negative values of $\Delta\theta_{\bar{1}33}$, the ratio $\xi/\xi_0 = .99$ or only slightly less than 1.0 i.e. the effect of the ($\bar{1}33$) reflection is small. As $\Delta\theta_{\bar{1}33}$ becomes less negative and passes through $\Delta\theta_{\bar{1}33} = 0.0$, however, ξ/ξ_0 decreases in magnitude until, at $\Delta\theta_{\bar{1}33} = .025$, $\xi/\xi_0 \approx .84$. In the range $.025 < \Delta\theta_{\bar{1}33} < .06$, it was found that both theoretical and experimental thickness extinction contours exhibited complex structure. As an example of this structure, Fig. 15 shows a microdensitometer trace taken across the image of a wedge-shaped specimen oriented so that the deviation of the ($\bar{1}33$) reflection from its Bragg condition lay within the range $.025 < \Delta\theta_{\bar{1}33} < .06$. It can be seen in this Figure that the contours do not exhibit a regular sinusoidal behaviour such as was shown in Fig. 12b but, instead, show marked variations in peak to peak spacing as well as distorted peak shapes. Such regions of complex structure were always found to be associated with marked changes in extinction distance. This can be seen by comparing the values of ξ/ξ_0 at $\Delta\theta_{\bar{1}33} = 0.075$ and 0.025 which are 1.28 and 0.84 respectively. For values of $\Delta\theta_{\bar{1}33}$ greater than those at which the complex periodicity occurs, the ratio ξ/ξ_0 decreases in magnitude with increasing $\Delta\theta_{\bar{1}33}$ until, at $\Delta\theta_{\bar{1}33} = .30$ $\xi/\xi_0 = 1.07$.

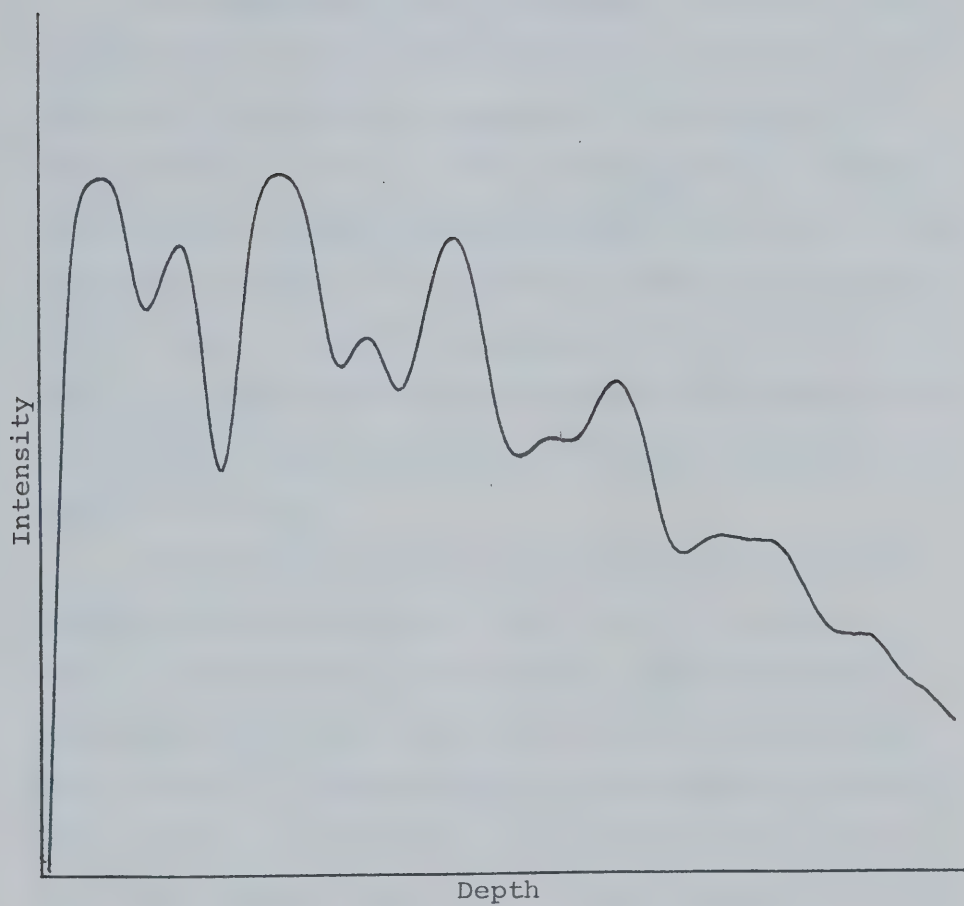


Fig. 15 A microdensitometer trace showing complex structure in the variation of the (220) intensity with depth.

5:2.2 Explanation of the Observed Variation of ξ/ξ_0 with $\Delta\theta_{\bar{1}33}$ for $\Delta\theta_{220} = 0.0$

The behaviour of the (220) extinction distance as described in the previous section can be explained in terms of Bloch wave parameters. It was seen in Sections 2:2.1 and 2:2.3 that the extinction distance is determined by the spacing between the branches of the dispersion surface corresponding to the important Bloch waves. Thus, in order to explain the variation of ξ/ξ_0 with $\Delta\theta_{\bar{1}33}$, it is necessary to examine the behaviour of the different branches of the dispersion surface as a function of $\Delta\theta_{\bar{1}33}$.

In the theoretical calculations carried out to determine the variation of ξ/ξ_0 with $\Delta\theta_{\bar{1}33}$ shown in Fig. 14, approximately twenty-five reflections were included, resulting in an equal number of Bloch waves being excited. The branches of the dispersion surface corresponding to these waves are shown in Fig. 16. It was found, however, that, at a given orientation, only a few Bloch waves made significant contributions to the (220) intensity. Thus, only the dispersion surface branches corresponding to these waves are important when considering the variation of ξ/ξ_0 with $\Delta\theta_{\bar{1}33}$. In Fig. 16, these branches are denoted by the dotted line segments. It is seen here that, in general, only three

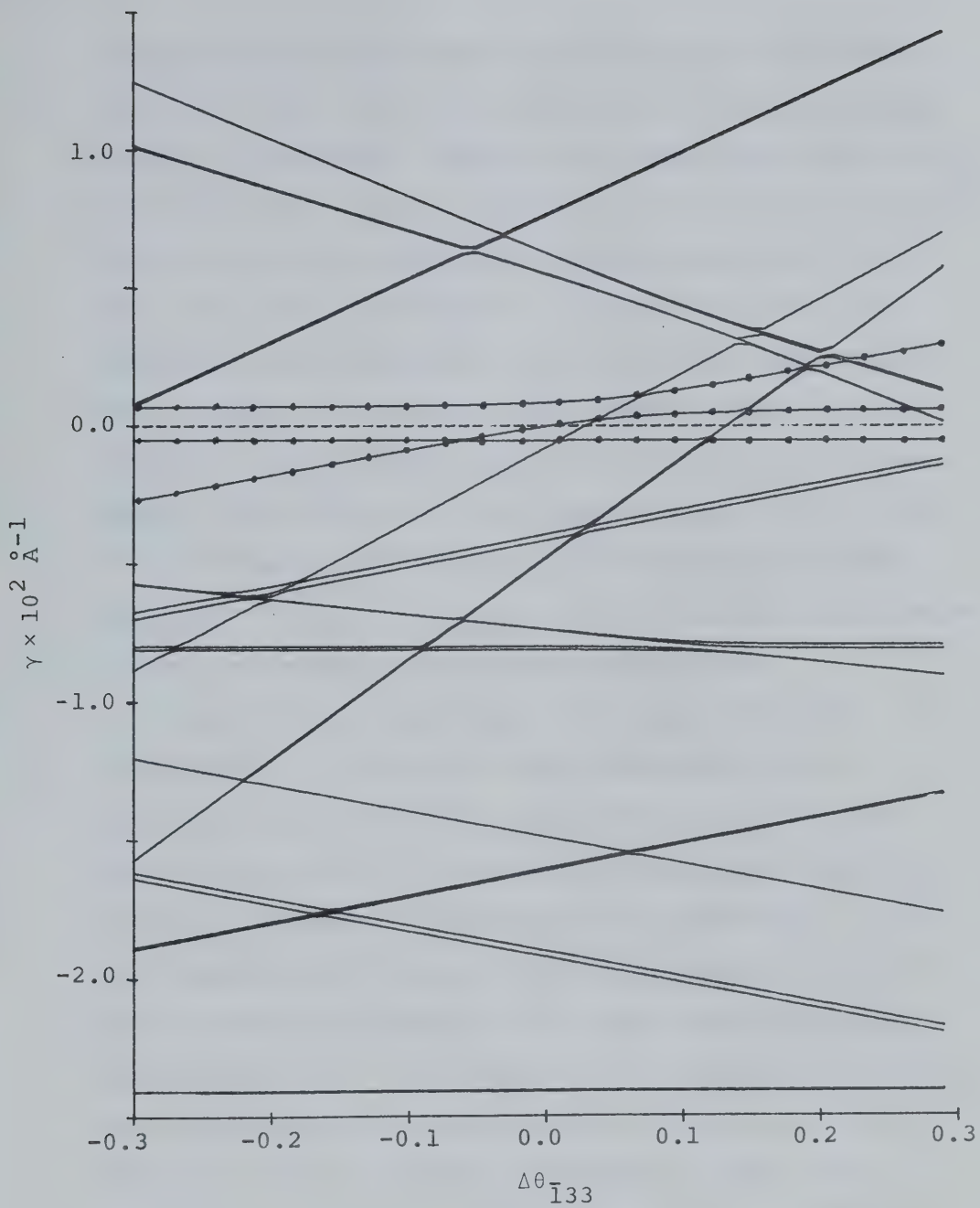


Fig. 16 The excited branches of the dispersion surface as given by a 25 beam calculation for $-0.30 \leq \Delta\theta_{\bar{1}33} \leq 0.30$ and $\Delta\theta_{220} = 0.0$.

Bloch waves are important at any orientation although it is not the same three Bloch waves over the whole range of $\Delta\theta_{\bar{1}33}$ considered. However, by comparison with Fig.17 which shows the three branches of the dispersion surface obtained from a calculation including only the (000), (220) and ($\bar{1}33$) reflections, it can be seen that the important branch segments in the many-beam case correspond closely in position to the branches given by the three-beam calculation. Because of this good agreement between the positions of the important branches in the three and many-beam calculations, the analysis of the variation of ξ/ξ_0 with $\Delta\theta_{\bar{1}33}$ will be carried out in terms of the much simpler three-beam approximation.

Even in the three-beam calculation, however, it is necessary to find which Bloch waves make large contributions to the (220) amplitude in order to know which branches of the dispersion surface are important in interpreting the variation of ξ/ξ_0 with $\Delta\theta_{\bar{1}33}$. In this regard, Fig. 18 shows the contributions, $|\phi_{220}^{(j)}|$'s, of the three Bloch waves to the (220) amplitude as a function of $\Delta\theta_{\bar{1}33}$. The values of the $|\phi_{200}^{(j)}|$'s shown here were calculated at the top surface of the crystal and, therefore, do not include any effects of absorption. These effects will be considered separately in Section 5:3. In Fig. 18 it can be seen that, in the range

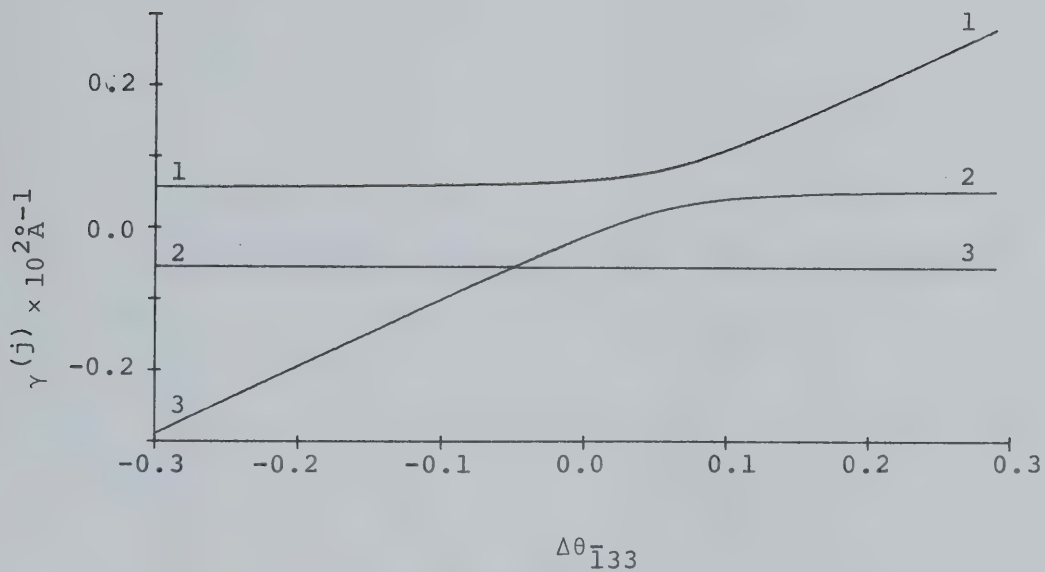


Fig. 17 The variation with $\Delta\theta_{\bar{1}33}$ of the branches of the dispersion surface as given by a three-beam calculation including the (000), (220) and ($\bar{1}33$) reflections. $\Delta\theta_{220} = 0.0$.

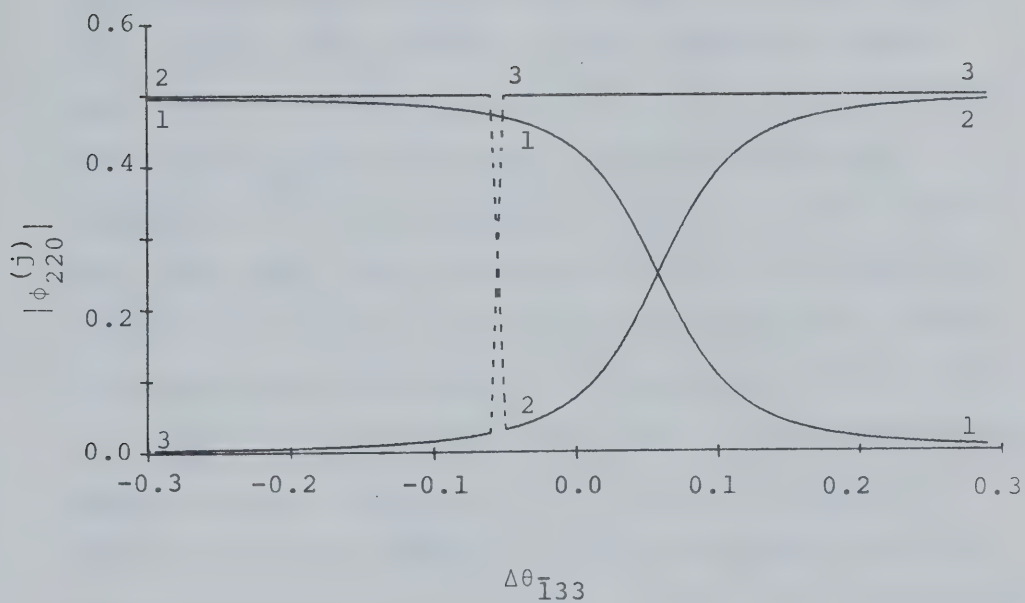


Fig. 18 The variation with $\Delta\theta_{133}$ of the contributions, $|\phi_{220}^{(j)}|$, of the different Bloch waves to the (220) amplitude as given by a three-beam calculation. $\Delta\theta_{220} = 0.0$.

$-0.3 \leq \Delta\theta_{\bar{1}33} < -0.5$, only Bloch waves 1 and 2 make significant contributions to the (220) amplitude. At $\Delta\theta_{\bar{1}33} \approx .05$, however, it can be seen that the contributions of Bloch waves 2 and 3 appear to interchange over a narrow range of values of $\Delta\theta_{\bar{1}33}$ as denoted by the dashed lines. Referring back to Fig. 17, it can be seen that at this point Bloch waves 2 and 3 have identical $\gamma^{(j)}$ values and are, therefore, degenerate. Sprague and Wilkins (1970) have shown that when absorption is taken into account in such a situation using first order non-degenerate perturbation theory, significant mixing of the Bloch waves corresponding to the degenerate $\gamma^{(j)}$'s is predicted. Sheinin and Cann (1973) have shown that, when the more correct doubly degenerate perturbation theory is applied in this situation, there is a significant difference in the predicted (220) intensity from that obtained when the first order perturbation theory is used. However, in both cases the predicted effects due to the presence of the degeneracy take place over a very small range of $\Delta\theta_{\bar{1}33}$. Also, since both of the Bloch waves involved in the mixing have nearly identical values of $\gamma^{(j)}$ in this range, no detectable variation in the extinction distance which involves either $\gamma^{(1)} - \gamma^{(2)}$ or $\gamma^{(1)} - \gamma^{(3)}$ would be expected.

In the range of $\Delta\theta_{\bar{1}33}$ from $-.05$ to $.025$, the most important contributions to the (220) amplitude are made

by Bloch waves 1 and 3, although the contribution of Bloch wave 2 is increasing in magnitude while that of Bloch wave 1 is becoming smaller. This behaviour of Bloch waves 1 and 2 leads to all three Bloch waves making significant contributions to the diffracted beam intensity in the range $.025 \leq \Delta\theta_{\bar{1}33} \leq .075$. Finally, it can be seen from Fig. 18, that, for $.075 \leq \Delta\theta_{\bar{1}33} \leq .30$, Bloch waves 2 and 3 are the only waves making a significant contribution to the (220) amplitude.

These observations from Fig. 18 can now be applied in interpreting the variation of ξ/ξ_0 with $\Delta\theta_{\bar{1}33}$ in terms of the spacing between the important branches of the dispersion surface. Thus, in the range $-.30 \leq \Delta\theta_{\bar{1}33} < .05$, Bloch waves 1 and 2 make important contributions to the (220) amplitude and, therefore, the extinction distance, ξ , depends upon the difference $\gamma^{(1)} - \gamma^{(2)}$. Similarly, in the range $-.05 < \Delta\theta_{\bar{1}33} \leq .025$, ξ depends upon the difference $\gamma^{(1)} - \gamma^{(3)}$. By examining Fig. 17, it can be seen that, through the range of $\Delta\theta_{\bar{1}33}$ from $-.30$ to $.025$, the difference, $\gamma^{(i)} - \gamma^{(j)}$, determining the extinction distance is increasing in magnitude. Since ξ equals $(\gamma^{(i)} - \gamma^{(j)})^{-1}$, this behaviour results in a corresponding decrease in ξ/ξ_0 in agreement with the results shown in Fig. 14. In the region, $.025 \leq \Delta\theta_{\bar{1}33} \leq .075$, Fig. 18 shows that all three Bloch waves are important, and,

therefore, the (220) intensity variation with depth will be a function of three different periodicities; $(\gamma^{(1)} - \gamma^{(2)})^{-1}$, $(\gamma^{(1)} - \gamma^{(3)})^{-1}$ and $(\gamma^{(2)} - \gamma^{(3)})^{-1}$. This should result in a complicated non-sinusoidal variation with depth of the (220) intensity as was observed. For $.075 \leq \Delta\theta_{\bar{1}33} \leq .30$, Bloch waves 2 and 3, as noted previously, are the only waves making significant contributions to the (220) intensity and, thus, the extinction distance depends on $\gamma^{(2)} - \gamma^{(3)}$. If this difference at $\Delta\theta_{\bar{1}33} = .075$ is compared to the difference $\gamma^{(1)} - \gamma^{(3)}$ at $\Delta\theta_{\bar{1}33} = .025$ it is found to be much smaller. This marked change in the magnitude of $\gamma^{(i)} - \gamma^{(j)}$, where i and j are the important Bloch waves, in passing through the complex region explains the observed jump in ξ/ξ_0 in Fig. 14. Finally, in the range of $\Delta\theta_{\bar{1}33}$ from .075 to .30 the difference $\gamma^{(2)} - \gamma^{(3)}$ increases with the result that ξ/ξ_0 decreases again as observed.

From the foregoing discussion, it can be seen that an analysis in terms of Bloch wave parameters accurately describes the behaviour of the (220) extinction distance in the presence of the strongly excited ($\bar{1}33$) reflection for the case $\Delta\theta_{220} = 0.0$.

5:2.3 The Variation of the (220) Extinction Distance with $\Delta\theta_{\bar{1}33}$ for $\Delta\theta_{220} = 0.25$

The results of three sets of measurements of the variation of the (220) extinction distance with deviation of the ($\bar{1}33$) reflection from its Bragg condition for $\Delta\theta_{220} = 0.25$ are shown in Fig. 20. The reference spacings of the thickness fringes used in obtaining the experimental ξ/ξ_0 points were found from the average values of the spacing of the thickness contours measured at $\Delta\theta_{\bar{1}33} \approx -.70$. The value of 638 Å, used for ξ_0 in determining the theoretical variation of ξ/ξ_0 with $\Delta\theta_{\bar{1}33}$, was obtained from a many-beam calculation also carried out for $\Delta\theta_{\bar{1}33} \approx -.70$.

From Fig. 19 it can be seen that there is relatively good agreement between the experimental results and the theoretical predictions when the accuracy of the experimental results is taken into consideration. As $\Delta\theta_{\bar{1}33}$ varies from $-.30$ to $-.06$, the ratio ξ/ξ_0 remains close to 1.0 but then increases to a value of 1.05 at $\Delta\theta_{\bar{1}33} = .03$. In the range $-.03 < \Delta\theta_{\bar{1}33} < -.01$, the variation of the (220) intensity with depth was observed to become complex in structure. This region of complex periodicity is followed by a drop in the magnitude of ξ/ξ_0 to a value of .93 at $\Delta\theta_{\bar{1}33} = -.01$. As $\Delta\theta_{\bar{1}33}$ varies from $-.01$ to $.03$, ξ/ξ_0 remains nearly constant before

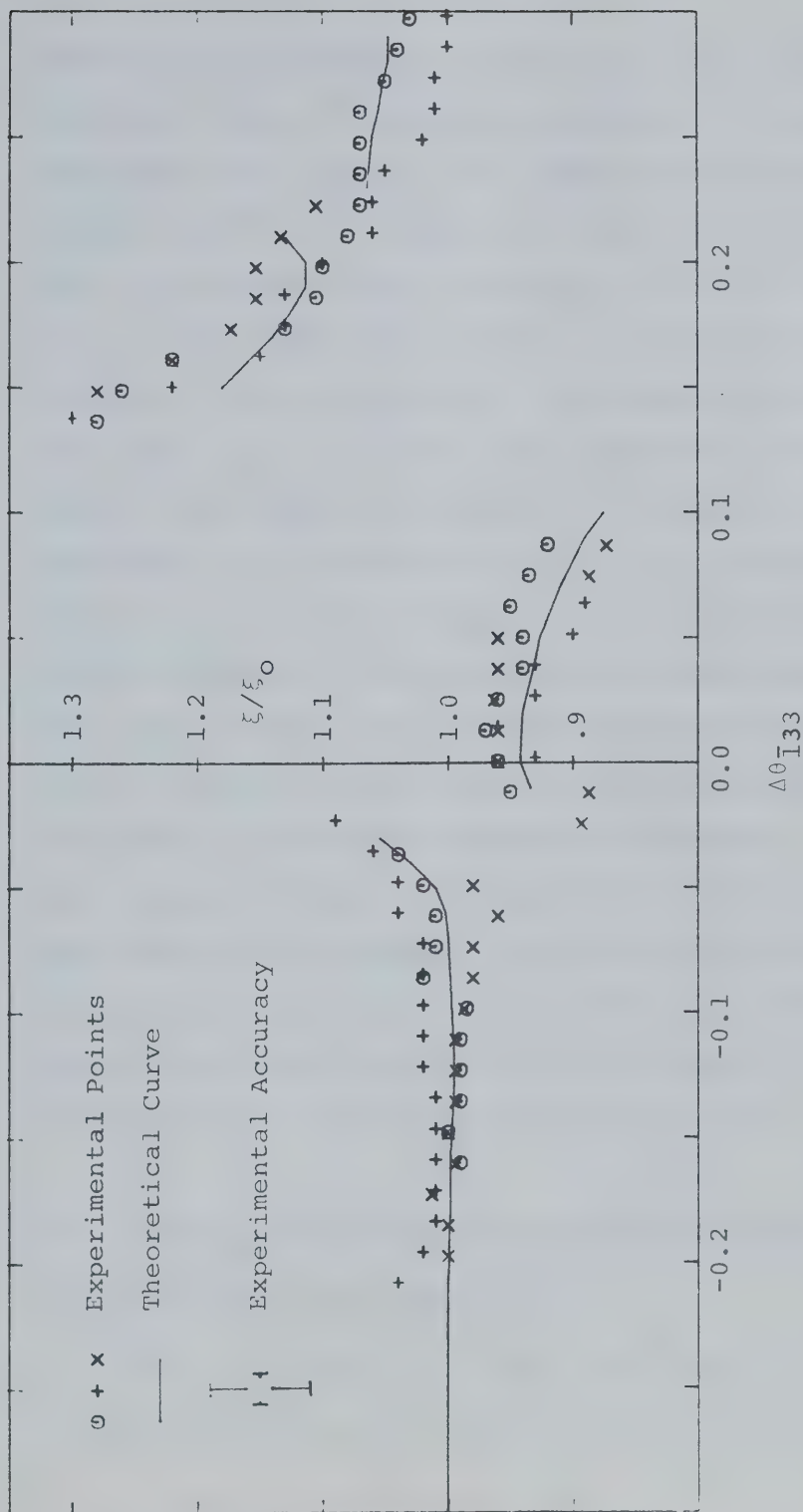


Fig. 19 The experimental and theoretical variation of the ratio ξ/ξ_0 for the (220) reflection in Si as a function of $\Delta\theta_{133}$ for the case $\Delta\theta_{220} = 0.25$.

decreasing to a value of .87 at $\Delta\theta_{\bar{1}33} = .10$. A second region of complex behaviour was observed to occur in the range $.10 \leq \Delta\theta_{\bar{1}33} \leq .14$. Associated with this complex region is a large jump in extinction distance with ξ/ξ_0 changing from .87 at $\Delta\theta_{\bar{1}33} = .10$ to 1.23 at $\Delta\theta_{\bar{1}33} = .14$. From $\Delta\theta_{\bar{1}33} = .14$, ξ/ξ_0 decreases to a value of 1.12 at $\Delta\theta_{\bar{1}33} = .20$. The theoretical curve then shows ξ/ξ_0 to increase to a value of 1.14 at $\Delta\theta_{\bar{1}33} = .21$. This is followed by a region of complex behaviour in the range $.21 < \Delta\theta_{\bar{1}33} < .22$ and an associated drop in ξ/ξ_0 to 1.06 at $\Delta\theta_{\bar{1}33} = .22$. The experimental results, however, do not behave in the same manner in this region. They show a continuous decrease in ξ/ξ_0 for this range of $\Delta\theta_{\bar{1}33}$. This lack of agreement may arise from experimental error as the predicted theoretical variation is small compared to the accuracy of the experimental measurements. Finally, in the range $.22 \leq \Delta\theta_{\bar{1}33} \leq .30$, ξ/ξ_0 for both the experimental and theoretical results shows similar behaviour in slowly decreasing to a value of 1.04 at $\Delta\theta_{\bar{1}33} = .30$.

5:2.4 Explanation of the Observed Variation of ξ/ξ_0 with $\Delta\theta_{\bar{1}33}$ for $\Delta\theta_{220} = 0.25$

The behaviour of the (220) extinction distance as a function of $\Delta\theta_{\bar{1}33}$ for $\Delta\theta_{220} = 0.25$ can be explained,

as in the case for $\Delta\theta_{220} = 0.0$, in terms of Bloch wave parameters. Fig. 20 shows the branches of the dispersion surface as given by a three-beam calculation including the (000), (220) and ($\bar{1}33$) reflections. Fig. 21 shows the contributions of the Bloch waves, corresponding to these branches, to the (220) diffracted beam amplitude. From this latter Figure, it can be seen that, in the region $-.30 \leq \Delta\theta_{\bar{1}33} \leq -.03$, only Bloch waves 1 and 2 make large contributions to the (220) amplitude. Therefore, the extinction distance depends on the spacing between the corresponding branches of the dispersion surface. Since this spacing, as shown in Fig. 20, remains constant, except near $\Delta\theta_{\bar{1}33} = -.03$ where it starts to decrease, the extinction distance would also be expected to be constant except for a small increase near $\Delta\theta_{\bar{1}33} = -.03$. This is in agreement with the observed results. Again, from Fig. 21, it can be seen that in the range $0.03 < \Delta\theta_{\bar{1}33} < -.01$ all three Bloch waves are important with the result that a complex variation of intensity with depth is obtained. For $\Delta\theta_{\bar{1}33}$ between $-.01$ and $.10$, however, only Bloch waves 1 and 3 make large contributions to the (220) amplitude with the result that the variation of intensity with depth is again sinusoidal. The period of this variation, ξ , depends upon the spacing between branches 1 and 3 in this region.

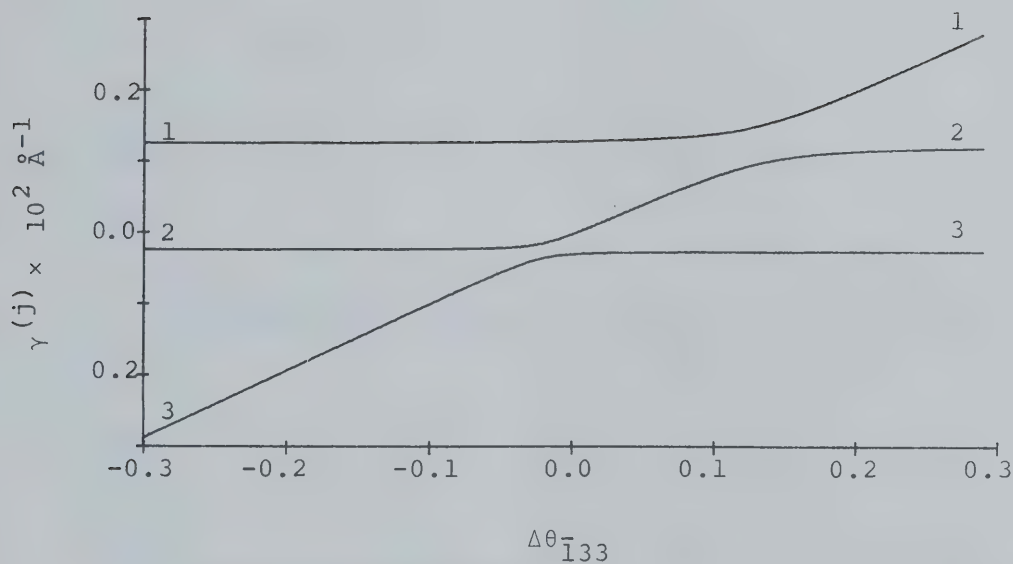


Fig. 20 The variation with $\Delta\theta_{\bar{1}33}$ of the branches of the dispersion surface as given by a three-beam calculation including the (000), (220) and ($\bar{1}33$) reflections. $\Delta\theta_{220} = .25$.

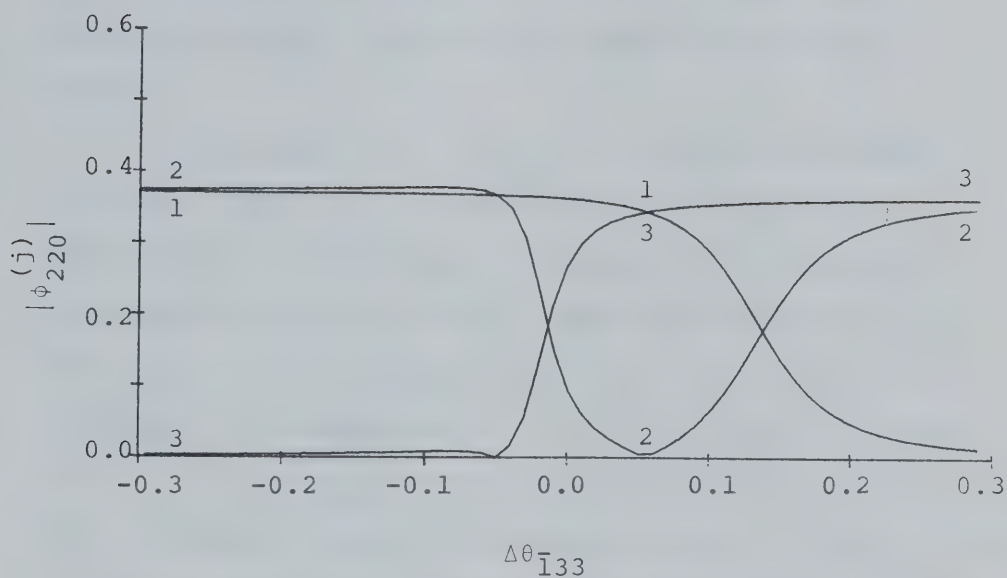


Fig. 21 The variation with $\Delta\theta_{\bar{1}33}$ of the contributions, $|\phi_{220}^{(j)}|$, of the different Bloch waves to the (220) amplitude as given by a three-beam calculation. $\Delta\theta_{220} = .25$.

Since $\gamma^{(1)} - \gamma^{(3)}$ at $\Delta\theta_{\bar{1}33} = -.01$ is significantly larger than $\gamma^{(1)} - \gamma^{(2)}$ at $\Delta\theta_{\bar{1}33} = -.03$, the drop in extinction distance in passing through the region of complex structure centred at $\Delta\theta_{\bar{1}33} = -.02$ is explained. The difference $\gamma^{(1)} - \gamma^{(3)}$ remains relatively constant in the range $-.01 < \Delta\theta_{\bar{1}33} < .03$ before slowly increasing as $\Delta\theta_{\bar{1}33}$ approaches .10. This is in agreement with the observed behaviour of the extinction distance which remained constant before slowly decreasing in this region.

In the range $.10 < \Delta\theta_{\bar{1}33} < .14$, the three Bloch waves are again all important as shown in Fig. 21. This results in the complex variation of the intensity with depth observed for this range of values of $\Delta\theta_{\bar{1}33}$. For $\Delta\theta_{\bar{1}33} > .14$, however, only Bloch waves 2 and 3 are important. By comparing $\gamma^{(2)} - \gamma^{(3)}$ at $\Delta\theta_{\bar{1}33} = .14$ and $\gamma^{(1)} - \gamma^{(3)}$ at $\Delta\theta_{\bar{1}33} = .10$, the jump in the value of ξ/ξ_0 in passing through the complex region $.10 < \Delta\theta_{\bar{1}33} < .14$ is again explained. Finally, since the spacing between branches 2 and 3 is increasing as $\Delta\theta_{\bar{1}33}$ varies from .14 to .30, a corresponding decrease in ξ/ξ_0 in this range is predicted. As can be seen in Fig. 19, such a decrease was indeed observed.

Although the three-beam approximation can predict the general behaviour of the experimental results for the case $\Delta\theta_{220} = .25$, it does not explain the observed

jump in the theoretical variation of ξ/ξ_0 with $\Delta\theta_{\bar{1}33}$, which occurs at $\Delta\theta_{\bar{1}33} = .21$. This jump was found to be associated with the presence of another non-systematic reflection. Because of the particular crystal orientation used, the $(\bar{1}\bar{7}\bar{5})$ reflection was found to be close to its Bragg condition at $\Delta\theta_{\bar{1}33} = .21$. The fact that the effect of this reflection was not observed experimentally may be explained, as noted in Section 5:2.3, by the large experimental error in comparison with the magnitude of the effect. Also, because of the small range of angle over which the $(\bar{1}\bar{7}\bar{5})$ reflection is important, divergence in the incident beam in the electron microscope would tend to decrease the already small effect. Therefore, except for the perturbation due to the presence of the $(\bar{1}\bar{7}\bar{5})$ reflection, the Bloch wave parameters, as given by the three beam approximation, successfully explain, as in the case $\Delta\theta_{220} = 0.0$, the observed variation of ξ/ξ_0 , with $\Delta\theta_{\bar{1}33}$.

5:2.5 A Discussion of the Results Obtained at

$$\Delta\theta_{220} = 0.0 \text{ and } \Delta\theta_{\bar{1}33} = 0.25$$

A comparison of the results presented in Sections 5:2.1 and 5:2.3 shows that the presence of the $(\bar{1}33)$ non-systematic reflection results in marked changes in

the (220) extinction distance for both the case $\Delta\theta_{220} = 0.0$ and $\Delta\theta_{220} = 0.25$. The actual manner in which these changes occur, however, differs in two important aspects. The first of these is that a region of complex variation of the (220) intensity with depth is observed for $\Delta\theta_{\bar{1}33}$ negative in the case $\Delta\theta_{220} = 0.25$ but not in the case $\Delta\theta_{220} = 0.0$. The second difference involves the different ranges of positive values of $\Delta\theta_{\bar{1}33}$ over which the complex variation is observed in the two cases. For $\Delta\theta_{220} = 0.0$ this range is $.025 \leq \Delta\theta_{\bar{1}33} \leq .06$ but for $\Delta\theta_{220} = 0.25$ the complex region is observed to be $.10 \leq \Delta\theta_{\bar{1}33} \leq .14$.

It is of interest to compare these results with the results reported by Ayroles and Mazel (1970) in their study of the effects of the simultaneous excitation of pairs of non-systematic reflections on the (200) extinction distance in MgO. They found that, when the (024) and (224) pair of reflections were simultaneously tilted through their Bragg conditions, the (200) diffracted beam intensity showed a complex variation with depth through only one region of tilt located at $\Delta\theta_{024} = \Delta\theta_{224} \approx 0.0$. This behaviour is similar to the results obtained in this thesis in the case $\Delta\theta_{220} = 0.0$ except that, in this case, the complex region was found to occur at a marked positive deviation of the ($\bar{1}33$) reflection from its Bragg condition. Ayroles and Mazel (1970) also

examined the effects of the $(\bar{2}24)$ and (424) pair of reflections. For these reflections they observed two regions of tilt in which the (200) intensity variation with depth exhibited complex structure. As in the case $\Delta\theta_{220} = 0.25$ described in Section 5:2.3, one of these regions occurred for positive deviations and the other for negative deviations of the non-systematic reflections from their Bragg conditions.

Thus, the results obtained by Ayroles and Mazel (1970) in the more complex four-beam situation are, in general, very similar to those obtained in the simpler three-beam case. The occurrence of either one or two regions of complex behaviour as observed by them is, therefore, not specifically associated with the special case of the simultaneous excitation of two non-systematic reflections. Such behaviour, as has been shown in this thesis, also occurs in the more general case where only one non-systematic reflection is strongly excited.

Two important questions arise from the results presented in this thesis and those of Ayroles and Mazel (1970). The first of these is under what circumstances will one or two regions of complex intensity variation with depth be obtained in the presence of a non-systematic reflection. The second question is at what deviations of the non-systematic reflection from its

Bragg condition will these regions occur. The answer to these questions is of great importance to the electron microscopist who normally wishes to minimize the effects of non-systematic reflections. Bloch wave analyses can explain, for a particular case, why the complex regions with their corresponding marked changes in extinction distance take place. This was shown here in Sections 5:2.2 and 5:2.4 and by Ayroles (1971). However, such analyses do not answer the questions posed above for the general non-systematic case.

In order to predict under what circumstances and at what deviations of the non-systematic reflection from its Bragg condition complex regions will be obtained for the general case, analytical solutions of the dynamical theory have been examined. This examination has been carried out for the case of a single non-systematic reflection close to its Bragg condition since this represents the simplest and yet most commonly occurring non-systematic situation obtained in practice. The results of this examination are presented in the following Section.

5:2.6 Analysis of Extinction Distance Behaviour in Terms of the Three-Beam Analytical Solution of the Dynamical Theory

Before proceeding with this analysis, it is first useful to make some general observations of the Bloch wave analyses which have already been carried out. It can be seen by examining Figs. 17 and 18 that the branches of the dispersion surface important in determining the extinction distance are those with $\gamma^{(j)}$ values closest to $\pm 5.25 \times 10^{-4} \text{ \AA}^{-1}$. These values, $\pm 5.25 \times 10^{-4} \text{ \AA}^{-1}$, are the $\gamma^{(j)}$ values of the two important Bloch waves in the absence of the non-systematic reflection. Similarly, in Fig. 20, the important branches are those with $\gamma^{(j)}$ values lying closest to $1.23 \times 10^{-3} \text{ \AA}^{-1}$ and $-2.3 \times 10^{-4} \text{ \AA}^{-1}$. These are the $\gamma^{(j)}$ values of the two important Bloch waves for the case $\Delta\theta_{220} = 0.25$ when the $(\bar{1}33)$ reflection is absent.

A second observation that can be made from the Bloch wave analyses is that the regions of complex variation of beam intensity with depth, in general, take place when there is an interchange in the branches lying closest to the two beam $\gamma^{(j)}$ values. This can be seen in Fig. 17 where the complex region at $.025 \leq \Delta\theta_{\bar{1}33} \leq .075$ is associated with a marked departure of branch 1 away from the $\gamma^{(j)}$ value of $5.25 \times 10^{-4} \text{ \AA}^{-1}$

while branch 2 is asymptotically approaching this $\gamma^{(j)}$ value. Similar behaviour at the two complex regions found for the case $\Delta\theta_{220} = 0.25$ can be seen by examining the relevant branches of the dispersion surface in Fig. 20. Returning to Fig. 18, it can be seen that an interchange in branches also takes place at $\Delta\theta_{\bar{1}33} = -.05$. However, complex behaviour of the (220) intensity with depth is not observed at this point. This can be explained both by the fact that Bloch waves 2 and 3 have identical $\gamma^{(j)}$'s here and that the interchange in the importance of the contributions of these waves to the (220) intensity takes place over an extremely narrow region of $\Delta\theta_{\bar{1}33}$.

These observations drawn from the Bloch wave analyses in Sections 5:2.2 and 5:2.4 suggest the following approach with regard to a study of the three beam analytical solution to the dynamical theory. In order to determine under what conditions one or two regions of complex intensity behaviour are obtained in the presence of a non-systematic reflection, the analytical solution should be examined for those situations which give two equal $\gamma^{(j)}$ values. Secondly, in order to predict at what deviations of the non-systematic reflection from its Bragg condition the complex regions occur, the conditions under which an interchange takes place in the $\gamma^{(j)}$'s lying closest to the two beam $\gamma^{(j)}$

values should be determined.

The three beam analytical solution of the dynamical theory starts with the set of equations 2.10. When only three reflections are taken into account and a centrosymmetric crystal is assumed, this set of equations reduces to three equations of the form:

$$\begin{aligned}
 -\gamma C_o + \frac{U_g}{2K} C_g + \frac{U_h}{2K} C_h &= 0 \\
 \frac{U_g}{2K} C_o + (s_g - \gamma) C_g + \frac{U_{g-h}}{2K} C_h &= 0 \\
 \frac{U_h}{2K} C_o + \frac{U_{g-h}}{2K} C_g + (s_h - \gamma) C_h &= 0
 \end{aligned} \tag{5.1}$$

In order for non-zero solutions to exist for the C's, the determinant of the coefficients of the C's must equal zero. This results in the following cubic equation in γ ,

$$\begin{aligned}
 \gamma^3 - (s_g + s_h) \gamma^2 + (s_g s_h - \frac{U_g^2}{4K^2} - \frac{U_h^2}{4K^2} - \frac{U_{g-h}^2}{4K^2}) \gamma \\
 + (\frac{U_g^2}{4K^2} s_h + \frac{U_h^2}{4K^2} s_g - \frac{2U_g U_h U_{g-h}}{8K^3}) = 0
 \end{aligned} \tag{5.2}$$

The analytical expressions for the roots of this equation are, in general, quite complicated. However, Gjønnes and Høier (1971) in a study of line displacements

at Kikuchi line intersections, derived the following conditions that s_g and s_h must satisfy in order that two of the $\gamma^{(j)}$'s be equal. These conditions are

$$s_g = \left(\frac{U_g}{U_h}\right) \left(\frac{U_{g-h}^2 - U_h^2}{2KU_{g-h}}\right) \quad (5.3)$$

and

$$s_h = \left(\frac{U_h}{U_g}\right) \left(\frac{U_{g-h}^2 - U_g^2}{2KU_{g-h}}\right) \quad (5.4)$$

If the three reflections (000), (220) and ($\bar{1}33$) are now considered, $U_g = U_{220}$, $U_h = U_{\bar{1}33}$ and $U_{g-h} = U_{313} = -U_{\bar{1}33}$. In this case equation 5.3 reduces to $s_{220} = 0.0$ and equation (5.4) becomes

$$s_{\bar{1}33} = \frac{U_{\bar{1}33}^2 - U_{220}^2}{2KU_{220}} \quad (5.5)$$

Thus, it can be seen that two of the three branches of the dispersion surface will touch only when $\Delta\theta_{220} = 0.0$ and $\Delta\theta_{\bar{1}33}$ is such that equation 5.5 is satisfied. For $\Delta\theta_{220} \neq 0$, no value of $\Delta\theta_{\bar{1}33}$ will exist at which two of the Bloch waves will be degenerate. This is in agreement with the observations in Sections 5:2.2 and 5:2.4. For $\Delta\theta_{220} = 0.0$, branches 2 and 3 were found to have equal $\gamma^{(j)}$ values at $\Delta\theta_{\bar{1}33} = -.05$. However, for $\Delta\theta_{220} = 0.25$, the branches of the dispersion surface did not

touch at any value of $\Delta\theta_{133}$.

From the above discussion, it can be seen that, in general, two regions of complex variation of the intensity of the systematic reflection with depth will be observed when a single non-systematic reflection is tilted through its Bragg condition. For one particular deviation of the systematic reflection from its Bragg condition, however, one of these regions will disappear because two of the Bloch waves become degenerate in a previously complex region.

It is next of interest to examine the particular deviations of the non-systematic reflection from its Bragg condition at which these complex regions occur. The locations of these regions will be such that one occurs at a positive deviation and the other at a negative deviation of the non-systematic reflection from its Bragg condition. This can be seen from the following discussion starting with the set of equations 5.1. When the non-systematic reflection h is far from its Bragg condition, these equations reduce to the two-beam approximation

$$\begin{aligned}
 -\gamma C_o + \frac{U_g}{2K} C_g &= 0 \\
 \frac{U_g}{2K} C_o + (s_g - \gamma) C_g &= 0 .
 \end{aligned}
 \tag{5.6}$$

The values of γ satisfying these equations for non-zero

values of C_o and C_g are of the form

$$\gamma = [s_g \pm (s_g^2 + \frac{U_g^2}{K^2})^{1/2}] / 2.0 \quad (5.7)$$

Thus, it is seen that, of the two solutions for γ , one will be positive and the other negative. If we label these solutions $\gamma_2^{(1)}$ and $\gamma_2^{(2)}$, then, for $s_g = 0.0$, $|\gamma_2^{(1)}| = |\gamma_2^{(2)}|$. Also, for s_g positive, $|\gamma_2^{(1)}| > |\gamma_2^{(2)}|$ while for s_g negative $|\gamma_2^{(1)}| < |\gamma_2^{(2)}|$.

The values of these $\gamma_2^{(j)}$'s play an important role in determining the values of s_h at which the regions of complex periodicity occur. This can be seen from the following argument. If the terms in C_h are eliminated from equations 5.1 by algebraic substitution, the following pair of equations is obtained:

$$(-\gamma - \frac{U_h^2}{4K^2(s_h - \gamma)})C_o + (\frac{U_g}{2K} - \frac{U_h U_{g-h}}{4K^2(s_h - \gamma)})C_g = 0 \quad (5.8)$$

$$(\frac{U_g}{2K} - \frac{U_h U_{g-h}}{4K^2(s_h - \gamma)})C_o + (s_g - \gamma - \frac{U_{g-h}^2}{4K^2(s_h - \gamma)})C_g = 0$$

In these equations the terms $U_h^2/4K^2(s_h - \gamma)$, $U_{g-h}^2/4K^2(s_h - \gamma)$ and $U_h U_{g-h}/4K^2(s_h - \gamma)$ can be seen, by comparison with equation 5.6, to represent corrections to the two beam approximation due to the presence of the third reflection

h. The importance of these corrections is determined by the term $s_h - \gamma$ appearing in all the denominators of equations 5.8. When this term is large, the correction terms will be small and the values obtained for γ will be approximately those given by the two-beam approximation. On the other hand, when $s_h - \gamma$ is small, the correction terms will be large and there will be marked deviations of the γ 's from their two beam values. As discussed at the beginning of this Section, such marked deviations are associated with complex variations of the intensity with depth. These marked deviations of the γ 's from their two beam values will occur when s_h approaches one of the $\gamma_2^{(j)}$ values. This can be seen if $\gamma = \gamma_2^{(j)}$ is substituted into equations 5.8. The correction terms in these equations will then become infinite when $s_h = \gamma_2^{(j)}$.

Thus, the values of s_h at which complex periodicity will occur can be predicted by an examination of the $\gamma_2^{(j)}$ values found from a two-beam calculation in which only the directly transmitted and systematic reflections are considered. When the deviation of the systematic reflection from its Bragg condition is equal to zero, the regions of complexity should occur for equal positive and negative deviations of the non-systematic reflection from its Bragg condition as

$\gamma_2^{(1)} = -\gamma_2^{(2)}$. For $s_g \neq 0$, however, $\gamma_2^{(1)} \neq -\gamma_2^{(2)}$ and the complex regions will no longer be symmetric about the Bragg condition.

For example, in the three-beam situation examined previously in Sections 5:2.1 and 5:2.2, $\Delta\theta_{220} = 0.0$ and $\gamma_2^{(1)} = -\gamma_2^{(2)} = 5.25 \times 10^{-4} \text{ \AA}^{-1}$. The corresponding values of $s_{\bar{1}33}$ at which the complex regions are predicted to occur are $s_{\bar{1}33} = \pm 5.25 \times 10^{-4} \text{ \AA}^{-1}$ or $\Delta\theta_{\bar{1}33} \approx \pm .05$. An examination of Fig. 14 confirms this prediction for the case $\Delta\theta_{\bar{1}33} \approx +.05$. As discussed previously in this Section, complex behaviour of the (220) intensity will not be observed in this case for $\Delta\theta_{\bar{1}33}$ negative due to Bloch wave degeneracy. At $\Delta\theta_{220} = .25$ the values of $\gamma_2^{(1)}$ and $\gamma_2^{(2)}$ are $1.23 \times 10^{-3} \text{ \AA}^{-1}$ and $-2.3 \times 10^{-4} \text{ \AA}^{-1}$ respectively and the corresponding values of $\Delta\theta_{\bar{1}33}$ at which the complex regions are predicted to occur are $.128 \theta_{\bar{1}33}$ and $-.029 \theta_{\bar{1}33}$. An examination of Fig. 19 verifies the accuracy of these predictions.

In summary, it has been found that, as a non-systematic reflection is tilted through its Bragg condition, two complex regions with associated marked changes in extinction distance will, in general, be observed. For one deviation of the systematic reflection from its Bragg condition, however, one of the complex regions will vanish due to the degeneracy of

two of the Bloch waves. The particular deviation at which this occurs is determined by the Fourier coefficients of the lattice potential corresponding to the reflections involved. A second result that was obtained is that the locations of the regions of complex periodicity are dependent upon the $\gamma_2^{(j)}$'s corresponding to the Bloch waves excited in the absence of the non-systematic reflection. Since these $\gamma_2^{(j)}$'s depend upon the deviation of the systematic reflection from its Bragg condition, the location of the complex regions will also depend upon this deviation.

5:2.7 The Variation of Extinction Distance in the Presence of Higher Order Non-Systematic Reflections

The variation of the (220) extinction distance was examined as a function of the deviation of the higher order ($\bar{1}35$) and ($\bar{1}37$) non-systematic reflections from their Bragg conditions. Three sets of measurements were obtained in each case and compared with the theoretical variation as given by a many-beam calculation. The results of these measurements are shown in Figs. 22 and 23 for the ($\bar{1}35$) and ($\bar{1}37$) reflections respectively. These results were obtained for the case of $\Delta\theta_{220} = 0.0$. As can be seen by comparing these Figures to Fig. 14, the behaviour of the extinction distance in the presence

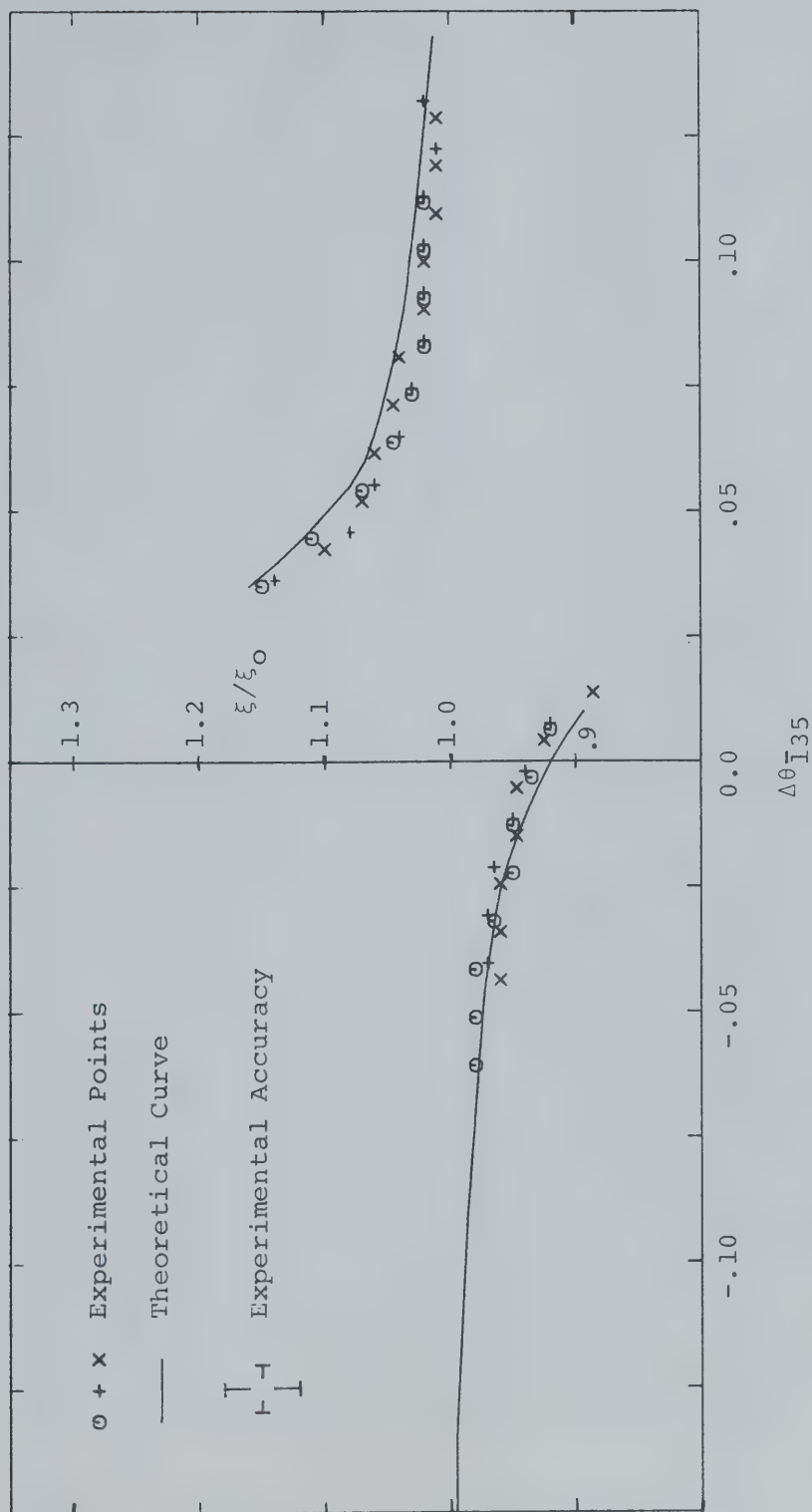


Fig. 22 The experimental and theoretical variation of the ratio ξ/ξ_0 for the (220) reflection in Si as a function of $\Delta\theta_{135}$. $\Delta\theta_{220} = 0.0$.

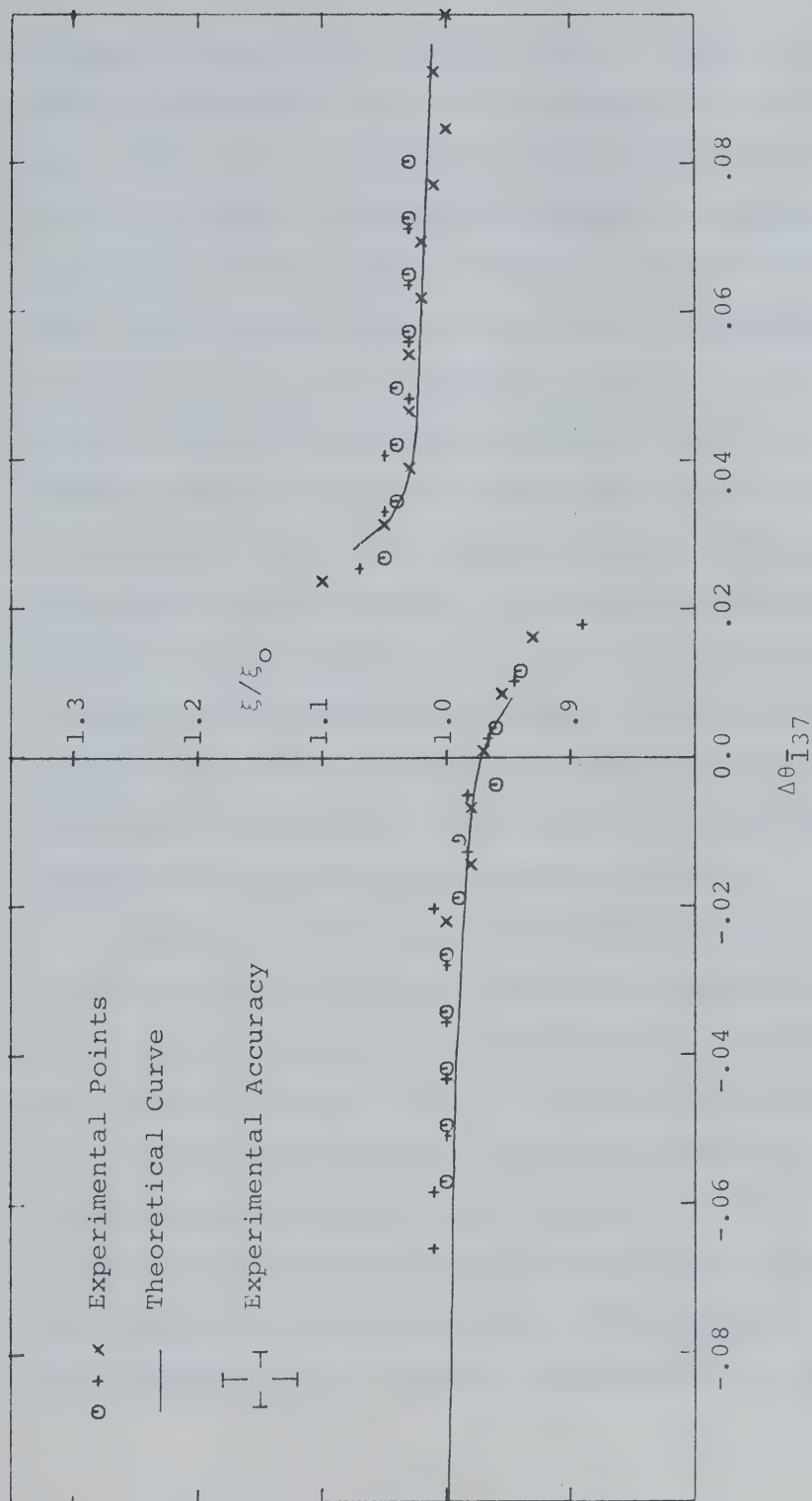


Fig. 23 The experimental and theoretical variation of the ratio ξ/ξ_0 for the (220) reflection in Si as a function of $\Delta\theta_{137}$. $\Delta\theta_{220} = 0.0$.

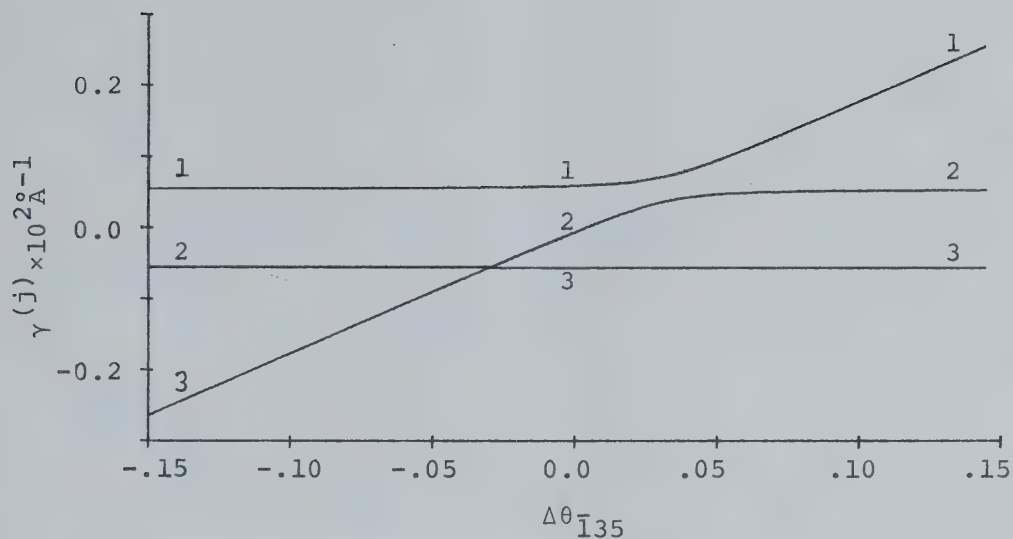
of these non-systematic reflections is very similar to that obtained for the ($\bar{1}33$) reflection in the case $\Delta\theta_{220} = 0.0$. For negative and small positive values of the deviation of the non-systematic reflection from its Bragg condition, the extinction distance falls below the reference value obtained in the absence of strongly excited non-systematic reflections. The smallest value of extinction distance is obtained at a small positive deviation, just less than the range of values for which the variation of the (220) intensity with depth becomes complex. For positive deviations just greater than the complex range, the extinction distance is found to have undergone a marked change in value and is now larger than the reference value. For even larger deviations, however, the extinction distance slowly decreases back towards this reference value.

Although the general behaviour of the extinction distance is similar for all three non-systematic reflections, there are significant differences in the results when the magnitudes of the variations of the extinction distance from the reference value are compared. This is particularly evident in the magnitudes of the jumps in the extinction distance which take place at the complex region. In the case of the ($\bar{1}33$) reflection, this jump corresponds to a change of approximately .45 in

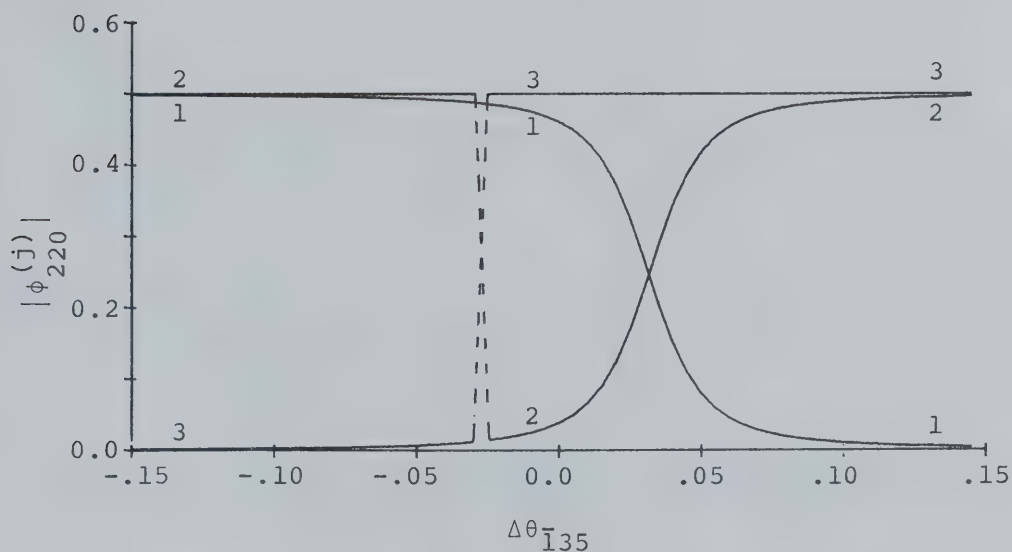
the ratio ξ/ξ_0 . For the ($\bar{1}35$) reflection, however, this change is only .25 and even less, .15, for the ($\bar{1}37$) reflection. Therefore, although the behaviour is qualitatively the same for all three reflections, quantitatively the magnitude of the effect decreases with increasing order of the non-systematic reflection.

5:2.8 Explanation for the Observed Behaviour in the Presence of Higher Order Reflections

It was seen in Sections 5:2.2 and 5:2.4 that the magnitude of the jump in extinction distance is determined by the distance between the branches of the dispersion surface whose corresponding Bloch waves are undergoing significant changes in their contributions to the (220) diffracted beam amplitude. In the case of the ($\bar{1}35$) and ($\bar{1}37$) reflections, Fig. 24a and 25a show the branches of the dispersion surface corresponding to the Bloch waves excited as these reflections are tilted through their Bragg conditions. From Figs. 24b and 25b, it can be seen that, in the complex regions, marked changes in the contributions of Bloch waves 1 and 2 to the (220) amplitude take place in the presence of these two reflections. This is in agreement with the results obtained for the ($\bar{1}33$) reflection in Section 5:2.2.

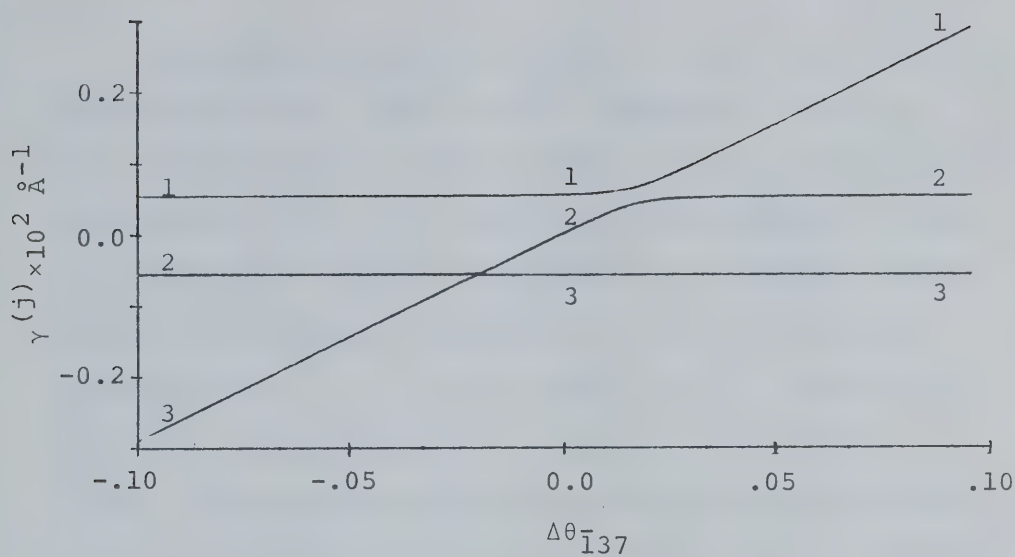


(a)

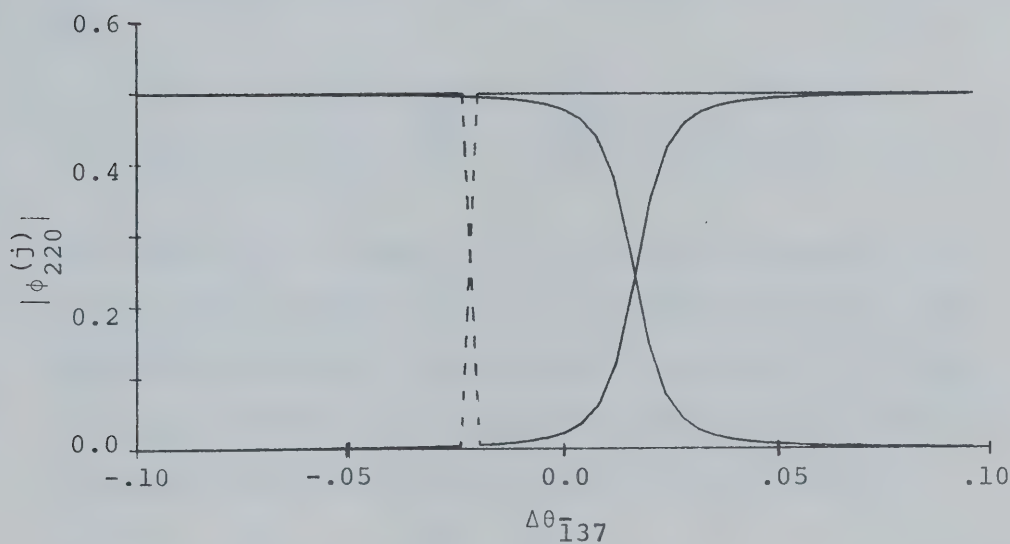


(b)

Fig. 24. (a) The variation with $\Delta\theta_{\bar{1}35}$ of the dispersion surface branches as given by a three beam calculation including the (000), (220) and ($\bar{1}35$) reflections. (b) The variation with $\Delta\theta_{\bar{1}35}$ of the contributions to the (220) amplitude of the Bloch waves corresponding to the branches in (a).



(a)



(b)

Fig.25. (a) The variation with $\Delta\theta_{\bar{1}37}$ of the dispersion surface branches as given by a three beam calculation including the (000), (220) and ($\bar{1}37$) reflections. (b) The variation with $\Delta\theta_{\bar{1}37}$ of the contributions to the (220) amplitude of the Bloch waves corresponding to the branches in (a).

If the minimum spacing in the complex region between branches 1 and 2 of the dispersion surface are compared for the ($\bar{1}33$), ($\bar{1}35$) and ($\bar{1}37$) reflections by examining Figs. 17, 24a and 25a respectively, it is seen that this spacing decreases with increasing order of the non-systematic reflection. For the situation examined here [i.e. $s_g = 0.0$ and $U_h = -U_{g-h}$ where g is the (220) reflection and h is one of ($\bar{1}33$), ($\bar{1}35$), ($\bar{1}37$)], this spacing can be found quite easily from the three beam analytical theory. In this case, the general expression for the γ 's as given in equation 5.2 reduces to

$$\gamma^3 - s_h \gamma^2 + \left(-\frac{U_g^2}{4K^2} - \frac{2U_h^2}{4K^2}\right)\gamma + \frac{U_g^2 s_h}{4K^2} - \frac{2U_g U_h^2}{8K^3} = 0.0 \quad (5.9)$$

An examination of Figs. 17, 24a and 25a shows that one of the roots of this equation is independent of s_h and, therefore, equal to $-U_g/2K$, one of the roots of the two beam approximation. If $\gamma + U_g/2K$ is divided into equation 5.9, the following quadratic equation is obtained:

$$\gamma^2 + \left(-s_h - \frac{U_g}{2K}\right)\gamma + \left(\frac{s_h U_g}{2K} - \frac{2U_h^2}{4K^2}\right) = 0.0 \quad (5.10)$$

The roots of this equation, as given by the standard formulae, are

$$\gamma = \frac{1}{2} \left\{ s_h + \frac{U_g}{2K} \pm \left[\left(s_h - \frac{U_g}{2K} \right)^2 + \frac{2U_h^2}{4K^2} \right]^{1/2} \right\}. \quad (5.11)$$

The value of s_h at which the difference between these two roots is a minimum can be found by differentiating the expression for this difference with respect to s_h and setting the result equal to zero. When this is done, it is found that the minimum difference occurs at $s_h = U_g/2K$ and is equal to $U_h/\sqrt{2} K$. Therefore, this spacing is directly proportional to the Fourier coefficient of the lattice potential of the non-systematic reflection involved. Since these coefficients decrease in magnitude with increasing h due to their dependence on the electron scattering factors, the decrease in spacing between branches 1 and 2 with increasing order of the non-systematic reflection is explained.

It should be noted, however, that the minimum spacing between branches 1 and 2 is not exactly equal to the observed jump in extinction distance. This jump is determined, instead, by the difference between the values of $\gamma^{(1)}$ and $\gamma^{(2)}$ calculated at two different deviations of the non-systematic reflection from its Bragg condition. These deviations depend upon the limits set for the region of complex variation in the (220) intensity with depth. For deviations just less than those associated with the complex region, the

extinction distance is given by $1/(\gamma^{(1)} - \gamma^{(3)})$. However, for deviations just larger than the complex region, the extinction distance is given by $1/(\gamma^{(2)} - \gamma^{(3)})$. Since $\gamma^{(3)}$ is a constant in this region, the jump in extinction distance will depend upon the difference between $\gamma^{(1)}$ and $\gamma^{(2)}$. However, since these $\gamma^{(j)}$'s are calculated at slightly different orientations, this difference will not be exactly equal to $U_h/\sqrt{2}$ K.

Thus, it can be seen that the magnitude of the effect of a non-systematic reflection depends upon its Fourier coefficient of the lattice potential. Since these coefficients, in general, decrease with increasing order of a reflection, the observed decreasing effects on extinction distance with increasing order of the non-systematic reflections are explained.

5:3 The Effects of a Non-Systematic Reflection on Anomalous Absorption

Recent work by Sheinin (1970B) has shown that, in the case where only systematic reflections are assumed to be present, the effects of anomalous absorption can be drastically altered if the deviations of these reflections from their Bragg conditions are changed by tilting the crystal. This behaviour results

primarily from the fact that changes in Bloch wave excitation occur under these circumstances. Thus, for example, when the lowest order reflection, g , of a systematic set is in the exact Bragg condition, pronounced effects of anomalous absorption can normally be observed. The reason for this is that the two Bloch waves which make a significant contribution to the diffracted beam intensity at this orientation have widely differing absorption coefficients. If the crystal is tilted outside the reflection $3g$ in the Bragg condition, on the other hand, the effects of anomalous absorption are found to be small. The explanation for this behaviour lies in the fact that in thick crystals, the two Bloch waves which make a significant contribution to the diffracted beam intensity have nearly equal absorption coefficients.

Changes in Bloch wave excitation also occur in the presence of non-systematic reflections as was seen in Section 5:2 and as has been shown previously by Lehmpfuhl and Reissland (1968), Ayroles (1971) and Lehmpfuhl (1972). To examine what effects a non-systematic reflection might have on anomalous absorption, the variations of the Bloch wave absorption coefficients have been calculated as a function of the deviation of a non-systematic reflection from its Bragg condition. The

effects of these variations on the contributions of the different Bloch waves to the diffracted beam amplitude in thick specimens were then examined. This was done to determine the changes in anomalous absorption effects which take place in the presence of a non-systematic reflection.

5:3.1 Variation of Bloch Wave Absorption Coefficients in the Presence of a Non-Systematic Reflection

Using expression 2.32, the absorption coefficients, $q^{(j)}$, of the three important Bloch waves excited for the situation examined in Section 5:2.1 were calculated. This situation consisted of maintaining the (220) reflection in its Bragg condition while the deviation of the ($\bar{1}33$) reflection was systematically varied about $\Delta\theta_{\bar{1}33} = 0.0$. The results of the calculations are shown in Fig. 26. Each coefficient has been numbered so that its corresponding Bloch wave is associated with the similarly numbered branch of the dispersion surface in Fig. 17. The dashed line segments in Fig. 26 at $\Delta\theta_{\bar{1}33} \approx -.05$ show the region of degeneracy of branches 2 and 3 of the dispersion surface. As stated in Section 5:2.2, however, this region is quite small and does not affect the results.

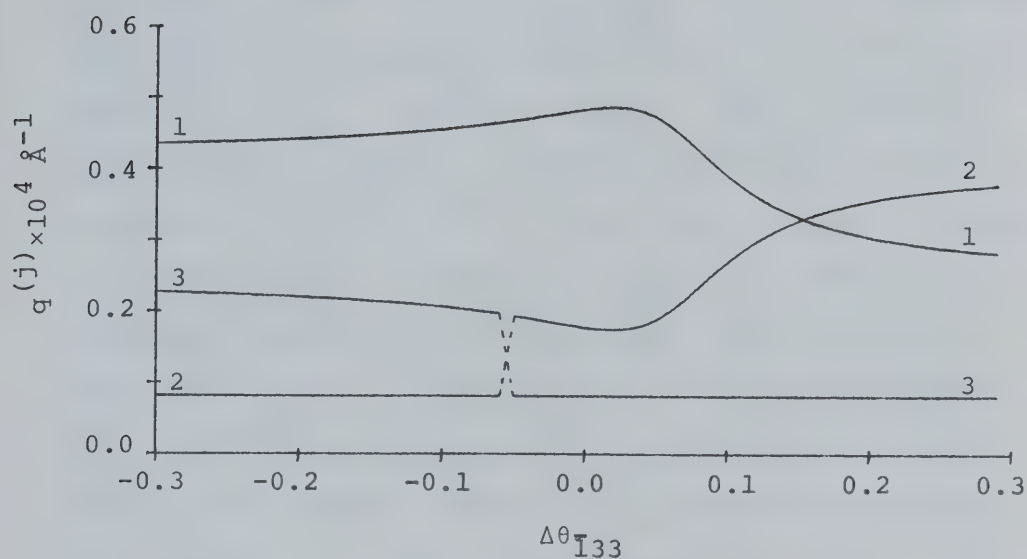


Fig. 26 The variation of the Bloch wave absorption coefficients, $q^{(j)}$, with $\Delta\theta_{\bar{1}33}$, the deviation of the $(\bar{1}33)$ reflection from its Bragg condition. $\Delta\theta_{\bar{1}33}$ is given in fractions of $\theta_{\bar{1}33}$, the $(\bar{1}33)$ Bragg angle.

As can be seen in Fig. 28, the absorption coefficients show a strong dependence on $\Delta\theta_{\bar{1}33}$, indicating that the presence of the non-systematic reflection does have a pronounced effect on the values of these coefficients. For example, $q^{(1)}$, which has an initial value of $.44 \times 10^{-4} \text{ \AA}^{-1}$ at $\Delta\theta_{\bar{1}33} = -.30$, slowly increases as $\Delta\theta_{\bar{1}33}$ increases until it reaches a maximum of $.48 \times 10^{-4} \text{ \AA}^{-1}$ at $\Delta\theta_{\bar{1}33} = .02$. From there it decreases to a value of $.29 \times 10^{-4} \text{ \AA}^{-1}$ at $\Delta\theta_{\bar{1}33} = .30$. $q^{(2)}$, on the other hand, is constant and equal to $.08 \times 10^{-4} \text{ \AA}^{-1}$ in the range $-.3 \leq \Delta\theta_{\bar{1}33} \leq -.05$. At $\Delta\theta_{\bar{1}33} \approx -.05$, it jumps in magnitude to a value of $.2 \times 10^{-4} \text{ \AA}^{-1}$ before decreasing to a minimum of $1.7 \times 10^{-4} \text{ \AA}^{-1}$ at $\Delta\theta_{\bar{1}33} = .02$. It then increases to a value of $.38 \times 10^{-4} \text{ \AA}^{-1}$ at $\Delta\theta_{\bar{1}33} = .30$. Finally, the absorption coefficient for Bloch wave 3 has an initial value of $.23 \times 10^{-4} \text{ \AA}^{-1}$ at $\Delta\theta_{\bar{1}33} = -.30$ before decreasing to $.2 \times 10^{-4} \text{ \AA}^{-1}$ at $\Delta\theta_{\bar{1}33} \approx -.05$. At this point it drops sharply to a value of $.08 \times 10^{-4} \text{ \AA}^{-1}$ and then remains constant through the range $-.05 \leq \Delta\theta_{\bar{1}33} \leq .30$.

In order to interpret these variations of the $q^{(j)}$'s with $\Delta\theta_{\bar{1}33}$, a study was carried out of the channelling of the Bloch waves in the crystal. Following the procedure of Metherell and Spring (1970), Bloch wave intensity distributions across a section of crystal perpendicular to the direction of current flow were calculated for the three Bloch waves at orientations of $\Delta\theta_{\bar{1}33}$

equal to $-.30$, $.02$ and $.30$. These distributions are shown in Fig. 27. Here, the light regions correspond to zones of high current flow while the lines extending vertically from the top and bottom of each display and those extending diagonally from the sides show the locations of (220) and ($\bar{1}33$) planes respectively. The black disks show the positions of the atomic rows which lie perpendicular to the plane of the displays.

Earlier, in Section 2:3 it was shown that the inelastic scattering potential is positive and localized at the atomic positions. Thus, Bloch waves whose intensities are also concentrated at these points will tend to be strongly absorbed. On the other hand, Bloch waves whose intensities are concentrated away from the atomic positions will tend to be well transmitted. Returning to Fig. 27a, it can be seen that at $\Delta\theta_{\bar{1}33} = -.30$, the intensity of Bloch wave 1 is concentrated along the (220) planes and, moreover, is localized near the atoms, thus resulting in it being highly absorbed. Bloch wave 2 is concentrated between the (220) planes and, therefore, is weakly absorbed while the intensity distribution of Bloch wave 3 is nearly uniform resulting in moderate absorption. At $\Delta\theta_{\bar{1}33} = .02$, as seen in Fig. 27b, the intensity of Bloch wave 1 is now very strongly concentrated at the atomic positions resulting in even higher

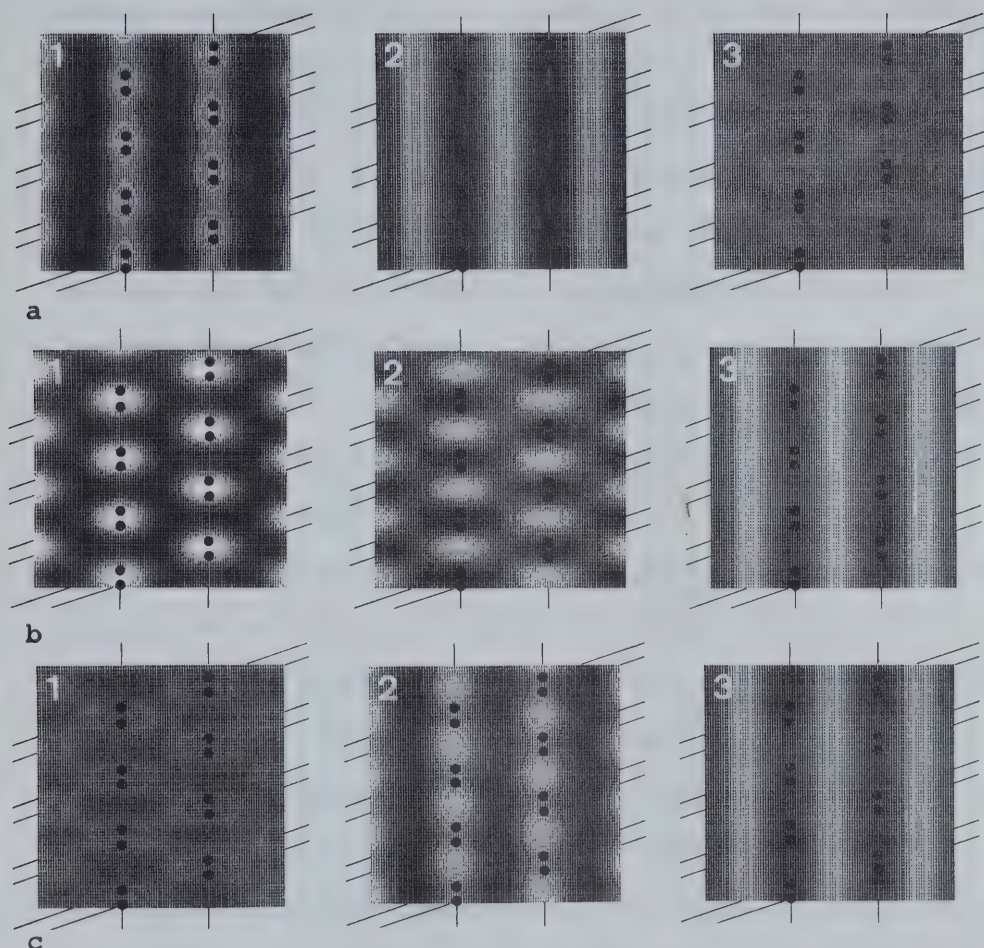


Fig.27. The intensity distribution of the 3 Bloch waves across a section of crystal perpendicular to the direction of current flow for values of $\Delta\theta_{\bar{1}33}$ of (a) $-.30$, (b) $.02$ and (c) $.30$. The light regions correspond to zones of high current flow while the lines extending vertically from the top and bottom of each display and those extending diagonally from the sides show the locations of the (220) and $(\bar{1}33)$ planes respectively. The black disks show the positions of the atomic rows which lie perpendicular to the plane of the display.

absorption than at $\Delta\theta_{\bar{1}33} = -.30$. In the case of Bloch wave 2, the intensity, although mainly lying along the (220) planes, is strongly concentrated between the atoms and, thus, a relatively low absorption coefficient is expected. For Bloch wave 3, weak absorption should be obtained as its intensity is principally located between the (220) planes. At $\Delta\theta_{\bar{1}33} = .30$, the intensity of Bloch wave 1, as seen in Fig. 27c, is nearly uniformly distributed with the result that this wave is now only moderately absorbed. Bloch wave 2 is no longer as strongly concentrated between the atoms on the (220) planes as at $\Delta\theta_{\bar{1}33} = .02$ with the result that it has become more strongly absorbed. Bloch wave 3 is concentrated between the (220) set of planes and, therefore, is weakly absorbed. These results indicate, therefore, that the non-systematic reflection has a pronounced effect on the channelling characteristics of the Bloch waves and that, as in the two-beam and systematic cases, these characteristics offer a physical explanation for the differences in the Bloch wave absorption coefficients.

5:3.2 Effects of the Variation of the Absorption Coefficients with $\Delta\theta_{133}$ on the Contributions of the Different Bloch Waves to the Diffracted Beam Intensity

In Section 2:3.2, it was shown that the amplitude of the g 'th diffracted beam at a crystal depth z is given by the expression

$$u_g(z) = \sum_{j=1}^N \phi_g^{(j)}(z) \exp(2\pi i \gamma^{(j)} z) \quad (5.12)$$

where the summation is over all Bloch waves excited and

$$\phi_g^{(j)}(z) = C_o^{(j)} C_g^{(j)} \exp(-2\pi q^{(j)} z) \quad (5.13)$$

From these two expressions, it can be seen that the contribution of a particular Bloch wave to the diffracted beam amplitude at a depth z is determined by $\phi_g^{(j)}(z)$. Therefore, it depends on both the product $C_o^{(j)} C_g^{(j)}$ and the exponential term $\exp(-2\pi q^{(j)} z)$. Thus, it can be seen that a change in the absorption coefficient of a Bloch wave will affect the contribution of that wave to the diffracted beam amplitude.

Before discussing the effects of the variations of the absorption coefficients with $\Delta\theta_{133}$ on the Bloch wave contributions, it is first useful to consider the situation of a single low-order reflection, g , in its

exact Bragg condition. Under these circumstances, only two of the Bloch waves, numbered 1 and 2 (Humphreys and Fisher, 1971), are strongly excited and the intensity of the diffracted beam g at a depth z is given by the expression

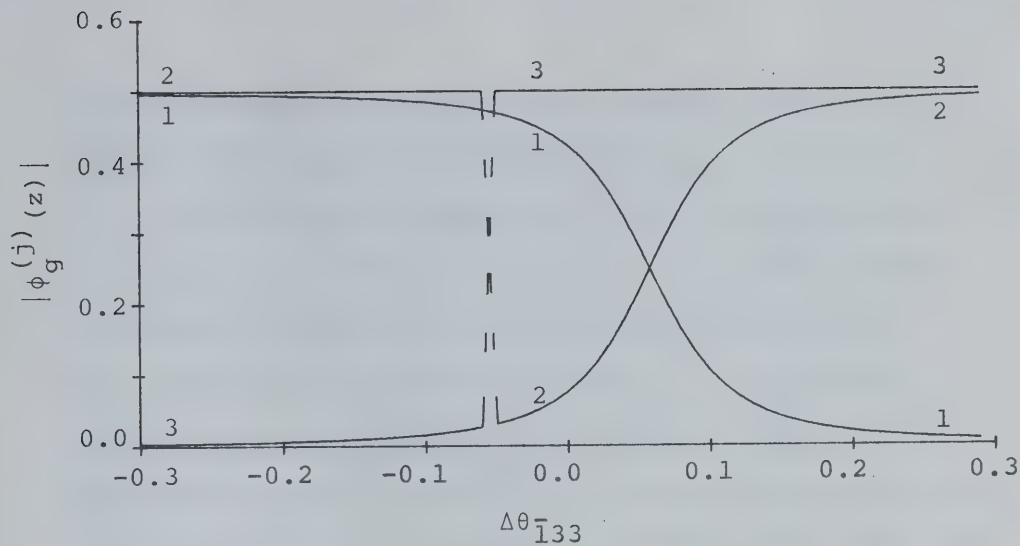
$$u_g^*(z)u_g(z) = \{\phi_g^{(1)}(z)\}^2 + \{\phi_g^{(2)}(z)\}^2 + 2\phi_g^{(1)}(z)\phi_g^{(2)}(z)\cos\{2\pi(\gamma^{(1)} - \gamma^{(2)})z\} \quad (5.14)$$

It can be seen from this expression that excellent thickness fringe contrast will be obtained near the top surface of the crystal since in this case, $|\phi_g^{(1)}(z)| \approx |\phi_g^{(2)}(z)|$. However, because the absorption coefficient of Bloch wave 1 is usually five to ten times greater than that of Bloch wave 2, $|\phi_g^{(1)}(z)| \ll |\phi_g^{(2)}(z)|$ in thick regions of the crystal and equation 5.14 shows that poor fringe contrast will result, although appreciable intensity is still present due to the $\{\phi_g^{(2)}(z)\}^2$ term. This is the anomalous absorption effect described earlier in Section 2:3.2.

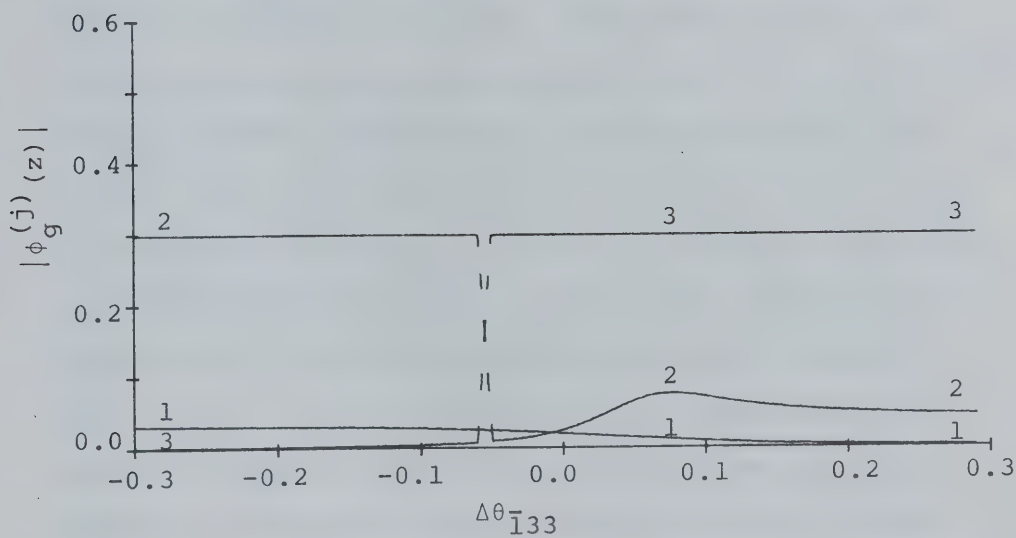
For a more general crystal orientation than that considered above, such as the case when a non-systematic reflection is present, the magnitudes of the $\phi_g^{(j)}(z)$'s need not be equal at the top surface of the crystal. However, the effect of the differences in the absorption coefficients is to still change the relative

magnitudes of the $\phi_g^{(j)}(z)$'s with increasing thickness. Thus, by examining how these relative magnitudes, as defined by the ratio $|\phi_g^{(j)}(z)|/|\phi_g^{(i)}(z)|$, vary with depth in the crystal, the effects of anomalous absorption on thickness fringe contrast due to the dependence of the $q^{(j)}$'s on $\Delta\theta_{\bar{1}33}$ can be predicted.

The variations of the $|\phi_g^{(j)}(z)|$'s of the three important Bloch waves with $\Delta\theta_{\bar{1}33}$ at the top or incident surface of the crystal and at a depth of 10,000 Å are shown in Fig. 28. It is first of interest to examine the situation at large deviations from the Bragg condition. At $\Delta\theta_{\bar{1}33} = -.30$ and at the top surface of the crystal $|\phi_g^{(1)}(z)| \approx |\phi_g^{(2)}(z)| \gg |\phi_g^{(3)}(z)|$. At a depth of 10,000 Å, on the other hand, all of the Bloch waves have been attenuated, but Bloch wave 1 much more so than Bloch wave 2, with the result that $|\phi_g^{(2)}(z)| \gg |\phi_g^{(1)}(z)|$. The ratio $|\phi_g^{(1)}(z)|/|\phi_g^{(2)}(z)|$ changes from ≈ 1.0 at the top surface to .11 at 10,000 Å. Similarly, at $\Delta\theta_{\bar{1}33} = .30$ and at the top surface $|\phi_g^{(2)}(z)| \approx |\phi_g^{(3)}(z)| \gg |\phi_g^{(1)}(z)|$. At a depth of 10,000 Å, however, Bloch wave 2 has now been attenuated much more than Bloch wave 3 with the result that $|\phi_g^{(2)}(z)|/|\phi_g^{(3)}(z)| \approx .15$. These results indicate that anomalous absorption effects will be important for both large positive and negative deviations of the ($\bar{1}33$) reflection from its Bragg condition although



(a)



(b)

Fig.28 The variation of the $|\phi_g^{(j)}(z)|$'s, the contributions of the different Bloch waves to the (220) diffracted beam amplitude, with $\Delta\theta_{\bar{1}33}$ at (a), the top surface of the crystal and (b), a depth of 10000 Å.

slightly better thickness fringe contrast should be observed for $\Delta\theta_{\bar{1}33} = .30$ than for $\Delta\theta_{\bar{1}33} = -.30$.

It is next of interest to look at the variation of the relative values of the $|\phi_g^{(j)}(z)|$'s with crystal thickness for small positive and negative values of $\Delta\theta_{\bar{1}33}$ where the variations in the $q^{(j)}$'s are more marked. Figs. 28a and 28b show that, at $\Delta\theta_{\bar{1}33} = -.10$, the values of $|\phi_g^{(1)}(z)|/|\phi_g^{(2)}(z)|$ near the top surface of the crystal and at a depth of 10000 Å are about 1 and 0.1 respectively. At $\Delta\theta_{\bar{1}33} = +.10$ the corresponding values of $|\phi_g^{(2)}(z)|/|\phi_g^{(3)}(z)|$ are about 0.7 and 0.25. These ratios indicate that a marked decrease in thickness fringe contrast occurs with increasing thickness for $\Delta\theta_{\bar{1}33} = -.01$ ($|\phi_g^{(1)}(z)|/|\phi_g^{(2)}(z)|$ decreases by a factor of 10) while for $\Delta\theta_{\bar{1}33} = +.10$, the decrease in contrast is relatively small ($|\phi_g^{(2)}(z)|/|\phi_g^{(3)}(z)|$ decreases by a factor of 3). As a consequence, thickness fringes in thick crystals should exhibit considerably better contrast at small positive values of $\Delta\theta_{\bar{1}33}$ than for small negative values even though in thin crystals, somewhat worse contrast is expected. Since a decrease in fringe contrast with crystal thickness is associated with anomalous absorption, these results indicate that for small negative values of $\Delta\theta_{\bar{1}33}$, anomalous absorption effects are much more pronounced than for small positive values.

The enhanced thickness fringe contrast at small positive values of $\Delta\theta_{\bar{1}33}$, noted in the previous paragraph, should result in thickness fringes being observed there in thicker crystals than for small negative values. That this is, in fact, so can be seen from Figs. 29a and 29b which show a computed and experimental (220) dark field image of a bent wedge-shaped Si specimen. The computed image in Fig. 29a was obtained by calculating the variation of the (220) diffracted beam intensity with depth for a range of values of $\Delta\theta_{\bar{1}33}$ from +.21 to -.21 and with the (220) reflection in its exact Bragg condition. These calculated results were then displayed using a computer line printer to give a two dimensional intensity plot (Head, 1967; Spring and Steeds, 1970). The experimental results in Fig. 29b show thickness fringes in a Si specimen which was found bent in such a manner that approximately the same range of values of $\Delta\theta_{\bar{1}33}$ and $\Delta\theta_{220}$ were obtained as in the computed image. It can be seen in these Figures that the thickness fringes are predicted and, indeed, are observed to be visible in thicker regions of the crystal for $\Delta\theta_{\bar{1}33}$ positive than for $\Delta\theta_{\bar{1}33}$ negative. Thus, the effects of anomalous absorption are more pronounced for small negative values of $\Delta\theta_{\bar{1}33}$ than for small positive values.

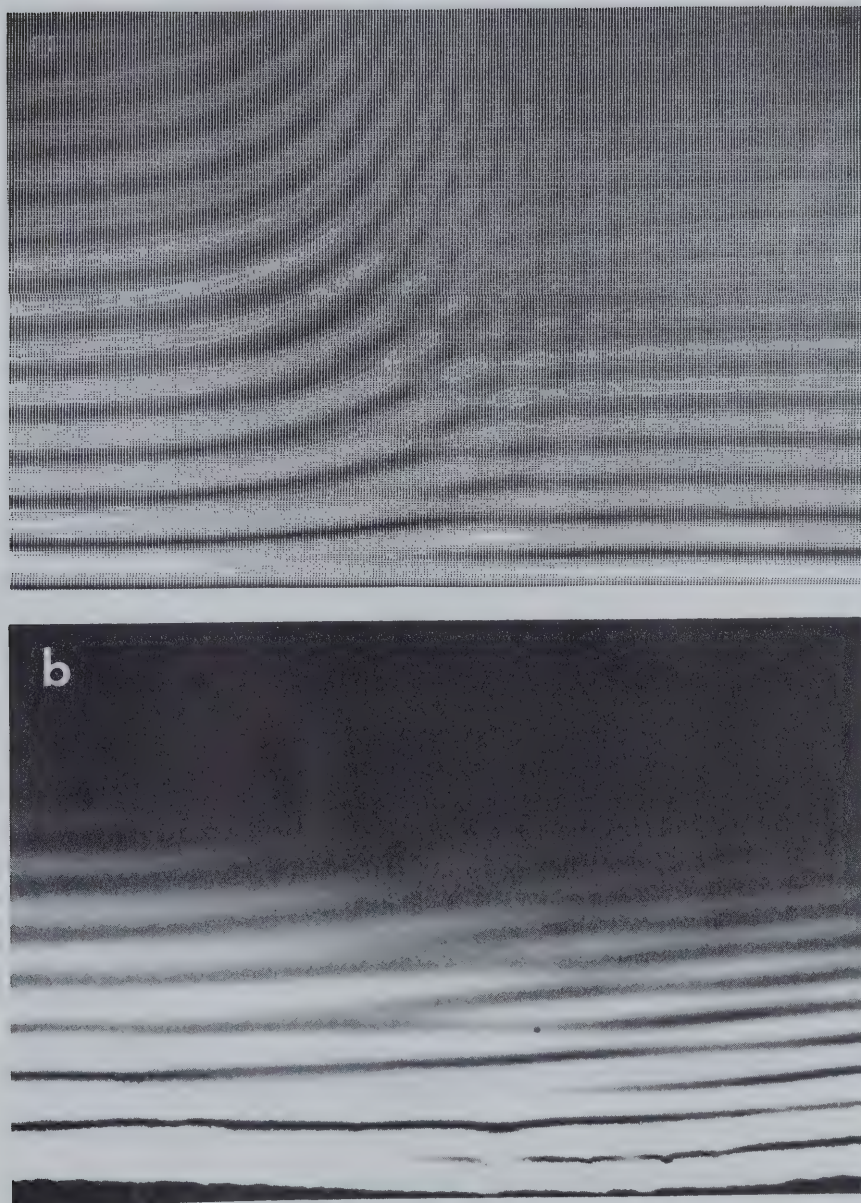


Fig.29. A computed, a, and experimental, b, (220) dark field image of a bent wedge-shaped silicon crystal. The (220) reflection is in its Bragg condition while $\Delta\theta_{133}$ varies from + to - in moving from left to right.

Finally, it is of interest to compare the effects of anomalous absorption obtained close to the Bragg condition of the non-systematic reflection with those obtained in the two beam limit (i.e. for large values of $|\Delta\theta_{\bar{1}33}|$). It was found, that under these circumstances, the values of $|\phi_g^{(1)}(z)|/|\phi_g^{(2)}(z)|$ at the top surface and a depth of 10,000 Å are 1 and 0.12 respectively. A comparison of these values with those for the small values of $\Delta\theta_{\bar{1}33}$ quoted above indicate that anomalous absorption effects for large values of $|\Delta\theta_{\bar{1}33}|$ are very similar to those obtained for small negative values. For small positive values of $\Delta\theta_{\bar{1}33}$, on the other hand, the marked changes in the effect of anomalous absorption which have already been noted occur. This behaviour is consistent with the results in Fig. 26 which show that small changes in absorption coefficient occur for negative values of $\Delta\theta_{\bar{1}33}$ whereas marked changes occur for positive values.

5:3.3 Effects of Beam Divergence on Thickness Fringe Contrast

The results presented in Section 5:3.2 on the contrast associated with thickness fringes assumed a parallel incident beam of electrons. In practice, however, a parallel beam is not achieved and, instead,

the electrons are incident on the specimen through a small angular range, known as the beam divergence. This divergence is of particular importance when the extinction distance is very sensitive to crystal orientation. In such cases, thickness fringe contrast in thicker regions of the crystal may be diminished due to interference effects. This is because in these thick regions intensity maxima associated with electrons at one angle of incidence may coincide with the intensity minima associated with electrons at a slightly different angle of incidence and thus, result in diminished contrast.

It will be noted by examining Fig. 14 that at $\Delta\theta_{\bar{1}33} \approx .09$, where the effects of anomalous absorption are smallest, the rate of change of extinction distance with $\Delta\theta_{\bar{1}33}$ is relatively large. In order to estimate how beam divergence might affect thickness fringe contrast at this orientation, a thickness fringe profile was calculated by taking the average of three profiles corresponding to $\Delta\theta_{\bar{1}33} = .083, .090$ and $.097$. These orientations were chosen as they correspond closely to an angular beam divergence of $.015^\circ$. This was approximately the value of divergence at which most of the experimental results described here were obtained as determined from measurements of diffraction spot size.

The thickness fringe profile found in this way is shown in Fig. 30b, while Fig. 30a shows a normal profile calculated for $\Delta\theta_{\bar{1}33} = .09$ only. As can be seen by comparing these two figures, the effect of the beam divergence is to significantly decrease the fringe contrast in thicker regions of the specimen. If contrast is defined as $\Delta I/I$ where ΔI is the difference between the maximum and minimum values of intensity observed in the region of thickness considered, and I is the mean intensity at the same depth, then, at $z \approx .8\mu$, $\Delta I/I \approx 1.33$ for a parallel electron beam situation. However, when beam divergence is taken into account in the manner described, $\Delta I/I$ is only equal to .85 at the same depth. Even with this marked reduction in $\Delta I/I$ the fringe contrast at $\Delta\theta_{\bar{1}33} = .09$ is still significantly better than that obtained at $\Delta\theta_{\bar{1}33} = -.09$. This can be seen by comparing Figs. 30b and 31a. Fig. 31a shows the variation of the (220) intensity with depth for $\Delta\theta_{\bar{1}33} = -.09$ again taking into account a beam divergence of $.015^\circ$. Here, at a depth of $z \approx .8\mu$, $\Delta I/I \approx .43$ and the contrast is only half as good as that at $\Delta\theta_{\bar{1}33} = .09$. It is interesting to note that, for thick crystals, the contrast at $\Delta\theta_{\bar{1}33} = .09$ is also slightly better than at $\Delta\theta_{\bar{1}33} = .70$, where the effects of non-systematic reflections are very small. This can

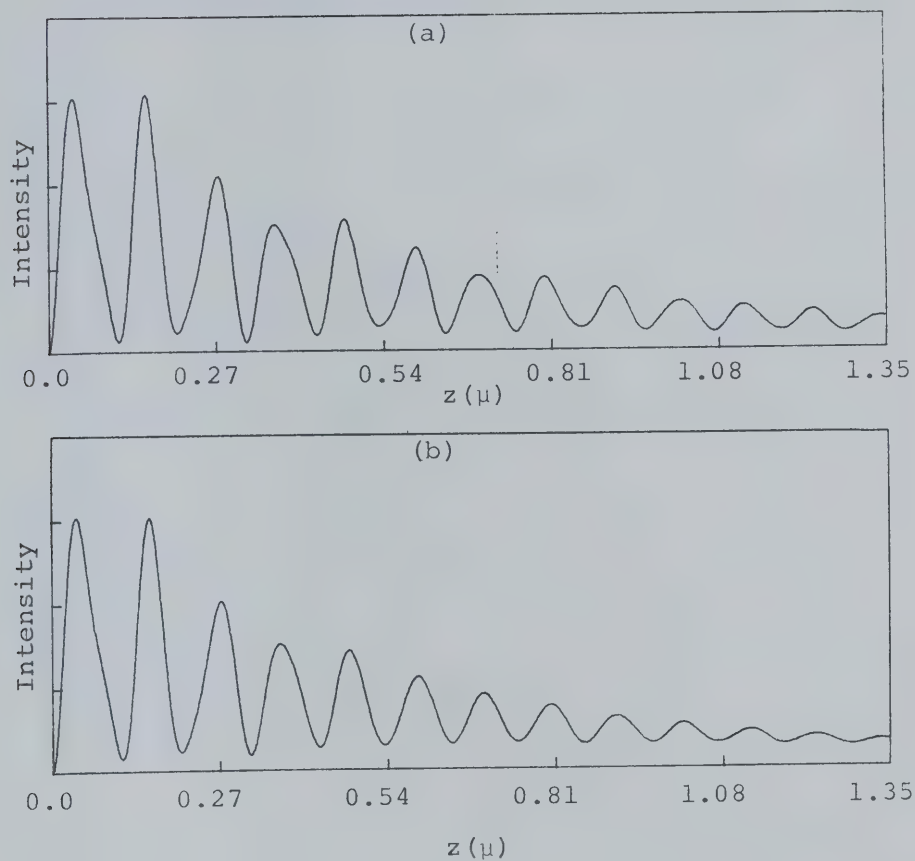


Fig. 30 The computed variation of the (220) intensity with depth, z , for $\Delta\theta_{133} = .09$ for the cases of (a) a parallel incident electron beam and (b) an incident electron beam with an angular divergence of 0.015° .

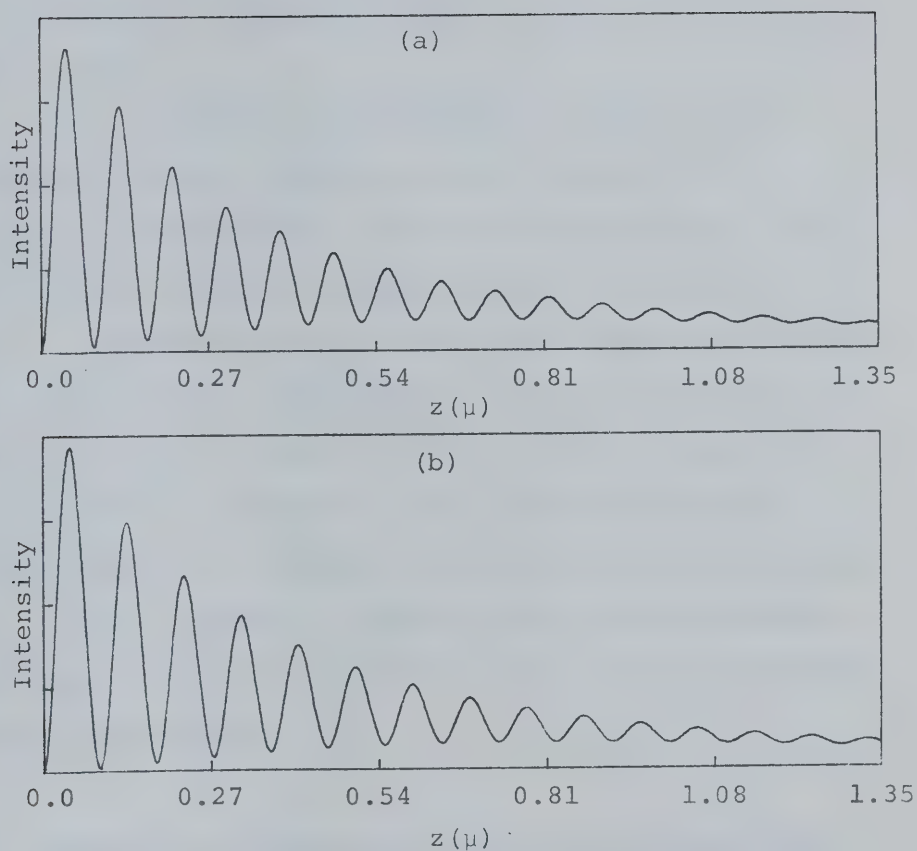


Fig. 31 The computed variation of the (220) intensity with depth, z , taking into account a beam divergence of $.015^\circ$ for (a) $\Delta\theta_{\bar{1}33} = -.09$ and (b) $\Delta\theta_{\bar{1}33} = .70$.

be seen by comparing Figs. 31b and 30b where Fig. 31b shows a thickness intensity profile computed at $\Delta\theta_{133} = .70$ taking beam divergence into account. Here, at $z = .8\mu$, $\Delta I/I \approx .75$ as compared to $\Delta I/I \approx .85$ for $\Delta\theta_{133} = .09$.

Thus, although beam divergence results in a decrease in fringe contrast in the region of low anomalous absorption due to interference effects, this contrast will still be better in thick crystals at $\Delta\theta_{133} = .09$ than at $\Delta\theta_{133} = -.09$, i.e. where the effect of a non-systematic reflection is small as was seen in Fig. 29. Also, it should be noted that divergence is an experimental problem and that the angle can be reduced further by suitable adjustment of the condenser lens current. However, proportionally longer exposure times would then be required to obtain properly exposed electron micrographs.

5:4 Variation of Bright and Dark Field Rocking Curves in the Presence of Non-Systematic Reflections

When examining specimens in the electron microscope, it is usually desirable to orient the specimen so that the maximum intensity is obtained in the image. The orientation at which this maximum penetration of the specimen by the electrons is obtained, can be found

theoretically by calculations of the variation of beam intensity with orientation. The resulting curves are commonly known as rocking curves. These curves were first used by several investigators to examine the effects of anomalous absorption on the directly transmitted and diffracted beam intensities of perfect crystals. Hashimoto, Howie and Whelan (1960, 1962) showed that, in the two-beam case, the bright field intensity was a maximum when the deviation parameter s_g was slightly positive, while the diffracted beam intensity was maximum at $s_g = 0$. Their results, which were in good agreement with experimental observations of absorption bands in bent crystals, have proven to be of considerable value to the electron microscopist in helping him choose the diffraction conditions for which optimum electron transmission can be obtained.

The two beam theory does not, however, take into account the possible effects of additional reflections which might be excited. The effect of systematic reflections on rocking curves was first investigated by Howie and Whelan (1960). They showed that, at low accelerating voltages, these reflections did not result in any qualitative changes in the predictions of the two beam theory. A number of authors (Humphreys and Lally, 1970; Humphreys, Thomas, Lally and Fisher, 1971;

Humphreys, 1972) have recently examined the effects of these reflections at very high accelerating voltages. In this case, they found that these effects can be of much greater significance, resulting in a maximum in the directly transmitted intensity which may occur anywhere from the symmetry position to $3g$ near its Bragg condition. The exact location depended upon the accelerating voltage and material being considered.

None of the theoretical rocking curves reported in the literature, up to the present time, have, however, taken the effects of non-systematic reflections into account. Since the excitation of these reflections is dependent on crystal orientation, the possibility exists that, for some orientations, non-systematic rocking curves may be significantly different from those obtained by taking only systematic reflections into account. An investigation (Sheinin and Cann, 1971) was undertaken with a view to exploring this possibility. In order to study the effects of non-systematic reflections in a variety of circumstances, rocking curves were obtained for a number of crystal orientations at both low and high accelerating voltages.

5:4.1 Procedures Used in Calculating Theoretical Rocking Curves

The rocking curve calculations were carried out for molybdenum at accelerating voltages of 150 and 1000 kV. Absorption was taken into account in the usual manner by assuming a complex part of the lattice potential. The absorption parameters used were those obtained experimentally by Sheinin, Botros and Cann (1970), while the electron scattering factors employed were those tabulated by Smith and Burge (1962). The Fourier coefficients of the lattice potential were temperature corrected using a Debye-Waller B factor of $.20 \text{ \AA}^2$.

The orientations used in the calculations were obtained in the following manner. The (110), (220), ... row of reflections was assumed to constitute the systematic set. The initial orientation for each rocking curve calculated was defined by specifying initial values of deviation parameters s_{110} and $s_{1\bar{1}0}$. The initial value of s_{110} chosen in each calculation was such that $s_{110} = s_{1\bar{1}0}$ (i.e. the symmetry position of the (110) row of reflections). In order to study the effects of different non-systematic reflections, the initial values of $s_{1\bar{1}0}$ were varied from $s_{1\bar{1}0} = s_{110}$ (the symmetry position of the (1 $\bar{1}$ 0) row of reflections) to a value of $s_{1\bar{1}0}$ corresponding to the (10, $\bar{1}$ 0,0)

reflection in the Bragg condition. Once the initial values of s_{110} and $s_{1\bar{1}0}$ were specified, (110) diffracted beam and directly transmitted intensities were calculated for various angles of tilt about an axis in the $[1\bar{1}0]$ direction. Bright and dark field rocking curves were then obtained by plotting these intensities as a function of the deviation parameter s_{110} .

The reflections taken into account in non-systematic calculations such as these must be limited to some reasonably small number if prohibitively long computing times are to be avoided. In order to accomplish this, a method similar to the criterion to be discussed in Section 5:5 was used to ensure that only those reflections which might significantly affect the final result were included in the calculation. Although in the criterion used, the importance of a non-systematic reflection was measured in terms of its effect on extinction distance rather than beam intensity, convergence calculations showed that it was quite accurate in predicting the importance of reflections in this latter case also. Using this criterion then, additional reflections in order of importance were included in a calculation until general convergence of the calculated results was obtained. Once some facility was gained with such convergence calculations, it was possible to obtain

results in computing times which were not unduly long. It should be noted that the reflections taken into account in calculations carried out in this manner would change with orientation and would, therefore, not necessarily be the same for each point on the rocking curve.

5:4.2 The Variation of Bright and Dark Field Intensity at an Accelerating Voltage of 150 kV

The bright and dark field rocking curves obtained for several different initial orientations and for an accelerating voltage of 150 kV are shown in Fig. 32. Fig. 32a shows the results obtained when only systematic reflections were taken into account. These curves illustrate the well established results that intensity maxima in bright and dark field images occur when the lowest order reflection of a systematic set is close to the exact Bragg condition, while relatively low intensities result when the crystal is near the symmetry position of the systematic row. Fig. 32b,c, and d show typical examples of rocking curves obtained when non-systematic reflections are taken into account. The accompanying diffraction patterns show the reflections taken into account at the initial values of s_{110} and $s_{1\bar{1}0}$. The initial orientation assumed in Fig. 32b was an exact $[00\bar{1}]$ or symmetry orientation, while in Figs. 32c and d, the initial orientations were obtained by tilting

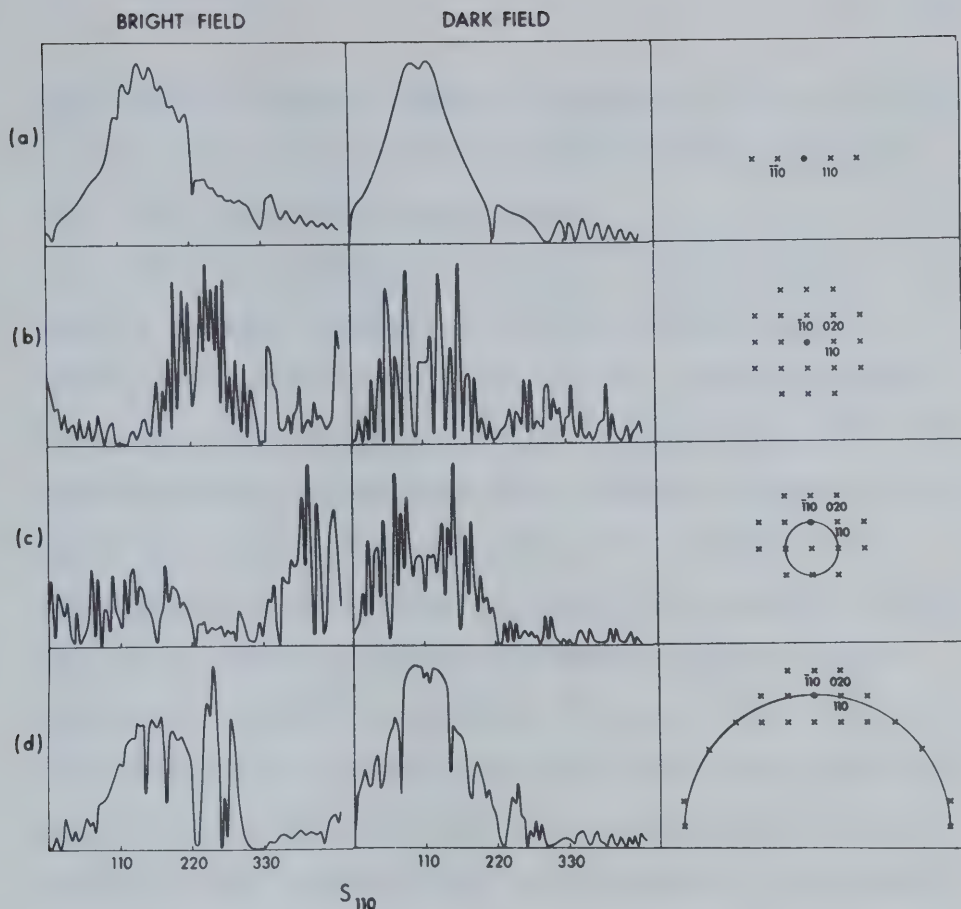


Fig. 32. Bright and dark field rocking curves for molybdenum at an accelerating voltage of 150 kV and a crystal thickness of 5000 Å. The accompanying diffraction patterns show the reflections taken into account at the initial value of s_{110} . In (a) systematic reflections only were considered, while in (b), (c) and (d) non-systematic reflections were also taken into account. The initial orientation in (b) was exactly $(00\bar{1})$, while in (c) and (d) the initial orientations were obtained by tilting the crystal from an exact $(00\bar{1})$ orientation by two and ten Bragg angles of the $(1\bar{1}0)$ reflection respectively. Also shown in each case is the intersection of the Ewald sphere with the (001) reciprocal lattice plane.

the crystal from the symmetry orientation about an axis in the $[110]$ direction by two and ten Bragg angles of the $(1\bar{1}0)$ reflection respectively.

The first general feature to be noted about the rocking curves, obtained by taking non-systematic reflections into account, is that for the same crystal thickness, changes in intensity with deviation from the Bragg condition occur much more rapidly than when only systematic reflections are taken into consideration. These detailed variations in intensity, however, become less pronounced as crystal thickness increases (see results for 1000 kV in Section 5:4.3). Thus, they are less important in determining the diffraction conditions for obtaining optimum electron transmission than are the general broad intensity maxima and minima which persist regardless of thickness. It is, therefore, of interest to examine the curves in Fig. 32 with a view to comparing the values of s_{110} at which these broad intensity maxima and minima occur. In the dark field rocking curves shown in Figs. 32b, c, and d, it can be seen that, regardless of orientation, relatively high intensities occur when the (110) reflection is close to the Bragg condition, while lower intensities result for values of s_{110} near the symmetry position of the (110) row. These results show that non-systematic reflections, although affecting

the detailed variation of diffracted beam intensity with deviation from the Bragg condition, do not have any significant effect on the values of s_{110} at which relatively high or low intensities are to be expected.

A comparison of the bright and dark field results in Fig. 32 shows that the effects of non-systematic reflections on bright field rocking curves are more pronounced than in the dark field. This can be seen from the fact that the values of s_{110} at which intensity maxima occur in the bright field vary considerably with the non-systematic reflections excited. Thus, for example, in Fig. 32b, the intensity maximum occurs at a value of s_{110} which is intermediate between those at which the (220) and (330) reflections are in the Bragg conditions, while in Fig. 32c, the intensity maximum occurs when the (440) reflection is close to the Bragg condition. Fig. 32d shows that relatively high intensities occur in the same range of values predicted by systematic calculations but, in addition, also occur for values of s_{110} which are intermediate between those for which the (220) and (330) reflections are in the Bragg condition. It should be noted that in each of these cases, relatively low intensities were obtained for values of s_{110} near the symmetry position of the (110) row. These results show that the bright

field rocking curves, taking non-systematic reflections into account, are similar to systematic rocking curves in that relatively low intensities occur near the symmetry position followed by an intensity maximum when the crystal is tilted away from this position. The angles of tilt at which these intensity maxima occur, however, vary with orientation and may be quite different from the value predicted by taking only systematic reflections into account.

Thus, it is seen that the effects of non-systematic reflections on dark and bright field rocking curves are quite different. This is illustrated by the fact that the values of s_{110} at which intensity maxima occur in the bright field vary considerably with crystal orientation, while those in the dark field do not. Also, the appearance of extinction bend contour bands in bent crystals will be similar to that predicted by systematic reflection calculations. The reason for this lies in the fact that both systematic and non-systematic calculations result in a rocking curve which is characterized by a relatively high intensity at some positive value of s_g and relatively low intensities near the symmetry position of the systematic row. Since quantitative measurements of s_g cannot normally be made from bend extinction contour measurements, the fact that the value

of s_g at which the intensity maximum occurs varies with orientation would remain undetected.

5:4.3 The Variation of Bright Field Intensity at an Accelerating Voltage of 1000 kV

In order to determine whether or not the conclusions drawn from the results at 150 kV are valid at higher accelerating voltages, calculations at 1000 kV were also carried out. Fig. 33 shows bright field rocking curves obtained at two different crystal thicknesses and for an orientation that was defined in the same way as in Fig. 32d. The first point to note about these curves is that the detailed variations in intensity decrease considerably with increasing crystal thickness but that the broad intensity maxima and minima remain essentially unchanged. The second point to note is that, in contrast to the results at 150 kV, the effects of non-systematic reflections produce a qualitative change in the shape of the rocking curve. The rocking curves in Fig. 33a, which were obtained by taking effects of systematic reflections only into account, are similar to those obtained by Humphreys and Lally (1970) and show an intensity maximum at the symmetry position of the systematic row. Fig. 33b shows that the effects of non-systematic reflections result in

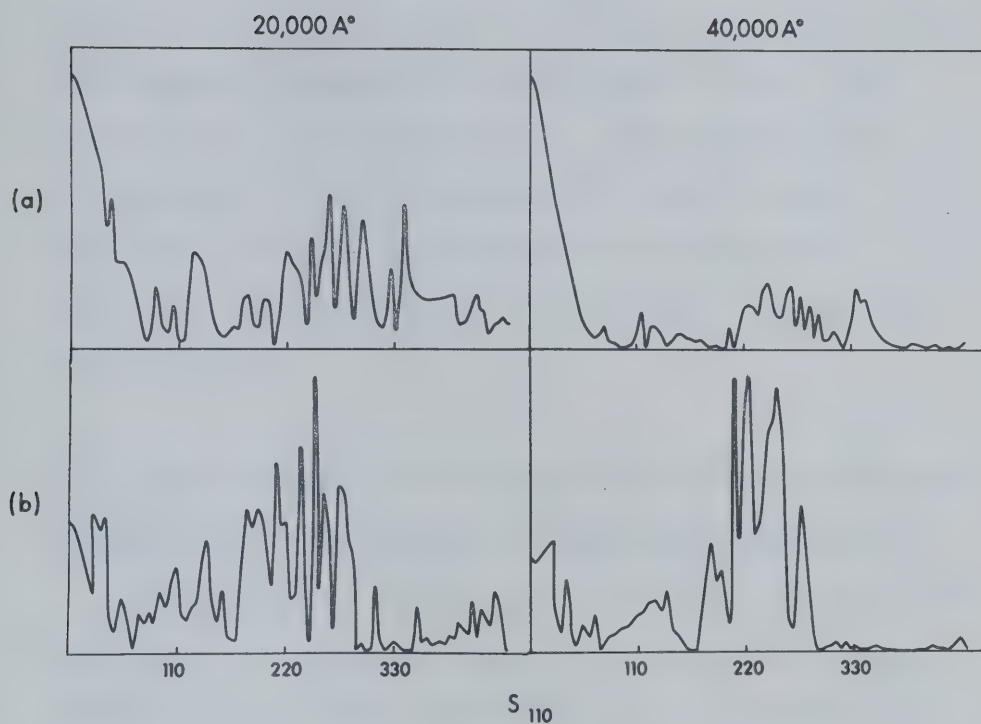


Fig. 33 Bright field rocking curves for molybdenum at an accelerating voltage of 1000 kV and for crystal thicknesses of 2 and 4μ . In (a) systematic reflections only were taken into account and in (b) the initial orientation assumed was defined in the same way as in Fig. 32d.

an intensity maximum which occurs when the (220) reflection is close to the Bragg condition with relatively low intensities resulting when the crystal is tilted toward the symmetry position of the systematic row. Thus, these results indicate that, at least under certain circumstances, the non-systematic rocking curves obtained at high and low accelerating voltages can be similar in character while the systematic curves are quite different.

5:5 The Development of a Criterion for the Inclusion of Non-Systematic Reflections in Many-beam Calculations

As stated in Section 1:7.4, whenever calculations involving the dynamical theory are carried out, some decision must be made concerning which reflections are to be included. This decision is usually based on a number of factors including the accuracy desired in the results, the number of strongly excited reflections present at the orientations involved as well as the important consideration of the computing facilities available to carry out the calculation.

It was noted in Section 3:2.2 that, when only systematic reflections or a high symmetry non-systematic situation is examined, the desired accuracy in a calculation can be obtained by systematically including higher

and higher order reflections. The justification for using this technique in these two cases is that the deviation of a reflection from its Bragg condition increases with increasing order of the reflection. Thus, the effect of any higher order reflection will be less than that of a reflection of lower order. The convergence technique used in these cases, therefore, includes additional reflections in a calculation in decreasing order of importance. Thus, the desired accuracy can easily be obtained in a many-beam calculation with the minimum number of reflections being included.

The inclusion of only the necessary reflections in a calculation is an important consideration when carrying out many-beam calculations. This is because the computing time required for such calculations is directly related to the number of reflections involved. For example, the time required to find the eigenvalues and eigenvectors of the A matrix varies approximately as the square of the number of reflections considered. In addition, the time used to compute extinction contour profiles, rocking curves and other diffraction phenomena from these parameters is also proportional to the number of reflections included. Since it is often necessary to minimize computing time, it is desirable, therefore,

to include only important reflections in a calculation.

For a general low-symmetry non-systematic situation where the importance of the reflections does not necessarily decrease with increasing order, it is essential to find an alternative method of ranking the reflections in decreasing order of their importance. For the strong-beam diffracting conditions examined in this thesis, the method developed to obtain such a ranking is described in the following section.

5:5.1 Ranking of Non-Systematic Reflections in Order of Their Importance for Inclusion in a Many-Beam Calculation

In general, the inclusion of a non-systematic reflection in a many-beam calculation will affect the values of all the Bloch wave parameters. In determining the importance of a non-systematic reflection for inclusion in a many-beam calculation, a method based on the predicted changes in the Bloch wave $\gamma^{(j)}$'s was used. The $\gamma^{(j)}$'s rather than the $q^{(j)}$'s or $c_g^{(j)}$'s were employed because the $\gamma^{(j)}$'s are directly related to the extinction distance, the physical quantity of primary interest in the work described in this thesis. Also, small changes in the $\gamma^{(j)}$'s, as evidenced by corresponding changes in the extinction distance, are more easily

detected than small changes in either the $q^{(j)}$'s or $C_g^{(j)}$'s.

The method used for predicting the importance of a non-systematic reflection was based on Bethe's Second Approximation as outlined in Section 2:2.2. If only three beams, 0, g and h, are considered and the reflection h is taken into account by using the correction terms given by this approximation, equations 2.17 reduce to

$$\left\{ \left(K^2 - \frac{U_h U_{-h}}{K^2 - k_h^2} \right) - k_o^2 \right\} C_o + \left\{ U_g - \frac{U_{g-h} U_{-h}}{K^2 - k_h^2} \right\} C_g = 0 \quad (5.15)$$

$$\left\{ U_g - \frac{U_{g-h} U_{-h}}{K^2 - k_h^2} \right\} C_o + \left\{ \left(K^2 - \frac{U_{h-g} U_{g-h}}{K^2 - k_h^2} \right) - k_g^2 \right\} C_g = 0 .$$

In equation 2.18, it was seen that the term $K^2 - k_h^2$ is approximately equal to $2K(s_h - \gamma_2^{(j)})$ where $\gamma_2^{(j)}$ is one of the two $\gamma^{(j)}$'s given by a two-beam calculation including only the 0 and g'th reflections. From equations 5.12 it can then be seen that the terms of the form $U_g, U_h, / (K^2 - k_h^2)$ will become infinite as s_h , approaches either of the two $\gamma_2^{(j)}$ values. Because of this behaviour the condition that $|s_h| \gg |\gamma_2^{(j)}|$ is generally imposed when applying the Second Bethe Approximation to take into account

the effect of a reflection h . Under this condition the term $2K(s_h - \gamma_2^{(j)})$ reduces to $2Ks_h$. In developing the method of ranking reflections in order of their importance described here, it was also assumed that the $\gamma_2^{(j)}$'s could be neglected in comparison with s_h . This assumption facilitates the application of the ranking procedure although it may introduce some inaccuracies which will be discussed in Section 5:5.3.

Using the assumption that the $\gamma_2^{(j)}$'s can be neglected in comparison with s_h , equations 5.15 become

$$\left\{ \left(K^2 - \frac{U_h U_{-h}}{2K s_h} \right) - k_o^2 \right\} C_o + \left\{ U_g - \frac{U_{g-h} U_{-h}}{2K s_h} \right\} C_g = 0 \quad (5.16)$$

$$\left\{ U_g - \frac{U_{g-h} U_{-h}}{2K s_h} \right\} C_o + \left\{ \left(K^2 - \frac{U_{h-g} U_{g-h}}{2K s_h} \right) - k_g^2 \right\} C_g = 0 .$$

Since $K \approx 30 \text{ \AA}^{-1}$ and $U_h \approx .02 \text{ \AA}^{-2}$, $K^2 \gg (U_h U_{-h})/2Ks_h$ except for the case s_h very small which is excluded, however, by the assumption that $|s_h| \gg |\gamma_2^{(j)}|$. Using the fact that $K^2 \gg (U_h U_{-h})/2Ks_h$, equations 5.16 reduce to

$$(K^2 - k_o^2) C_o + \left(U_g - \frac{U_{g-h} U_{-h}}{2K s_h} \right) C_g = 0 \quad (5.17)$$

$$\left(U_g - \frac{U_{g-h} U_{-h}}{2K s_h} \right) C_o + (K^2 - k_g^2) C_g = 0 .$$

The resulting eigenvalues $\gamma^{(j)}$ of this set of equations are found to be of the form

$$\gamma^{(j)} = \frac{s_g}{2} \pm \frac{1}{2} \left\{ s_g^2 + \frac{1}{K^2} \left(U_g - \frac{U_{g-h} U_{-h}}{2K s_h} \right)^2 \right\}^{\frac{1}{2}}. \quad (5.18)$$

In the strong-beam diffracting conditions considered in this thesis, $s_g \approx 0$ and this expression reduces to

$$\gamma^{(j)} \approx \pm \frac{1}{2K} \left(U_g - \frac{U_{g-h} U_{-h}}{2K s_h} \right). \quad (5.19)$$

Therefore, it can be seen that the change in the $\gamma^{(j)}$'s due to the presence of the reflection h will be of the order $(U_{g-h} U_{-h})/4K^2 s_h$. An analysis of this term, $(U_{g-h} U_{-h})/4K^2 s_h$, shows that the effect of the non-systematic reflection h on the $\gamma^{(j)}$'s is predicted to be directly proportional to the product $U_{g-h} U_{-h}$ and inversely proportional to s_h . The two Fourier coefficients U_{g-h} and U_{-h} are, thus, of equal importance in determining the effect of h . Therefore, not only is the order of the reflection h important but also the relationship of the reflection h to g . Consider, for example, two reflections h and h' which have equal Fourier coefficients, $U_h = U_{h'}$. If $|\vec{g} - \vec{h}| < |\vec{g} - \vec{h}'|$, then U_{g-h} will be larger than $U_{g-h'}$, and the effect of the

reflection h will be larger than that of the reflection h' for $s_h = s_{h'}$.

The prediction that the change in the $\gamma^{(j)}$'s will vary inversely with s_h is in agreement with previous observations in Section 5:2. There it was seen that the variation of the extinction distance from its value in the absence of a non-systematic reflection, in general, decreased with increasing $|\Delta\theta_h|$. Since $\xi = 1/(\gamma^{(i)} - \gamma^{(j)})$ and $s_h \approx |\vec{h}|\Delta\theta_h$, changes in the $\gamma^{(j)}$ with s_h will result in corresponding changes in ξ .

5:5.2 Development of a Criterion For Including Non-Systematic Reflections in a Many-Beam Calculation

In Section 5:5.1, it was shown that the presence of a non-systematic reflection results in a change, $U_{g-h}U_{-h}/4K^2s_h$, in the value of $\gamma^{(j)}$ from that calculated in the absence of that reflection. The corresponding change in the calculated extinction distance can then be found from the expression

$$\xi = \frac{1}{\gamma^{(i)} - \gamma^{(j)}} = \frac{K}{U_g - \frac{U_{g-h}U_{-h}}{2Ks_h}} \quad (5.20)$$

Since $|s_h| \gg \gamma_2^{(j)} \approx \frac{U_g}{2K}$, U_g will be much larger than $U_{g-h}U_{-h}/2Ks_h$ and equation 5.20 can be rewritten as

$$\xi \approx \frac{K}{U_g} \left(1 + \frac{U_{g-h} U_{-h}}{2U_g K s_h} \right) . \quad (5.21)$$

But K/U_g is the extinction distance in the absence of the non-systematic reflection. Therefore, the predicted fractional change in the extinction distance due to the presence of the non-systematic reflection is equal to $U_{g-h} U_{-h} / (2U_g K s_h)$. In the following discussion, this ratio will be denoted by ϵ .

Thus, it can be seen that the importance of a reflection in a calculation of extinction distance can be determined by finding its corresponding value of ϵ . Therefore, a convergence technique based on values of ϵ can be used to include only those beams which are necessary to obtain the desired accuracy. In this technique, many-beam calculations are carried out including all reflections with a value of ϵ greater than some reference value ϵ_0 . By decreasing the value of ϵ_0 more reflections are included in the calculation until the desired accuracy is obtained in the results.

In order to test the validity of using the parameter ϵ in this manner, a series of many-beam calculations of extinction distance were carried out in which the reference value, ϵ_0 , was systematically varied. Four situations were considered. In the first of these,

only systematic reflections were included. Since in the derivation of ϵ , no limitation was placed on the type of reflection involved, ϵ should predict the importance of systematic as well as non-systematic reflections. The second situation considered both systematic and non-systematic reflections at a high symmetry orientation such as studied by Howie and Basinski (1968), Lynch (1971), Ayroles (1971), and Lehmpfuhl (1972). The crystal orientation examined here was an exact $[1\bar{1}1]$ orientation in Si. Calculations were carried out for this case to test the applicability of the criterion in a situation which is not strictly a strong-beam diffracting situation. The third and fourth situations considered orientations used in the work described in Section 5:2 of this thesis. The first of these involved an orientation where no non-systematic reflections were strongly excited, i.e., $\Delta\theta_{220} = 0.0$ and $\Delta\theta_{\bar{1}33} = -.50$. The second considered an orientation at which the (220) extinction distance was varying rapidly with $\Delta\theta_{\bar{1}33}$. At this orientation, $\Delta\theta_{\bar{1}33} = .10$ while $\Delta\theta_{220} = 0.0$. All the calculations were carried out for Si at an accelerating voltage of 150 kV.

The results of these calculations are given in Tables 1, 2, 3, and 4 below. Here, ϵ_0 is the minimum

value allowed for ϵ , N is the number of beams and ξ is the calculated bright field extinction distance as determined from $1/(\gamma^{(j)} - \gamma^{(i)})$ where $\gamma^{(j)}$ and $\gamma^{(i)}$ are the γ 's corresponding to the two most important Bloch waves.

Table 1. The calculated extinction distance ξ found from many-beam calculations in which the reflections included were determined by the parameter ϵ . Only systematic reflections are considered.

ϵ_0	.05	.02	.01	.006	.002	.001	.0005
N	2	2	4	4	4	6	6
ξ	906	906	869	869	869	867	867

Table 2. The calculated extinction distance ξ found from many-beam calculations in which the reflections included were determined by the parameter ϵ . The orientation was an exact $[1\bar{1}1]$.

ϵ_0	.05	.02	.01	.006	.002	.001	.0005
N	4	7	9	12	26	47	73
ξ	275	285	286	287	290	289	286

Table 3. The calculated extinction distance ξ found from many-beam calculations in which the reflections included were determined by the parameter ϵ . The orientation is such that $\Delta\theta_{220} = 0.0$ while $\Delta\theta_{\bar{1}33} = -.50$.

ϵ_0	.05	.02	.01	.006	.002	.001	.0005
N	2	3	5	15	26	38	65
ξ	906	894	857	848	837	835	836

Table 4. The calculated extinction distance ξ found from many-beam calculations in which the reflections included were determined by the parameter ϵ . At the orientation considered, $\Delta\theta_{220} = 0.0$ and $\Delta\theta_{\bar{1}33} = .10$.

ϵ_0	.05	.02	.01	.006	.002	.001	.0005
N	3	4	7	15	26	41	68
ξ	1046	1047	1025	1020	1014	1015	1019

By examining these four Tables, it can be seen that by including all reflections with ϵ values greater than .002 in the many-beam calculations, good convergence can be obtained with regard to the extinction

distance. Doubling or even tripling the number of reflections included in the calculation does not significantly alter the calculated value of ξ . Thus, at $\epsilon_0 = .002$, all the reflections having a significant effect on the extinction distance have been included. An examination of the manner in which the extinction distance varies in the range of ϵ_0 from .05 to .002 shows that the reflections are brought into the calculations in order of decreasing importance. This can be seen by the fact that, as additional reflections are included, the resulting change in the extinction distance decreases.

Thus, it can be seen that, by finding the quantity $(U_{g-h} U_h) / 2Ks_h$ for each reflection h and comparing it to U_g , the magnitude of the effect of different non-systematic reflections on the extinction distance of the g 'th reflection can be predicted. Using these predictions, the non-systematic reflections can be ranked according to their importance. Many-beam calculations can then be carried out in which reflections are included in order of this ranking to permit the minimum number of beams possible to be used.

5:5.3 Additional Considerations In Using the Criterion

In employing the criterion described in the previous section in many-beam calculations, two points should be noted. The first of these is that the use of a particular value of the criterion parameter ϵ_0 does not necessarily imply that the extinction distance obtained in a many-beam calculation is accurate to this value. The reason for this lies in the cumulative nature of the effects of a number of non-systematic reflections. This was first pointed out by Hewat (1972) for the case of a centro-symmetric crystal where $U_h = U_{-h}$. In this case, the presence of the $-h$ 'th reflection will tend to cancel out the effect of the h 'th reflection when the reciprocal lattice point corresponding to one reflection lies inside the Ewald sphere, while the reciprocal lattice point corresponding to the other reflection lies outside. This is because the presence of one of these reflections will tend to increase the extinction distance, while the presence of the other reflection will tend to decrease it. For example, when a four-beam calculation including the (000) , (220) , $(\bar{1}11)$ and $(1\bar{1}\bar{1})$ reflections is carried out for $\Delta\theta_{220} = 0.0$ and $\Delta\theta_{\bar{1}11} \approx 25 \approx -\Delta\theta_{1\bar{1}\bar{1}}$, the net effect of the presence of the two non-systematic reflections on the (220) extinction distance is of the order of only .1 per cent.

This can be compared to the 1 per cent effect predicted for each reflection in the absence of the other. However, the presence of the $(\bar{1}11)$ reflection tends to increase the extinction distance, while the $(1\bar{1}\bar{1})$ reflection causes a decrease. The net result is that only a small change in the extinction distance takes place.

Similarly, if two non-systematic reflections are present, both of which lie outside or inside the Ewald sphere, the net effect on the extinction distance will, to a good approximation, be the sum of the two individual effects. For example, if an orientation is examined in Si for which the (220) and $(2\bar{2}0)$ reflections are present, it is found that the (400) reflection is also strongly excited. If $\Delta\theta_{220} = 0.0$ and $\Delta\theta_{2\bar{2}0} = -2.0$ then $\Delta\theta_{400}$ is found to be equal to -1.0 θ_{400} . When three-beam calculations including the (000) , (220) and either the $(\bar{2}20)$ or (400) reflections are carried out at these orientations, the change in extinction distance is found to be 3.7 per cent. However, when both the $(\bar{2}20)$ and (400) reflections are included in a four-beam calculation, the change in extinction distance is approximately 7.4 per cent. The effects tend to add here rather than cancel because the reciprocal lattice points corresponding to the $(2\bar{2}0)$ and (400) reflections both lie outside the Ewald sphere.

Thus, it is seen that using the criterion to include all reflections in a many-beam calculation of extinction distance whose effect is predicted to be 1 per cent or larger does not necessarily result in an extinction distance accurate to 1 per cent. This is because of the cumulative nature of the effects described above. Therefore, the desired accuracy in the calculations must be obtained by using the convergence technique described in Section 5:5.2. In this technique, the value of ϵ_0 is progressively decreased and more beams included in the calculation until the desired convergence is obtained.

An important point to note is that in these discussions of cumulative effects, the Fourier coefficients, U_h , were all considered to have the same sign. When this is not the case, the above discussion requires modification (see Appendix B) although the use of the parameter ϵ for determining the importance of a reflection is still valid.

The second point to be considered in using the criterion is the accuracy with which it predicts the effect of a non-systematic reflection. This, in turn, is determined by the validity of the assumption $|s_h| \gg |\gamma_2^{(j)}|$ used in deriving the parameter ϵ . Although this condition is unlikely to be fulfilled for all the reflections present at a given general orientation, this

does not necessarily introduce significant errors in the use of the criterion to include reflections in a calculation. This can be seen by considering the following example.

In Section 5:5.2, it was shown that a value of $\epsilon_0 = .002$ resulted in the necessary reflections being included in the many-beam calculations to give good convergence. It is of interest, therefore, to examine the s_h values of different order non-systematic reflections for which the calculated values of ϵ are equal to ϵ_0 . As defined in Section 5:5.2, the parameter ϵ is equal to $(U_{g-h}U_{-h})/(2U_gKs_h)$. For a low order (non-systematic reflection h of the same order) as g , $U_{g-h} \approx U_{-h} \approx U_g \approx .03 \text{ \AA}^{-2}$, while $K \approx 30 \text{ \AA}^{-1}$ for 100 keV electrons. When these values are substituted into the expression for ϵ and this expression set equal to .002, a value of $.5 \text{ \AA}^{-1}$ is obtained for s_h . Since the typical value of $|\gamma_2^{(j)}|$ is of the order of 10^{-3} \AA^{-1} , the condition that $|s_h| \gg |\gamma_2^{(j)}|$ is well fulfilled in this case. For medium order non-systematic reflections, $|\vec{h}| \approx 4|\vec{g}|$, $U_{g-h} \approx U_{-h} \approx .1 U_g$ and the value of s_h found in this case is $.005 \text{ \AA}^{-1}$ again fulfilling the condition $|s_h| \gg |\gamma_2^{(j)}|$. For high order non-systematic reflections, $|\vec{h}| \approx 10|\vec{g}|$, $U_{g-h} \approx U_{-h} \approx 10^{-3} \times U_g$ and the value of s_h found in this case is $.5 \times 10^{-6} \text{ \AA}^{-1}$. For these reflections, therefore, the condition $|s_h| \gg |\gamma_2^{(j)}|$ is not satisfied. As seen in Sections 5:2.7 and 5:2.8, however, the effects

of these high order reflections are small compared to the lower order reflections. Moreover, the range of deviations over which these reflections have a significant effect is quite narrow ($\approx 10^{-4}$ degrees) with the result that the effect will not, in general, be observed experimentally due to such limitations as beam divergence. Thus, due to these two factors, errors in the use of the criterion for including the higher order reflections in a many-beam calculation are not expected to be significant.

5:5.4 Application of the Criterion to Calculations Carried Out in This Thesis

For the theoretical results presented in Section 5:2 of this thesis, convergence calculations showed that a value of $\epsilon_0 = .002$ resulted in the inclusion of the necessary reflections to obtain good agreement with experimental results. The inclusion of additional reflections in the theoretical calculations by making ϵ_0 smaller did not result in any improvement in the agreement with experiment. As an additional test of the accuracy of the criterion, many-beam calculations were carried out in which all the reflections which could be detected in an experimental diffraction pattern were included. The results of these calculations were compared with many-beam calculations for the same orientations in which the reflections included were found using the criterion. No significant difference between the results of the calculations were noted

although many more reflections were included in the calculations based on the diffraction patterns.

5:6 Bloch Wave Labelling in the Presence of Non-Systematic Reflections

In the Bloch wave formulation of the dynamical theory of electron diffraction, it is necessary to identify in some manner the different Bloch waves excited in the crystal. This identification has usually been based on the magnitude of the wave vectors associated with the different waves. In the two-beam approximation, the Bloch wave with the larger wave vector has customarily been labelled as wave 2 while the Bloch wave with the smaller wave vector has been labelled 1. Humphreys and Fisher (1971) have suggested, however, that the Bloch wave labelling scheme which is simplest and the most logical, particularly in a many-beam situation, is a scheme in which the waves are labelled in order of decreasing wave vector. In this scheme, the wave with the largest wave vector would be labelled 1; the wave with the second largest wave vector would be labelled 2 and similarly for Bloch waves 3, 4,M. In comparison with the earlier labelling in the two-beam situation, it should be noted that the labels 1 and 2 are reversed in the Humphreys and Fisher scheme.

When Bloch waves are labelled in such a consistent manner, it is found for the case where only systematic reflections are considered that the different numbered Bloch waves will always have certain characteristics for a given set of diffraction conditions. For example, in the Humphreys and Fisher labelling scheme, Bloch wave 1 is symmetric and has a high absorption coefficient when the lowest order systematic reflection is in the Bragg condition. Similarly, for this diffracting situation, Bloch wave 2 is antisymmetric and has a low absorption coefficient. In Section 5:6.2 the effect of the presence of a non-systematic reflection on the association of certain characteristics with particular numbered Bloch waves will be examined. First, however, it is useful to consider the labelling of Bloch waves when two of the waves are degenerate due to the presence of a non-systematic reflection.

5:6.1 Bloch Wave Labelling at a Degeneracy Resulting from the Presence of a Non-Systematic Reflection

In Fig. 17 it was seen that, for the (220) reflection in its exact Bragg condition, two Bloch waves are degenerate at $\Delta\theta_{133} \approx -0.05$. These waves are labelled 2 and 3 following the convention of Humphreys and Fisher (1971). The labelling shown in Fig. 17 assumes that the branches of the dispersion surface

come together and touch at the degeneracy point before splitting apart again. However, it is also possible to consider a cross over of the two branches at this point and a subsequent relabelling of the branches as shown in Fig. 34. The labelling here is no longer consistent with that of Humphreys and Fisher.

To investigate the possibility of a cross over of the two branches of the dispersion surface at the degeneracy point, it is useful to examine the Bloch wave parameters $|\phi_{220}^{(j)}|$. In Fig. 18, it can be seen that an interchange in the values of $|\phi_{220}^{(2)}|$ and $|\phi_{220}^{(3)}|$, as denoted by the dashed lines, is required to take place if branches 2 and 3 are considered to touch and not cross. However, as can be seen in Fig. 35, if branches 2 and 3 are assumed to cross at the degeneracy point, this interchange is not present. Fig. 35 is, in fact, characteristic of the results obtained for $\Delta\theta_{220}$ exactly equal to zero in that, at this deviation of the (220) reflection from the Bragg condition, the numerical results indicated that no interchange occurred at or in the vicinity of the degeneracy point.

In the Bloch wave analyses carried out in this thesis, however, it has been assumed that branches 2 and 3 of the dispersion surface only touch and that an instantaneous interchange in the $|\phi_{220}^{(j)}|$ values takes place at the degeneracy point. This assumption is based

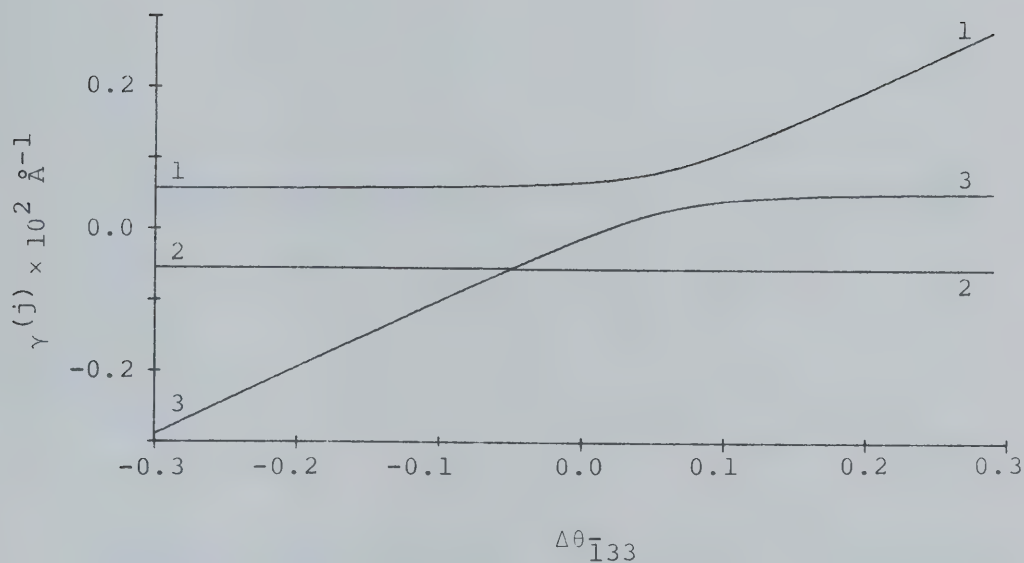


Fig. 34 The branches of the dispersion surface for a three-beam situation including the (000), (220) and ($\bar{1}33$) reflections. $\Delta\theta_{220} = 0.0$. The branches of the dispersion surface are considered to cross at the degeneracy point at $\Delta\theta_{\bar{1}33} \approx -0.05$.

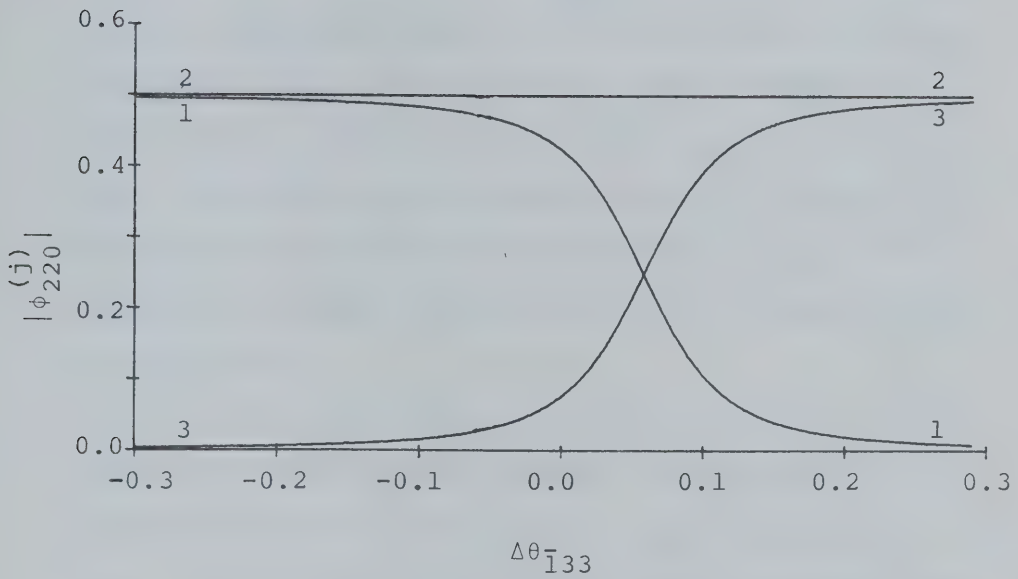


Fig. 35 The variation with $\Delta\theta_{133}$ of the contributions, $|\phi_{220}^{(j)}|$ of the different Bloch waves to the (220) amplitude assuming that branches 2 and 3 of the dispersion surface cross over at the degeneracy point.

on two separate results. First, calculations at values of $\Delta\theta_{220}$ not equal to zero showed that an interchange in the values of $|\phi_{220}^{(j)}|$ and $|\phi_{220}^{(3)}|$ took place over a range of values of $\Delta\theta_{\bar{1}33}$ at which dispersion surface branches 2 and 3 were closest together. Such an interchange is shown at $\Delta\theta_{\bar{1}33} \approx -.02$ in Fig. 21 for the case $\Delta\theta_{220} = .25$. The range of $\Delta\theta_{220}$ over which the interchange occurred was found to be proportional to $\Delta\theta_{220}$. The closer $\Delta\theta_{220}$ was made to zero the narrower the range of $\Delta\theta_{\bar{1}33}$ over which the interchange took place. Thus, continuity in the behaviour of $|\phi_{220}^{(2)}|$ and $|\phi_{220}^{(3)}|$ at the exact degeneracy point would require an instantaneous interchange in the values of $|\phi_{220}^{(2)}|$ and $|\phi_{220}^{(3)}|$ at this point.

A similar analysis of the behaviour of branches 2 and 3 of the dispersion surface also supports the assumption that the two branches touch rather than cross. For any deviation of the (220) reflection from its Bragg condition not equal to zero, branches 2 and 3 were found to behave in a hyperbolic fashion in the region of their closest approach as can be seen at $\Delta\theta_{\bar{1}33} \approx .02$ in Fig. 20. As $\Delta\theta_{220}$ was made to approach zero, however, it was found from numerical calculations that the distance of closest approach decreased and the behaviour of the two branches in the region about $\Delta\theta_{\bar{1}33} = .02$ more closely followed that shown in Fig. 17.

Thus, sharp bends in branches 2 and 3 of the dispersion surface at the degeneracy point are in agreement with the behaviour of the branches at small values of $\Delta\theta_{220}$ where the degeneracy is not present.

Another result which is in agreement with an interchange of the $|\phi_{220}^{(j)}|$ values at a degeneracy point can be seen from the results obtained in critical voltage measurements (Metherell and Fisher, 1969; Lally, Humphreys, Metherell and Fisher, 1972). For the case of the reflection $2g$ in the Bragg conditions, it is found that, below the critical voltage, Bloch wave 2 is antisymmetric and Bloch wave 3 is symmetric. Above the critical voltage, however, Bloch wave 2 is symmetric and Bloch wave 3 is antisymmetric. This interchange in symmetries of waves 2 and 3 is explained by an instantaneous interchange of the Bloch wave amplitudes at the critical voltage where Bloch waves 2 and 3 are degenerate.

Based on these results, therefore, a labelling system for the Bloch waves present in a non-systematic situation has been employed which assumes no cross over of branches of the dispersion surface at degeneracy points. This system is in agreement with that of Humphreys and Fisher (1971).

5:6.2 The Effect of the Presence of a Non-Systematic Reflection on Bloch Wave Labelling

In general, when only systematic reflections are considered and the low order reflection g is in its Bragg condition, it is found that the Bloch waves numbered 1 and 2 in the Humphreys and Fisher (1971) scheme make the most important contributions to the diffracted beam amplitude. This is also the case when the (220) systematic reflection is in its Bragg condition and the ($\bar{1}33$) non-systematic reflection is at a large negative deviation from its Bragg condition. This can be seen by examining Fig. 18 which shows that Bloch waves 1 and 2 make the largest contributions to the (220) amplitude at $\Delta\theta_{\bar{1}33} = -.30$. For large positive values of $\Delta\theta_{\bar{1}33}$, however, the same Figure shows that Bloch waves 2 and 3 are the important waves contributing to this amplitude.

It is next of interest to examine the characteristics of the important Bloch waves at the two deviations, $\Delta\theta_{\bar{1}33} = \pm .30$. In Fig. 26, it can be seen that at $\Delta\theta_{\bar{1}33} = -.30$, Bloch wave 1 is strongly absorbed, while Bloch wave 2 is weakly absorbed. At $\Delta\theta_{\bar{1}33} = +.30$, however, Bloch wave 2 is strongly absorbed, while Bloch wave 3 is weakly absorbed. Similarly, at $\Delta\theta_{\bar{1}33} = -.30$,

Bloch wave 1 is symmetric ($C_o^{(1)} \approx C_{220}^{(1)}$) and Bloch wave 2 antisymmetric ($C_o^{(2)} \approx -C_{220}^{(2)}$) while for $\Delta\theta_{133} = +.30$, Bloch wave 2 is symmetric and Bloch wave 3 antisymmetric. Thus, for large negative deviations of the non-systematic reflection from its Bragg condition, the important Bloch waves and their corresponding characteristics are found to be the same as those obtained in the case where only systematic reflections are considered. For large positive deviations, although the characteristics of the important Bloch waves are the same as those in the systematic case, the waves are numbered 2 and 3 rather than 1 and 2 due to the presence of the non-systematic reflection.

Therefore, it is seen that, when non-systematic reflections are taken into account, particular Bloch wave numbers no longer necessarily correspond to Bloch waves with certain characteristics. The characteristics associated with a particular Bloch wave will depend upon the number of non-systematic reflections considered and their deviations from their Bragg conditions.

CHAPTER 6

SUMMARY AND SUGGESTIONS FOR FURTHER WORK

6:1 Variation of Extinction Distance in the Presence of a Non-Systematic Reflection

Measurements of the variation of the (220) extinction distance in Si were carried out as a function of the deviation of a single strongly excited non-systematic reflection from its Bragg condition. These measurements were subsequently interpreted in terms of both Bloch wave parameters and three-beam analytical expressions.

6:1.1 Experimental Observations

It was found from measurements of the variation of the (220) extinction distance as a function of the deviation of the ($\bar{1}33$) non-systematic reflection from its Bragg condition that:

1. Marked variations of the extinction distance from its systematic value took place as the ($\bar{1}33$) reflection was tilted through its Bragg condition.
2. These variations were found, in general, to be largest at small positive and negative values of $\Delta\theta_{\bar{1}33}$.

3. Associated with these regions of maximum variation of the extinction distance were ranges of tilt through which the variation of the (220) intensity with depth became non-sinusoidal or complex in nature. Sharp changes in the observed extinction distance took place in tilting through such regions.

4. For large positive values of $\Delta\theta_{\bar{1}33}$, the observed extinction distance was larger than the systematic value. This difference increased as $\Delta\theta_{\bar{1}33}$ decreased until the first complex region was encountered.

5. For small positive and negative values of $\Delta\theta_{\bar{1}33}$ lying between the two complex regions, the extinction distance was smaller than the systematic value.

6. For values of $\Delta\theta_{\bar{1}33}$ more negative than that at which the second complex region occurred, the extinction distance was found to lie close to the systematic value.

7. For the particular case where the (220) reflection was in its exact Bragg condition, the complex region was not observed for negative $\Delta\theta_{\bar{1}33}$. The extinction distance in this case lay below the systematic value for all $\Delta\theta_{\bar{1}33} < 0$.

6:1.2 Bloch Wave Analysis

Three-beam calculations of Bloch wave parameters were carried out for a range of deviations of the non-systematic reflection about its Bragg condition. An analysis of the behaviour of the different branches of the dispersion surface and the contributions of their corresponding Bloch waves to the (220) amplitude was then undertaken. This analysis showed that the variation in extinction distance could be explained in terms of displacements of the different branches of the dispersion surface in the presence of the non-systematic reflection. The analysis also showed that the regions of complex variation of the (220) intensity with depth occurred when three Bloch waves made significant contributions to the (220) intensity.

6:1.3 Three-Beam Analytical Theory

In order to acquire insight into the observed behaviour of the extinction distance in the presence of a non-systematic reflection an analysis was carried out in terms of the three-beam analytical expressions as given by the dynamical theory of electron diffraction. These expressions showed that, in agreement with experiment, two regions of complex variation of intensity with

depth will occur, in general, whenever a non-systematic reflection is tilted through its Bragg condition. For one particular deviation of the systematic reflection from its Bragg condition, however, one of these regions will not be observed due to degeneracy of two of the Bloch waves. The particular values of the deviations of the systematic and non-systematic reflections from their Bragg conditions at which this degeneracy occurs are determined by the Fourier coefficients of the lattice potential of the reflections involved.

The analytical expressions were also examined to determine at what deviations of the non-systematic reflection from its Bragg condition the regions of complex variation of the systematic diffracted beam intensity with depth will occur. These deviations were found to depend upon the values of the $\gamma^{(j)}$'s corresponding to the important Bloch waves in the absence of the non-systematic reflection. As a result, when the systematic reflection is near its exact Bragg condition, the regions of complexity will occur at approximately equal positive and negative deviations of the non-systematic reflection from its Bragg condition. When the systematic reflection is far from its Bragg condition, however, the positions of the complex regions will be asymmetric with respect to the Bragg condition of the non-systematic reflection.

6:1.4 Effects of Higher Order Non-Systematic Reflections

The effects on the (220) extinction distance of the ($\bar{1}33$), ($\bar{1}35$) and ($\bar{1}37$) non-systematic reflections were measured. A comparison of the results of these measurements showed that the effect of the non-systematic reflection, although similar in the three cases, decreased with increasing order of the reflection involved. From an analysis in terms of the three-beam analytical theory, this decrease was found to be associated with a corresponding decrease in the Fourier coefficients of the lattice potential corresponding to the higher order reflections.

6:2 The Effect of the Presence of a Non-Systematic Reflection on Anomalous Absorption

It was found that the presence of a non-systematic reflection has a marked effect on the channelling of Bloch waves in a crystal. Since the Bloch wave absorption coefficients are dependent upon this channelling, these coefficients were found to be a function of the deviation of a non-systematic reflection from its Bragg condition. Since anomalous absorption effects are, in turn, dependent upon differences between the absorption coefficients, the presence of a non-systematic reflection was found to alter anomalous absorption effects. In the case of the (220) systematic reflection in Si, these

effects were found to be enhanced for negative values and diminished for positive values of the deviation of the ($\bar{1}33$) non-systematic reflection from its Bragg condition. These theoretical predictions were confirmed by observation of thickness extinction contours in wedge-shaped crystals.

6:3 Effect of the Presence of Non-Systematic Reflections on Image Intensity

Rocking curve calculations were carried out for both bright and dark field images in the presence of non-systematic reflections. It was found that the presence of these reflections did not significantly alter the position of the intensity maximum in the dark field rocking curve from that predicted when only systematic reflections are considered. In the bright field, however, the presence of the non-systematic reflections were found, under certain circumstances, to have marked effects on the location of the intensity maximum in the rocking curve. This maximum, which for low accelerating voltages usually occurs at a small positive deviation of the low-order diffracted beam, g , from its Bragg condition, was found to occur as far away as $4g$ in the Bragg condition depending upon the non-systematic reflections excited.

Calculations of bright field rocking curves were also carried out at high accelerating voltages. These calculations showed that the character of the rocking curve in such a case could be fundamentally changed by the presence of non-systematic reflections. In the absence of these reflections, the intensity maximum in the rocking curve occurs at the symmetry position. However, in the presence of certain configurations of non-systematic reflections, the maximum was found to occur instead near $2g$ in the Bragg condition. Thus, bend contours examined in such a situation would exhibit two bright lines rather than only the one which would be observed in the absence of non-systematic reflections.

6:4 Development of a Criterion for Inclusion of Reflections in a Many-Beam Calculation

A method was developed for predicting the importance of a reflection for inclusion in a many-beam calculation. This method used the approach of the Second Bethe Approximation to estimate the effect of the reflection in terms of changes in the two-beam extinction distance. By including reflections in decreasing order of their estimated effect, it was found that many-beam calculations could be carried out in which only the necessary reflections for the accuracy desired were taken into consideration.

6:5 The Effect of the Presence of a Non-Systematic Reflection on Bloch Wave Labelling

An examination of the Bloch waves excited in the presence of a non-systematic reflection was carried out to determine the effect of such a reflection on the characteristics of different numbered Bloch waves. It was found that when non-systematic reflections are taken into consideration, particular Bloch wave numbers no longer necessarily correspond to Bloch waves with certain characteristics.

Under certain conditions, the presence of a non-systematic reflection was also found to result in Bloch wave degeneracies. An analysis of these degeneracies suggested that the corresponding dispersion surfaces can be considered to touch but not cross at the degeneracy point. Such a behaviour is in agreement with similar degeneracies reported in critical voltage work.

6:6 Suggestions for Further Work

The measurements and analyses of the effects of a non-systematic reflection have been carried out in this thesis for a strong beam diffracting situation. Due to recent interest in weak beam imaging (Cockayne, 1972), a similar study of the effects of non-systematic reflections in the weak beam case would be of great interest.

In the examinations reported in this thesis, only the effects of a non-systematic reflection on perfect crystal image contrast have been considered. A most logical extension of this work would be to the case of defect image contrast. Some work on stacking fault images in the presence of non-systematic reflections (Humphreys, Howie and Booker, 1967) and dislocations (Skalicky and Papp, 1972; Oblak and Kear, 1972) has been carried out. However, analysis in terms of Bloch waves or an analytical theory has not been undertaken.

A third possible extension of this work is to the measurement of low-order coefficients of the lattice potential, V_g , by making measurements of the effect of a higher order non-systematic reflection, h , on the extinction distance of the reflection g . Since the coefficients V_h and V_{g-h} are more accurately known in such a case, the value of V_g could be varied in many-beam calculations until the best fit is obtained between experiment and theory.

In the case of anomalous absorption effects in the presence of a non-systematic reflection, an application of this work could be to the imaging of crystal defects in thick materials. It may be possible to introduce non-systematic reflections into a diffraction situation in such a manner as to enhance defect image

contrast in thick crystals by diminishing anomalous absorption effects. Richards and Stobbs (1972) have, in fact, reported such enhancement in the case of weak beam images.

Finally, in the results reported in this thesis on the effects of non-systematic reflections on the location of intensity maxima in rocking curves, only particular configurations of non-systematic reflections were considered. As an extension to this work, it is suggested that, instead of rocking curves, two-dimensional rocking surfaces be calculated in which the orientation of the crystal is varied in a continuous manner in both the systematic and non-systematic directions. Such surfaces would give better insight into the behaviour of intensity maxima in the presence of non-systematic reflections. These surfaces could also be compared directly with experimental convergent beam patterns.

REFERENCES

- Ayroles, R. (1971) J. Microsc. 11, 193.
- Ayroles, R. and Mazel, A. (1970) Proc. Septième Congrès International de Microscopie Electronique, Grenoble, 1, 97.
- Bethe, H.A. (1928) Ann. d. Physik 87, 55.
- Boersch, H. (1943) Zeit. fur Physik 121, 746.
- Booker, G.R. and Stickler, R. (1962) Brit. J. Appl. Phys. 13, 446.
- von Borries, B. and Ruska, E. (1940) Naturwiss. 28, 366.
- de Broglie, L. (1924) Phil. Mag. 47, 446.
- Brunel, J.C. (1968) unpublished.
- Cann, C.D. (1967) M.Sc. Thesis, Unpublished.
- Cann, C.D., Foxon, C.T.B. and Sheinin, S.S. (1968) Proc. 26'th Ann. Meeting, Electron Microscopy Soc. of America.
- Cann, C.D. and Sheinin, S.S. (1968) phys. stat. sol. 30, 791.
- Cockayne, D.J.H. (1972) Z. Naturforsch. 27a, 452.
- Cowley, J.M. and Moodie, A.F. (1957) Acta Cryst. 10, 609.
- Darwin, C.G. (1914) Phil. Mag. 27, 315 and 675.
- Davisson, C.J. and Germer, L.H. (1927) Nature 119, 558.
- Doyle, P.A. and Turner, P.S. (1968) Acta Cryst. A24, 390.

- Dupouy, G., Perrier, F., Uyeda, R., Ayroles, R., and Mazel, A. (1965) J. Microsc. 4, 429.
- Fisher, P.M.J. (1968) Japan J. Appl. Phys. 7, 191.
- Foxon, C.T.B. (1968) unpublished.
- Fujimoto, F. (1959) J. Phys. Soc. Japan 14, 1558.
- Fujimoto, F. (1960) J. Phys. Soc. Japan 15, 1022.
- Fujiwara, K. (1961) J. Phys. Soc. Japan 16, 2226.
- Fukuhara, A. (1966) J. Phys. Soc. Japan 21, 2645.
- Gevers, R. (1970) in Modern Diffraction and Imaging Techniques in Material Science, ed. S. Amelinckx, R. Gevers, G. Remaut and J. Van Landuyt, North-Holland.
- Gjønnes, J. (1966) Acta Cryst. 20, 240.
- Gjønnes, J. and Høier, R. (1969) Acta Cryst. A25, 595.
- Gjønnes, J. and Høier, R. (1971) Acta Cryst. A27, 313.
- Gjønnes, J. and Watanabe, D. (1966) Acta Cryst. 21, 297.
- Goringe, M.J. (1971) Electron Microscopy in Material Science, Ed. U. Valdré, Academic Press.
- Goringe, M.J., Howie, A. and Whelan, M.J. (1966) Phil. Mag. 14, 217.
- Hall, C.R. and Hirsch, P.B. (1965) Proc. Roy. Soc. A286, 158.
- Hashimoto, H. (1964) J. App. Phys. 35, 277.
- Hashimoto, H., Howie, A. and Whelan, M.J. (1960) Phil. Mag. 5, 967.

- Hashimoto, H., Howie, A., and Whelan, M.J. (1962)
Proc. Roy. Soc. A269, 80.
- Head, A.K. (1967) Aust. J. Phys. 20, 557.
- Heidenreich, R.D. (1942) Phys. Rev. 62, 291.
- Heidenreich, R.D. (1950) Phys. Rev. 77, 271.
- Heidenreich, R.D. and Sturkey, L. (1945) J. Appl. Phys.
16, 97.
- Herzberg, B. (1971) Z. Naturforsch. 26a, 1247.
- Hewat, E. (1972) Proc. 5'th Eur. Cong. on Electron
Microscopy, Manchester, 526.
- Hibi, T., Kambe, K. and Honjo, G. (1955) J. Phys. Soc.
Japan 10, 35.
- Hiller, J. and Baker, R.F. (1942) Phys. Rev. 61, 722.
- Hirsch, P.B., Howie, A., Nicholson, R.B., Pashley, D.W.
and Whelan, M.J. (1965) Electron Microscopy of
Thin Crystals, Butterworths.
- Hoerni, J.A. (1956) Phys. Rev. 102, 1534.
- Horstmann, M. and Meyer, G. (1963) Phys. Kondens.
Materie 1, 208.
- Howie, A. (1962) J. Phys. Soc. Japan, Suppl. BII, 17,
122.
- Howie, A. (1966) Phil. Mag. 14, 223.
- Howie, A. and Basinski, Z.S. (1968) Phil. Mag. 17, 1039.
- Howie, A. and Whelan, M.J. (1960) Proc. Eur. Regional
Conf., Electron Microscopy, Delft, 181.

- Howie, A. and Whelan, M.J. (1961) Proc. Roy. Soc. A263, 217.
- Humphreys, C.J. (1972) Phil. Mag. 25, 1459.
- Humphreys, C.J. and Fisher, R.M. (1971) Acta Cryst. A27, 42.
- Humphreys, C.J. and Hirsch, P.B. (1968) Phil. Mag. 18, 115.
- Humphreys, C.J., Howie, A. and Booker, G.R. (1967) Phil. Mag. 15, 507.
- Humphreys, C.J. and Lally, J.S. (1970) J. Appl. Phys. 41, 232.
- Humphreys, C.J., Thomas, L.E., Lally, J.S. and Fisher, R.M. (1971) Phil. Mag. 23, 87.
- Ibers, J.A. and Vainshtein, B.K. (1962) International Crystallographic Tables, Vol. III, Tables 3.3.3A(1) and A(2), Kynoch Press, Birmingham.
- IMSL (1972) International Mathematical and Statistical Libraries, Inc. Houston, Texas.
- Kambe, K. (1957) J. Phys. Soc. Jap. 12, 13.
- Kamiya, Y. and Uyeda, R. (1961) J. Phys. Soc. Japan 16, 1361.
- Kinder, E. (1943) Naturwiss. 31, 149.
- Knoll, M. and Ruska, E. (1932) Ann. d. Physik 12, 607.
- Lally, J.S., Humphreys, C.J., Metherell, A.J.F. and Fisher, R.M. (1972) Phil. Mag. 25, 321.

- Lehmpfuhl, G. (1970) Proc. Septième Congrès International de Microscopie Electronique, Grenoble, 1, 101.
- Lehmpfuhl, G. (1972) Z. Naturforsch. 27a, 425.
- Lehmpfuhl, G. and Reissland, A. (1968) Z. Naturforsch. 23a, 544.
- Lynch, D.F. (1971) Acta Cryst. A27, 399.
- Mazel, A. (1971) J. Microsc. 11, 207.
- Menzel-Kopp, C. (1962) J. Phys. Soc. Japan, Suppl. BII 17, 76.
- Metherell, A.J.F. and Fisher, R.M. (1969) phys. stat. sol. 32, 551.
- Metherell, A.J.F. and Spring, M.S. (1970) Proc. Septième Congrès International de Microscopie Electronique, Grenoble, 1, 105.
- Molière, K. (1939) Ann. d. Physik 34, 461.
- Monk, A.E.B. (1972) unpublished.
- Niehirs, H. (1959) Z. Naturf. 14a, 504.
- Oblak, J.M. and Kear, B.H. (1972) Proc. 30'th Ann. Meeting, Electron Microscopy Soc. of America, 646.
- Pfister, H. (1953) Ann. Phys. 11, 239.
- Radi, G. (1970) Acta Cryst. A26, 41.
- Reynaud, F. (1971) J. Microsc. 11, 179.
- Richards, C.G. and Stobbs, W.M. (1972) Sym. Abstracts, 5'th Eur. Cong. on Electron Microscopy, Manchester.
- Sheinin, S.S. (1966) Rev. Sci. Instr. 37, 232.
- Sheinin, S.S. (1967) phys. stat. sol. 27, 247.

- Sheinin, S.S. (1970A) *phys. stat. sol.* 37, 683.
- Sheinin, S.S. (1970B) *phys. stat. sol.* 38, 675.
- Sheinin, S.S. and Botros, K.Z. (1970) *phys. stat. sol.(a)* 3, 271.
- Sheinin, S.S., Botros, K.Z. and Cann, C.D. (1970) *phys. stat. sol.(a)* 3, 537.
- Sheinin, S.S. and Cann, C.D. (1971) *phys. stat. sol.(a)* 5, 745.
- Sheinin, S.S. and Cann, C.D. (1973) To be published.
- Shimamoto, N., Fukamachi, T. and Ohtsuki, Y. (1972) *J. Phys. Soc. Japan* 33, 459.
- Shinohara, K. (1932) *Sci. Pap. Inst. Phys. Chem. Res., Tokyo*, 20, 39.
- Skalicky, P. and Papp, A. (1972) *Phil. Mag.* 25, 178.
- Smith, G.H. and Burge, R.E. (1962) *Acta Cryst.* 15, 182.
- Spencer, J.P. and Humphreys, C.J. (1971) *Proc. 25'th Ann. Meeting EMAG, Inst. Physics, Cambridge*, 310.
- Sprague, J.A. and Wilkens, M. (1970) *Proc. Septième Congrès International de Microscopie Electronique, Grenoble*, 1, 95.
- Spring, M.S. and Steeds, J.W. (1970) *phys. stat. sol.* 37, 303.
- Steeds, J.W. (1970) *phys. stat. sol.* 38, 203.
- Sturkey, L. (1957) *Acta Cryst.* 10, 858.
- Takahashi, H. (1969) *Japan J. Appl. Phys.* 8, 296.

- Tan, T.Y., Bell, W.L. and Thomas, G. (1971) Phil. Mag.
24, 417.
- Thomson, G.P. and Reid, A. (1927) Nature 119, 890.
- Uyeda, R. (1968) Acta Cryst. A24, 175.
- Uyeda, R. and Nonoyama, M. (1965) Japan J. App. Phys.
4, 498.
- Watanabe, D., Uyeda, R. and Fukuhara, A. (1968) Acta
Cryst. A24, 580.
- Whelan, M.J. (1965) J. App. Phys. 36, 2103.
- Williams, E.J. (1933) Proc. Roy. Soc. A139, 163.

APPENDIX A

Determination of the Exact Orientation of a Crystal for the Case of Two Reflections in Their Exact Bragg Conditions

In many diffraction situations, it is usually sufficient to express the orientation of a crystal in terms of the nearest low-order zone axis: $[111]$, $[013]$, etc. In electron diffraction, however, very small changes in orientation can have very marked effects on the observed images. Thus, in this case it is necessary to know the orientation of a crystal with greater accuracy than afforded by the zone axis approach.

The procedure used in this thesis for accurately determining the orientation of a crystal was based on a method developed by Foxon (1968). In this procedure, it is assumed that two reflections (h_1, k_1, l_1) and (h_2, k_2, l_2) whose reciprocal lattice vectors, \vec{g} and \vec{h} , are non-collinear are in their exact Bragg conditions. In this situation, as shown in Fig. A1, the corresponding reciprocal lattice points \vec{g} and \vec{h} as well as the origin of reciprocal space O are all equidistant from the points A and B . This distance is equal to $1/\lambda$ where λ is the wave length of the incident electrons. Only two orientations of the crystal, designated $\overrightarrow{OR1}$ and $\overrightarrow{OR2}$ in Fig. A1, will result in this situation.

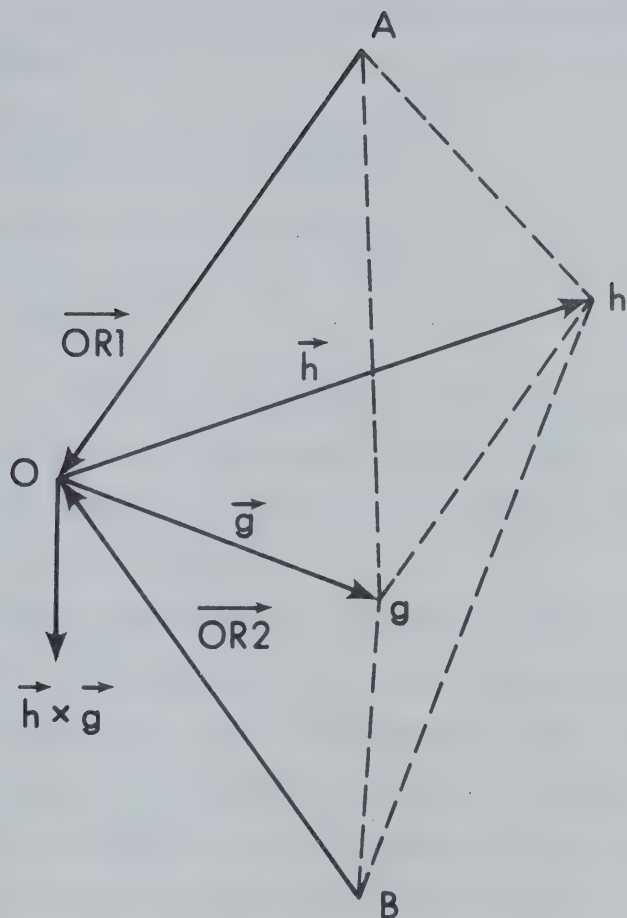


Fig. A1. A diagram in reciprocal space showing the the allowed orientation $\overrightarrow{OR1}$ and $\overrightarrow{OR2}$ of the crystal when the reflections corresponding to \vec{g} and \vec{h} are in their exact Bragg conditions. $OA = gA = hA = OB = gH = hB = \frac{1}{\lambda}$. The points h and g are at positions $\frac{1}{a_o} (h_2, k_2, l_2)$ and $\frac{1}{a_o} (h_1, k_1, l_1)$ respectively in the reciprocal lattice.

These orientations can be found by solving the set of equations

$$\begin{aligned}\overrightarrow{OR} \cdot \vec{g} &= |\overrightarrow{OR}| |g| \cos \theta_1 \\ \overrightarrow{OR} \cdot \vec{h} &= |\overrightarrow{OR}| |h| \cos \theta_2 \\ |\overrightarrow{OR}| &= \frac{1}{\lambda} \quad .\end{aligned}\tag{A.1}$$

Here, θ_1 , the angle between g and the vectors $\overrightarrow{OR1}$ and $\overrightarrow{OR2}$, is equal to $90^\circ + \sin^{-1}(|\vec{g}|\lambda/2)$ and, θ_2 , the corresponding angle between h and $\overrightarrow{OR1}$ and $\overrightarrow{OR2}$ is equal to $90^\circ + \sin^{-1}(|\vec{h}|\lambda/2)$.

These equations A.1 result in two distinct solutions for \overrightarrow{OR} corresponding to the two vectors $\overrightarrow{OR1}$ and $\overrightarrow{OR2}$ shown in Fig. A1. By convention, the orientation of a crystal is defined to be that direction in the crystal parallel to the direction of the incident electron beam. To determine which of the two solutions $\overrightarrow{OR1}$ and $\overrightarrow{OR2}$ is correct, it is necessary to examine the relationship of the reflection g to the reflection h . If the electron beam is incident in the direction $\overrightarrow{OR1}$, the reflection g will occur at a clockwise position with respect to h in a diffraction pattern. If the electron beam is incident in the direction $\overrightarrow{OR2}$, the reflection g will occur at a counterclockwise position with respect to h . Thus, it is necessary to consider

the actual experimental situation to determine which of the two orientations should be chosen.

In practice, in the computer subroutine which was used to calculate orientations, the reflections g and h were assumed to be in a counterclockwise order and the orientation chosen was the one closest to the direction $\vec{h} \times \vec{g}$.

APPENDIX B

The Effect of the Signs of the Fourier Coefficients of the Lattice Potential

In a centro-symmetric crystal, the Fourier coefficients, U_g , are all real. If, in addition, the centre of symmetry coincides with the centre of an atom, the U_g 's will usually be positive (Hashimoto, Howie and Whelan, 1962). When this centre of symmetry does not coincide with an atomic position, however, the U_g 's may be either positive or negative depending upon the structure factor. For example, in Si a centre of symmetry lies at the point $(\frac{1}{8}, \frac{1}{8}, \frac{1}{8})a_0$ midway between atoms at the positions $(0,0,0)a_0$ and $(\frac{1}{4}, \frac{1}{4}, \frac{1}{4})a_0$. When the (220) systematic reflection and one of the $(\bar{1}33)$, $(\bar{1}35)$ and $(\bar{1}37)$ non-systematic reflections are considered, it is found that U_g and U_h are negative but U_{g-h} is positive. An examination of equation 5.18, which is reproduced below, shows that, for these reflections, the extinction distance will increase for s_h positive but decrease for s_h negative.

$$\xi \approx \frac{K}{U_g} \left(1 + \frac{U_{g-h}U_{-h}}{2U_g K s_h} \right) \quad . \quad (5.18)$$

This behaviour is in agreement with that obtained when the Fourier coefficients are all of positive sign.

When the reciprocal lattice point corresponding to the non-systematic reflection of interest lies inside the Ewald sphere, the systematic extinction distance will have increased over its value obtained when the non-systematic reflection is absent. Also, when the lattice point is outside the Ewald sphere, a decrease will be found in the extinction distance. For the $(\bar{3}13)$ non-systematic reflection, however, U_g is negative but U_h and U_{g-h} are both positive. An examination of equation 5.18 in this case reveals that the extinction distance will decrease for s_h positive and increase for s_h negative in contrast to the previously described behaviour.

Thus, in considering the cumulative aspect of the effects of non-systematic reflections in a material such as Si, no general statement can be made with regard to their effects on the extinction distance and the positions of their corresponding reciprocal lattice points with respect to the Ewald sphere. In this case, the effects of two reflections, both of which have negative s_h values, may tend to cancel, while the effects of reflections with deviations of opposite signs may add.

Finally, it may be noted that the criterion developed in Section 5:6 is independent of the signs of the Fourier coefficients. Therefore, the use of this

criterion for including reflections in a many-beam calculation will not be affected by the presence of both positive and negative coefficients.

B30052